Pedro Libânio de Abreu Martins

Magnetoelectric nanocomposites based on electroactive polymers

Magnetoelectric nanocomposites based on electroactive polymers

Pedro Libânio de Abreu Martins

UMinho | 2012
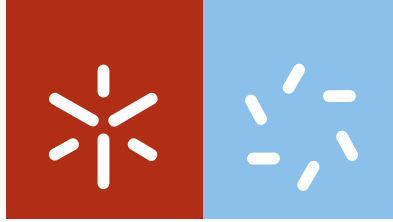
Universidade do Minho

Escola de Ciências

Pedro Libânio de Abreu Martins

Magnetoelectric nanocomposites based on electroactive polymers

Tese de Doutoramento
Doutoramento em Ciências
Especialidade de Física

Trabalho realizado sob orientação do
Professor Doutor Senentxu Lanceros-Méndez
e do
Professor Doutor José Manuel Barandiarán Garcia

Setembro de 2012

DECLARAÇÃO

Nome

Pedro Libânio de Abreu Martins

Endereço electrónico: pmartins@fisica.pt

Número do Bilhete de Identidade: 12306249

Título da tese:

Magnetoelectric nanocomposites based on electroactive polymers

Orientador(es): Senentxu Lanceros-Méndez e José Manuel Barandiarán Garcia

Ano de conclusão: 2012

Designação do Mestrado ou do Ramo de Conhecimento do Doutoramento: Física

Universidade do Minho, 04/09/2012

Assinatura: _____

Magnetoelectric nanocomposites based on electroactive polymers

Escola de Ciências

Pedro Libânio de Abreu Martins

Setembro de 2012

Acknowledgements

I am ever grateful to God, the Creator and the Guardian, and to whom I owe my existence.

In my daily work I have been blessed with a nice and cheerful group of friends, for this reason I thank to the Electroactive Smart Materials Friends. In a special way I wish to thank Carlos Costa due to the help and friendship transmitted in the beginning of the PhD.

I also want to thank the memorable and never forgotten good times spent in the Cambridge University, thanks Xavier, Sohini and Neil Mathur.

I am very grateful by the friendly and welcoming way I was received in the Basque Country University, thanks Andoni, Javier, Iñaki and Jon Gutierrez.
I wish to extend my thanks to my co-supervisor Jose Manuel Barandiaran for helping me whenever I needed and for always having a kind word when I worked in Bilbao.
I want to thank my supervisor Senentxu Lanceros-Mendez for giving me the opportunity to work with him, for his continuous support, patience, and wisdom. It was a pleasure to have been your PhD student.

I wish to thank my parents. They raised me, supported me, taught me and loved me. What I am today I owe it to you.

I want to thank my brother Joel for inspiring me to be a better person, he's my pride since the day he was born.

Lastly, and most importantly, I thank my wife Clarisse that has been, always, my pillar, my joy and my guiding light. Love you.

To Clarisse, Joel, and my parents, I dedicate this thesis.

Pedro Martins

Abstract

The magnetoelectric (ME) effect is a physical phenomenon with a wide range of device applications such as computer memories, smart sensors, actuators and high frequency microelectronic devices. There are few single-phase ME materials and most of them show weak ME coupling at room temperature. In order overcome this limitation, composite materials with increased ME effect are being developed. Most of the ME investigations have used as piezoelectric matrix ceramic materials, but ceramic composites may become fragile and are limited by deleterious reactions at the interface regions leading to low electrical resistivities and high dielectric losses, making those ceramic composites not attractive for applications. In this way, new multifunctional Poly(vinylidene fluoride) (PVDF) and copolymers based nanocomposites were produced with magnetostrictive $NiFe_2O_4$, $CoFe_2O_4$ and $Ni_{0.5}Zn_{0.5}Fe_2O_4$ nanoparticles. PVDF and copolymers were used due to their flexibility and high piezoelectric coefficient and ferrite nanoparticles due to their good magnetostrictive properties and distinct magnetic response.

The piezoelectric, dielectric, ferroelectric, magnetic and ME properties of the resulting nanocomposites were determined and discussed.

It was found that the dispersed ferrite nanoparticles strongly enhanced the nucleation of the β-phase of the PVDF matrix, essential for the ME response. The origin of such β-phase nucleation was attributed to the electrostatic interactions resulting from the presence of negative nanoparticle surfaces that interact with the polymeric CH_2 groups that have positive charge density.

It was also verified that macroscopic magnetic and dielectric responses of the composites strongly depend on the ferrite nanoparticle content, with both magnetization and dielectric constant increasing for increasing filler content. The β-relaxation in the composite samples was similar to the one observed for β-PVDF obtained by stretching. A superparamagnetic behaviour was observed for $PVDF/NiFe_2O_4$ composites, whereas $PVDF/CoFe_2O_4$ samples show a magnetic hysteresis cycle with coercivity of 0.3 T.

Ferroelectric and piezoelectric properties were improved when small amount of $CoFe_2O_4$ nanoparticles (up to 7% in weight percent (wt.%)) were added to the P(VDF-TrFE) matrix. The highest ME response of 41.3 mV/cm.Oe was found in the P(VDF-TrFE)/$CoFe_2O_4$ (28/72 wt.%) composite when a H_{DC}=0.25T was transversely applied

to the sample surface and a ME voltage coefficient of $\approx$5mV/cm.Oe was obtained at a H_{DC}=0.5T for the PVDF/CoFe$_2$O$_4$ (93/7 wt.%) sample. This ME response for the PVDF based composites was possible after stretching of the samples, which also led to the formation of voids.

Direct ME effects up to 1.35 mV/cm.Oe were obtained in a H_{DC} =0,5T, for the P(VDF-TrFE)/Ni$_{0.5}$Zn$_{0.5}$Fe$_2$O$_4$ (15/85 wt.%). P(VDF-TrFE)/Ni$_{0.5}$Zn$_{0.5}$Fe$_2$O$_4$ nanocomposites show, as compared to P(VDF-TrFE)/CoFe$_2$O$_4$ nanocomposites, linear and non-hysteretic direct magnetoelectric responses up to 0.5 T.

It is in this way, novel polymer based ME composites were produced and characterized in such way that it was demonstrated their suitability for sensor applications.

Pedro Martins

Resumo

O efeito magnetoeléctrico (ME) é um fenómeno físico que tem uma vasta gama de aplicações de que são exemplo as memórias de computador, sensores inteligentes, atuadores e aparelhos microeletrónicos de alta frequência. Existem muito poucos materiais ME de fase única e a maior parte deles exibem um efeito ME muito baixo à temperatura ambiente. Para ultrapassar esta limitação, estão a ser desenvolvidos materiais compósitos com efeito ME melhorado. Contudo, a maior parte das investigações no âmbito dos materiais ME têm usado como matriz piezoelétrica materiais cerâmicos, estes podem-se tornar frágeis e são limitados por reações deletérias nas interfaces levando a resistividades elétricas muito baixas e a elevadas perdas dielétricas, o que faz com que estes compósitos cerâmicos não sejam atrativos do ponto de vista ads aplicações. Desta forma, novos compósitos multifuncionais baseados no Poli(fluoreto de vinilideno) (PVDF) ou nos seus copolímeros foram produzidos através da incorporação de partículas magnetostrictivas de $NiFe_2O_4$, $CoFe_2O_4$ e $Ni_{0.5}Zn_{0.5}Fe_2O_4$. O PVDF e os seus copolímeros foram utilizados devido à sua flexibilidade e alto coeficiente piezoelétrico. Por sua vez, as nanopartículas de ferrites foram usadas devido às suas propriedades magnetostritivas e resposta magnética distinta.

As propriedades piezoelétricas, dielétricas, ferroelétricas, magnéticas e ME dos nanocompósitos resultantes foram determinadas e discutidas.

Foi descoberto que as nanopartículas de ferrites dispersas no PVDF melhoravam, significativamente a nucleação da fase β do polímero, fase essa que é essencial à resposta ME do compósito.

A origem desta nucleação foi atribuída às interações eletrostáticas resultantes da presença de nanopartículas com superfícies negativas que interagiam com os grupos CH_2 do polímero que possuem densidade de carga negativa.

Verificou-se também que a resposta magnética e dielétrica dos compósitos era fortemente dependente da quantidade de ferrites adicionada, com a magnetização e constante dielétrica a aumentarem com o aumento da quantidade de partículas adicionadas.

A relaxação β nos compósitos foi similar aquela observada no β-PVDF obtido através de estiramento.

Pedro Martins

Foi ainda observado um comportamento superparamagético nos compósitos PVDF/NiFe$_2$O$_4$ enquanto que, nas amostras PVDF/CoFe$_2$O$_4$ observou-se um ciclo de histerese magnética com coercividade de 0.3 T.

As propriedades piezoelétricas e ferroelétricas também foram melhoradas quando se adicionaram pequenas quantidades de nanopartículas de CoFe$_2$O$_4$ (até 7 % de percentagem em massa (wt.%)) ao P(VDF-TrFE).

A maior resposta ME foi verificada na amostra P(VDF-TrFE)/CoFe$_2$O$_4$ (28/72 wt.%) quando um campo magnético H$_{DC}$=41.3 mV/cm.Oe foi aplicado transversalmente à superfície da amostra, foi também obtido um coeficiente ME de ≈5mV/cm.Oe na amostra PVDF/CoFe$_2$O$_4$ (93/7 wt.%) quando se aplicou um H$_{DC}$=0.5T. Esta resposta ME em amostras baseadas em PVDF foi possível graças ao estiramento da amostra, estiramento esse que também deu origem a vazios dentro do compósito.

Foram também obtidas respostas ME diretas até 1.35 mV/cm.Oe na amostra P(VDF-TrFE)/Ni$_{0.5}$Zn$_{0.5}$Fe$_2$O$_4$ (15/85 wt.%). Quando sujeitas a H$_{DC}$ até 0.5T estas amostras mostraram um comportamento linear e sem histerese.

Desta forma, novos compósitos ME baseados em polímeros foram produzidos e caracterizados de tal forma que foi demonstrada a sua adequação para aplicações na área dos sensores.

Pedro Martins

Table of contents

Pedro Martins

Pedro Martins

Pedro Martins

List of figures

Pedro Martins

Pedro Martins

Pedro Martins

List of Tables

List of symbols

A

A_α Absorbance at 766 cm^{-1} of PVDF

A_β Absorbance 840 cm^{-1} of PVDF

B

B VTF energy

C

D

d_{3n} Piezoelectric coefficient

E

E_{act} Activation energy

E_C Coercive Electric Field

E_Y Young's modulus

H

H   Magnetic Field

H_{AC} Alternating Current Magnetic Field

H_{DC} Direct Current Magnetic Field

K

K_{eff} Anisotropy constant

k_B Boltzmann constant

K_α Absorption coefficient of α-PVDF

K_β Absorption coefficient of β-PVDF

M

M	Magnetization
M_s	Saturation magnetization

N

n	Avrami exponent

P

P_{Max}	Maximum Polarization
P_{Rem}	Remnant Polarization

R

R	Ideal gas constant
R^2	Linear regression coefficient
R_g	Radius of gyration

T

T	Stress
T_0	Vogel temperature
$t_{1/2}$	Crystallization half-time
$\tan \delta$	Dielectric loss
Tg	Glass transition temperature
T_c	Crystallization temperature
T_m	Nominal melting temperature

W

wt.%	Weight percent

X

x	Weight fraction of the α-PVDF

X_c	Degree of crystallinity
X_c^c	Degree of crystallinity calculated from the melting crystallization scans
X_c^m	Degree of crystallinity calculated from the melting scans
X_t	Relative crystallinity
X_α	Degree of crystallinity of α-PVDF
X_β	Degree of crystallinity of β-PVDF

Y

y	Weight fraction of the β-PVDF

Greek

α	Magnetoelectric coefficient
ΔG	Gibbs free energy
$\Delta H_{100\%crystalline\ \alpha}$	Enthalpy of pure crystalline α-PVDF
$\Delta H_{100\%crystalline\ \beta}$	Enthalpy of pure crystalline β-PVDF
ΔH_c	Crystallization enthalpy
ΔH_m	Melting enthalpy
ΔS	Entropy variation
ε	Dielectric constant
ξ	Magnetic permeability
ρ	Density
φ	Volume fraction
χ	Magnetic susceptibility
τ_0	Preexponential factor
τ	Relaxation time

List of Abbreviations

A

ATR   Attenuated Total Reflectance

B

BFO $BiFeO_3$

C

CB   Carbon black

CTAB   Cetrimonium bromide

D

DMF   *N*,*N*-dimethylformamide

DSC   Fourier transformed infrared spectroscopy

F

$F(\alpha)$ α-phase content of PVDF

$F(\beta)$ β-phase content of PVDF

FC   Field cooled

FTIR   Fourier transformed infrared spectroscopy

H

HDPE   High-density polyethylene

I

iPP   Isotactic polypropylene

L

Li^+-PEO   Lithium perchlorate-doped PEO

M

MCE	Magnetocaloric effect
ME	Magnetoelectric
MF	Multiferroic

N

NZFO	$Ni_{0.5}Zn_{0.5}Fe_2O_4$

O

OMPL	Optical microscopy with polarized light

P

P(VDF-TrFE)	Poly(vinylidene trifluorethylene)
PANI	Polyaniline
PEN	Poly(ethylene 2,6-naphthalate)
PEO	Polyethylene oxide
PET	Poly(ethylene terephthalate)
PMMA	Poly(methyl methacrylate)
POM	Polarized optical microscopy
PP	Polypropylene
ppm	Parts per million
PU	Polyurethane
PVDF	Polyvinylidene fluoride
PVDF-HPFP	PVDF hexafluoropropylene
PZT	Lead zirconate titanate

S

Pedro Martins

SDS	Sodium dodecyl sulfate
SEM	Scanning Electron Microscopy
SQUID	Superconducting quantum interference device

T

T	Stress
TEM	Transmission electron microscopy
TGA	Thermogravimetric analyses

V

VER	Vinyl ester resin
VFT	Vogel–Fulcher–Tammann

X

XRD	X-ray diffraction

Z

ZFC	Zero field cooled

1 Introduction

1.1
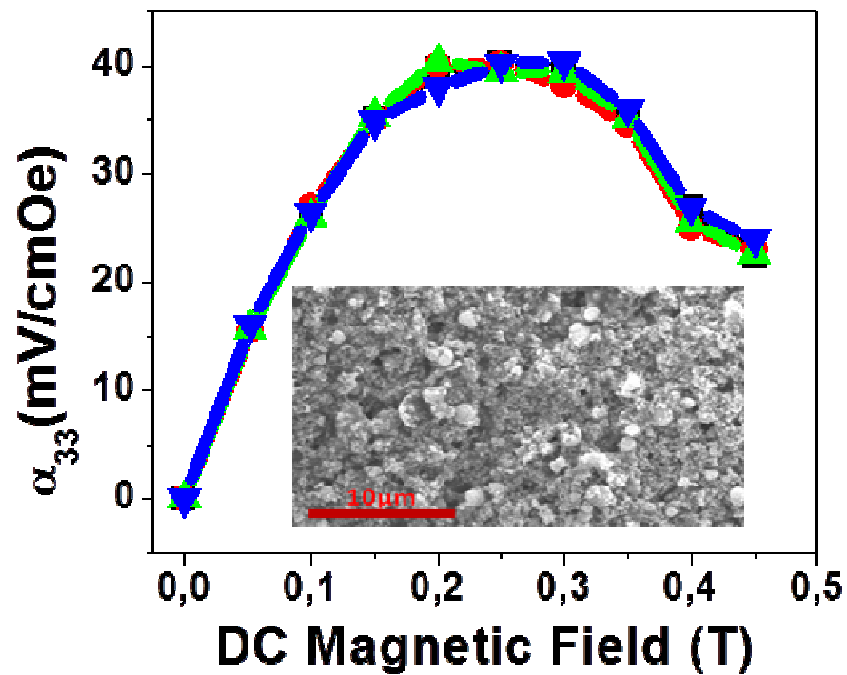
Magnetoelectric (ME) materials have attracted large interest of the scientific community due to the application potential of the cross-correlation between the magnetic and the electric orders for technological applications such as multifunctional devices, transducers, actuators and sensors.

There are few single-phase ME materials and most of them show weak ME coupling at room temperature and in order to obtain materials with higher ME effect than the single-phase ME materials, composites materials are being developed and investigated.

Over the past few years, ME multilayer ceramic and particulate composite materials have attracted growing attention. Ceramic composites may become fragile and are limited by deleterious reactions at the interface regions making such ceramic composites not appropriate for device applications. In this way, one of the major current challenges in the ME area is to obtain composites with an uncomplicated production method, a flexible structure and without large leakage currents. One possible way to overcome this quest is to use Polyvinylidene fluoride (PVDF) and its copolymers as piezoelectric phase of the ME nanocomposite. Since copolymer Poly(vinylidene trifluorethylene) (P(VDF-TrFE)) crystallizes from the melt directly in the electroactive β-phase which is an essential requirement for the preparation of ME composites, P(VDF-TrFE) is being used in ME composites instead of PVDF, but due to their distinct morphological and physical properties, it would be useful to implement also PVDF based ME composite materials. Regarding the other required component in a ME nanocomposites, ferrite nanoparticles such as $NiFe_2O_4$, $CoFe_2O_4$ and $Ni_{0.5}Zn_{0.5}Fe_2O_4$ have been used as magnetostrictive phase as, among different magnetic oxide materials, show the largest magnetostrictive coefficients with high Curie temperature, good processability, chemical agent resistance, easy production and chemically inertness. However there are only few studies taking advantage of the simultaneously use of both materials (PVDF and ferrite nanoparticles) in order to obtain the ME.

This thesis investigation is related to the development and characterization of ME nanocomposites consisting of PVDF and its copolymer P(VDF-TrFE) as piezoelectric phase and ferrite nanoparticles as magnetostrictive phase.

1.2 Objectives

Since one of the main challenges in the ME area is to replace the ceramic piezoelectric phase by polymer based piezoelectric matrices to achieve larger sensor areas and/or non-planar structures, the main objective of this thesis was to obtain new types of ME polymer composites suitable for advanced applications. The composites needed to be produced, the origin of the effects investigated and the range of applicability determined. In particular, the main scientific objectives of the investigation were:

1. To obtain new composites based in electroactive polymers with good ME properties. Prepare PVDF and P(VDF-TrFE) composites by producing particulate composites of the polymers with magnetostrictive ferrite nanoparticles such as $NiFe_2O_4$, $CoFe_2O_4$ and $Ni_{0.5}Zn_{0.5}Fe_2O_4$.
2. To get a deeper knowledge of the physical origin of the dielectric, magnetic, mechanical and thermal properties of the composites.
3. To obtain a relationship between the processing conditions, the structural and microscopic properties of the materials and their macroscopic response.
4. To obtain and investigate the main characteristics of the ME response of the developed nanocomposites.

1.3 Structure

This thesis is divided in 10 chapters and is intended to provide a comprehensive and logic report of the progress achieved during the present investigation. The chapters are presented in such a way that show the sequential progress obtained during this investigation and are related to a variety of published works.

In the first part of this thesis (Chapter 1) are presented the objectives, the thesis structure and the state of the art on ME materials and their applications.

In the Chapters 2 to 4 it is reported and discussed the nucleation of the electroactive β-phase of PVDF and its influence in the crystallization kinetics of the polymer.

The β-phase nucleation phenomenon is discussed and a nucleation mechanism is presented in Chapters 5 and 6.

In the next three chapters (7, 8 and 9) of the thesis are presented, evaluated and discussed the dielectric, piezoelectric, magnetic and ME properties of the polymer based nanocomposites.

The last chapter is focused on the final conclusions of the work and in the suggestion for future work research directions.

1.4   State of the art

A short introduction on the main topics related to this thesis as well as the state of the art on the investigation in polymer based and non-polymer based magnetoelectric materials is presented.

1.4.1   Basic Concepts

In the Table 1.1 are listed and defined the basic concepts related to the ME field.

Table 1.1 – Basic Concepts.

Concept	Definition	References
Multiferroic	Material that possesses two or all three ferroic properties (ferroelectricity, ferromagnetism and ferroelasticity).	[1-2]
Ferroelectric	Material that possesses a spontaneous and stable polarization that can be hysteretically switched by an applied electric field.	[3-4]
Ferromagnetic	Material that possesses a spontaneous and stable magnetization that can be hysteretically switched by an applied magnetic field.	[5-6]
Ferroelastic	Material that possesses a spontaneous and stable deformation that can be hysteretically switched by an applied stress.	[7-8]
Piezoelectricity	Alteration in the strain of a material as a linear function of an applied electric field or a change in the material polarization as a linear function of applied stress.	[8-9]
Piezomagnetism	Alteration in the strain of a material as a linear function of an applied magnetic field or a change in the material magnetization as a linear function of applied stress.	[10-11]
Electrostriction	Alteration in the strain of a material as a quadratic function of an applied electric field.	[12-13]
Magnetostriction	Alteration in the strain of a material as a quadratic function of an applied magnetic field.	[14-15]

Pedro Martins

Piezoelectric coefficient	Relates the mechanical strains produced by an applied electric field and are called the strain constants, or the "d" coefficients. d is a tensor, with components d_{ij}, where i indicates the direction of polarization generated in the material when the electric field is zero (or the direction of the applied field), and j is the direction of the applied stress (or the induced strain).	[12-13]
Piezomagnetic coefficient	Relates the mechanical strains produced by an applied magnetic field and are called the "d_m" coefficients. d is a tensor, with components d_{ijm}, where i indicates the direction of magnetization generated in the material when the magnetic field is zero (or the direction of the applied field), and j is the direction of the applied stress (or the induced strain).	[14, 16]
Magnetostrictive coefficient	Relates the mechanical strains produced by an applied magnetic field and are called the "λ" coefficients. λ is a tensor, with components λ_{ij}, where i indicates the direction of magnetization generated in the material when the magnetic field is zero (or the direction of the magnetic field), and j is the direction of the applied stress (or the induced strain).	[14-15]
ME coefficient	Relates the polarization/voltage produced by an applied magnetic field and are called the "α" coefficients. A is a tensor, with components α_{ij}, where i indicates the direction of polarization/voltage generated in the material when the electric field is zero (or the direction of the applied electric field), and j is the direction of the applied magnetic field (or the induced magnetization).	[17-18]

1.4.2   ME Effect

The ME effect, defined as the variation of the electrical polarization of a material in the presence of an applied magnetic field or as the induced magnetization in the presence of an applied electric field [19-21] has drawn increasing interest due to their potential applications in areas such as information storage, spintronics, multiple-state memories, magnetic sensors, transformers, gyrators, microwave devices, optical waves and diodes among others [22-26].

Four years (1888, 1894, 1905 and 1926) are intimately related to the emergence of the ME (Figure 1.1):

- In 1888, Röntgen, before winning the Nobel Prize due to the discovery of the X-rays, observed that a dielectric moving in a electric field became magnetized [27];
- The reverse effect, the electrical polarization of a dielectric moving in a magnetic field was discovered by Wilson in 1905 [28];
- Between the first and second discoveries indicted above, Pierre Curie, in 1894 and on the basis of symmetry considerations enunciated the possibility of ME effect in non-moving crystals [24, 29];
- In 1926, Debye introduced and coined the term "*magnetoelectricity*" for the effect that was at time unsuccessfully proved experimentally [30].
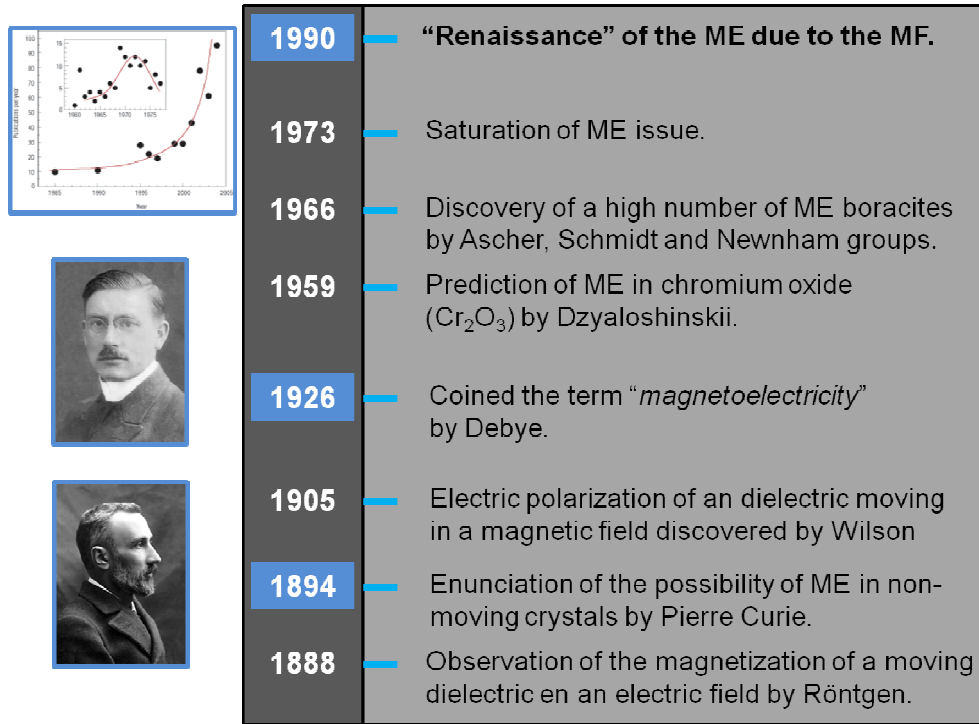
Figure 1.1 – Evolution Highlights in the investigation of the ME effect.

In 1959, the ME effect was predicted to occur in Cr_2O_3 by Dzyaloshinskii [31], prediction that was experimentally confirmed in the following year by Astrov [32].

In 1966, the groups of Ascher and Schmidt at the Battelle Institute in Geneva and Newnham at the Pennsylvania State University discovered a high number of ME boracites [33] and phosphates [34].

ME coupling coefficients, defined as

$$\alpha = \frac{\partial P}{\partial H} \tag{1.1}$$

were not as high as necessary for applications, but the number of new ME materials increased significantly.

Thus, in 1973 the scientific work about ME materials reached a saturation since it was felt that single-phase ME were not technologically applicable due to the weak ME coupling and the need of low temperatures. Further, the theoretical considerations gave no hope towards significant solutions and improvements [35]. As a result of this dead-end the intensity of the ME scientific activity strongly declined for almost 20 years.

It was in the 1990s that the interest in ME materials strongly increased again due to the relationship of the ME and MF concepts: the main object of the ME scientific investigations shifted from single phase ME materials, to the search for MF compounds with higher ME coupling [36]. In those novel composites the ME response is due to elastic coupling between the two constituent phases, one piezoelectric and the other magnetostrictive [22].

Three main types of bulk ME composites have been investigated both experimentally and theoretically: a) magnetic metals/alloys e.g., laminated Terfenol-D or Metglas and piezoelectric ceramics, e.g., Lead zirconate titanate (PZT); b) laminated Terfenol-D and Metglas and piezoelectric polymers; c) particulate composites of ferrite and piezoelectric ceramics [3].

Today ME research is a strong research area, showing still plenty of mysteries, promises and challenges. One of the main challenges is to replace the ceramic in bimorphs or superlattice composites with a polymer or polymer based piezoelectric matrix to achieve larger areas or non-planar structures [37].

The main goal of this review is to report the state of the current research, advantages, disadvantages, merits and risks of the polymer based ME materials.

The review is divided into the following topics: it will start by discussing the problems in the application of non polymeric ME materials, followed by a summary of results on the three main types of polymeric ME materials; nanocomposites (Figure 1.2a), laminated composites (Figure 1.2b) and *polymer as a binder* composites (Figure 1.2c).
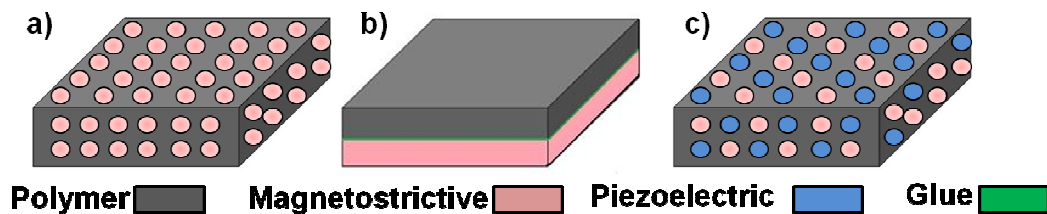
Figure 1.2 – Types of polymer based ME materials.

After some applications for the different polymer-based ME materials being presented, the review will be ended with a summary and an outlook.

1.4.3 Non polymeric ME materials: problems faced for application developments

The magnitude of α in most of the single phase MF materials is in the range of 1-20 mV/cm.Oe which is considered insufficient for most of the proposed practical applications [38]. Also there is a wide variation of the transition temperatures (paraelectric to ferroelectric, paramagnetic to antiferromagnetic, antiferromagnetic to ferromagnetic) for the single-phase ME materials and there is a limited number of materials that exhibits MF behaviour at room temperature [39]. In this way, most of these ME can be only used at low temperatures, ≈ 10 K, which further complicates the design and applications of devices. As an effective alternative, with the product property based on the concept proposed by van Suchtelen [40], composites can be fabricated to obtain MF materials with large ME coefficient (α) at room temperature arising from an elastic coupling between magnetostrictive and piezoelectric phases. The fabricated composites morphology can be particulate, *in situ* growth or laminated [1, 6].

Despite ME coefficients obtained in ceramic MF composites being three orders of magnitude higher than in single phase materials [9-10], such composites may become fragile and are limited by deleterious reactions at the interface regions, leading to low electrical resistivity and high dielectric losses >0.1, hindering in this way the incorporation into devices [11]. Apart from the aforementioned disadvantages, ceramic composites still have other problems such as being expensive, dense and brittle which can lead to failure during operation [41-42]. In this way, ceramic based ME materials are not attractive from the technological point of view.

A more recent approach to obtain highly flexible and non-brittle ME composites and to solve all the aforementioned problems is to use polymer based nanocomposites [37].

In comparison with the ceramic ME composites, polymeric based ME materials can be easily fabricated by a conventional low-temperature processing into a variety of forms such as thin sheets or molded shapes and can exhibit improved mechanical properties [37].

1.4.4 Polymer based ME materials

As previously mentioned, three main types of ME polymer based composites can be found in the literature: Nanocomposites, *polymer as a binder* and laminated composites. In the following, the main characteristics, materials, achievements and limitations of each type will be discussed.

1.4.4.1   Particulate nanocomposites

When compared to their ceramic ME counterparts, a much lower variety of 0-3 type ME polymer based nanocomposites have been reported in the last two decades. Polymers such as piezoelectric PVDF and Polyurethane (PU) have been used in such ME nanocomposites due to their good piezoelectric/electrostrictive properties [43].

In the electrostrictive PU based ME composites several interesting results have been obtained, including the extraction of the true ME current from the total output current response and the coexistence of both linear and quadratic ME responses in the filled PU film. The obtained linear ME effect is of the same order of magnitude than that of Cr_2O_3 single crystal (up to 18 mV/cm.Oe) and a possible *linear* magnetoelastoelectric coupling between fillers and polymer matrix not triggered by magnetostriction has been also proposed [44].

The linear voltage ME coefficients (α) obtained in PU/ Fe_3O_4 and PU/Nickel composites were 11.4 and 6.0 mV/cm.Oe, respectively at 7 Hz, H_{DC}=0 and H_{AC}=1 Oe. Even when it is predicted that due to the magnetostriction it should be found an optimal value H_{DC} and therefore a peak in the α value *vs* H_{DC} [45], experiments show that α remains more or less constant with increasing H_{DC}. This experimental observation strongly suggests that the magnetostrictive properties of the material have no influence in the PU/ Fe_3O_4 and PU/Nickel ME composites.

This interesting fact has been confirmed as the ME response in PU composites is independent of the magnetostrictive properties of the fillers such as Terfenol-D, Fe_3O_4 or Nickel [46]. In this way, the ME coupling does not have its origin in the magnetostriction of the particles but rather in the linear elastic interaction between those particle aggregates and the highly polar microdomains of the semi-crystalline PU [45, 47-48]. Consequently, the coupling in PU composites is mainly due to the particular nature of the elastomer PU matrix composed of both rubbery and polar domains. A support for the aforementioned mechanism is the fact that the simple of morphous carbon nanopowder into PU based ME composites enhances the quasistatic strain amplitude [49] since the bonding between the PU and the carbon nanopowder prevents slippage and effectively improves the strain in the nanocomposite [50]. In any case, the origin of the ME coupling in such nanocomposites is not clearly established yet [23].

Regarding the use PVDF as the piezoelectric constituent of ME nanocomposites and after the theoretical calculations of giant ME on ferromagnetic rare-earth-iron-alloys-filled ferroelectric polymers in 2001 by Nan *et al* [51-52], just one main experimental

Pedro Martins

report can be found in the literature. Zhang *et al* studied the effect of CoFe$_2$O$_4$ nanoparticles on the morphology, ferroelectric, magnetic and ME behaviours of P(VDF-TrFE)/CoFe$_2$O$_4$ nanocomposites. The ferroelectric and ME responses are strongly influenced by the concentration of ferrite nanoparticles [53]. A significant experimental α_{33} value around 40 mV/cm.Oe was obtained in this kind of nanocomposites and theoretical confirmed by a relatively simple model based on Wong and Shin´s (Figure 1.3) [54-55]. In this model, the ME response α_{33} can be expressed as:

$$\alpha_{33} = (1-\phi)\frac{L_E}{\varepsilon}(d_{31p}\frac{dY_{xp}}{dH_m} + d_{32p}\frac{dT_{yp}}{dH_m} + d_{33p}\frac{dT_{zp}}{dH_M})(\frac{dH_m}{dH}) \qquad \textbf{(1.2)}$$

where L_E and $\dfrac{dH_p}{dH}$ are given by:

$$L_E = \frac{[\varepsilon_m + 2\varepsilon_p]]}{[(1-\phi)\varepsilon_m + (2+\phi)\varepsilon_p]} \qquad \textbf{(1.3)}$$

$$\frac{dH_p}{dH} = \frac{3\xi_p}{(1-\phi)\left(\xi_m + \dfrac{dM_m}{dH_m}\right) + (2+\phi)\xi_p} \qquad \textbf{(1.4)}$$

Here, *p* and m indicate the polymer and magnetic phase respectively; ; d_{3n} the piezoelectric coefficients; ε the dielectric constant, ϕ the volume fraction of the magnetostrictive phase; *T* and *H* are the stress and applied magnetic field, respectively; ξ the magnetic permeability and *M* the magnetization. $\dfrac{dM_m}{dH_m}$ is obtained from the magnetization curve of the nanocomposites.
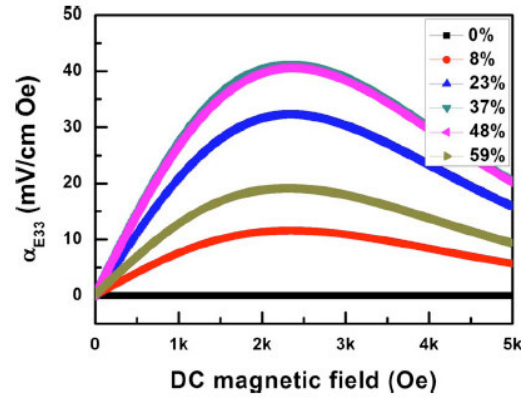
Figure 1.3 − Theoretical calculation of the ME coefficient as a function of H_{DC} field for the P(VDF-TrFE)/CoFe$_2$O$_4$ nanocomposites with different volume fractions.

Possible ME polymer nanocomposite structures (Figure 1.4) were also synthesized using conducting polyaniline and nanosized BiFeO$_3$ (BFO) particles through in situ sol–gel polymerization by Hemalatha *et al* [56].
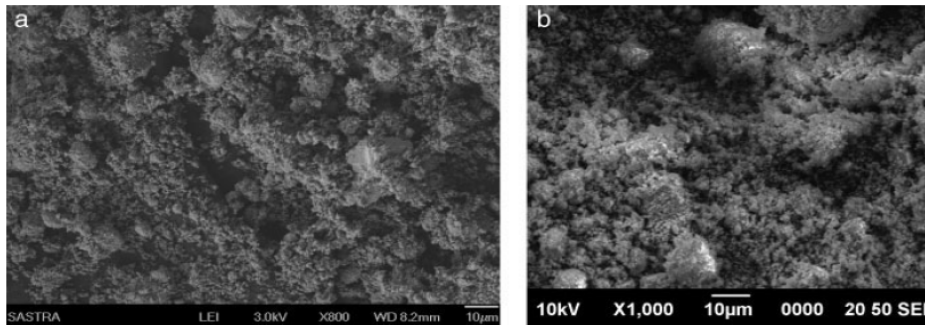
Figure 1.4 − (a) Scanning Electron Microscopy (SEM) micrograph of PANI/BFO composite at 800 magnification. (b) SEM micrograph of PANI/BFO composite at 1000 magnification.

The morphology, crystalline structure, magnetic, and optical properties of Polyaniline (PANI)/BFO composites with various concentrations of nanofiller were discussed but the ME response of such nanocomposites has not yet been reported.

1.4.4.2   *Polymer as a binder composites*

Unlike in the previous section, in the polymer *as a binder* composites the polymer is not used as the piezoelectric phase of the ME material but as a binder for the piezoelectric

and magnetostrictive particles that keep them together and provides the stress coupling between the piezoelectric matrix and the magnetostrictive fillers.

Three-phase particulate composites of Terfenol-D alloy, PZT and PVDF [57] (Figure 1.5) were the first to be studied.
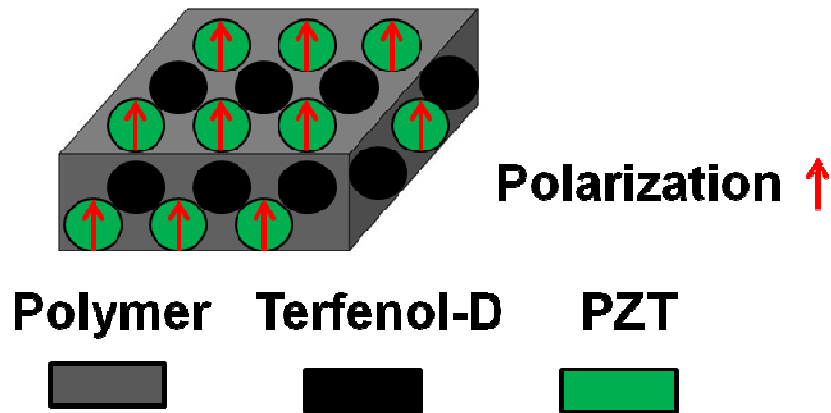
Figure 1.5 − Schematic representation of the particulate Terfenol-D/PZT/polymer composites [58].

In order obtain the ME response, a small ϕ, of Terfenol-D nanoparticles were dispersed in a PZT/PVDF mixture by a simple blending technique and the obtained dielectric, piezoelectric and ME properties demonstrate that a percolation transition occurs at $\phi \approx 0.12$. When ϕ is lower than 0.07 the MF composites exhibit good piezoelectric and ME responses but when $0.07 \leq \phi \leq 0.12$ the piezoelectric and ME response sharply drops and disappears at the percolation threshold, above which the composite becomes a conductor and only respond magnetostrictively. The maximum obtained value for α_{33} at 0,2 T was about 42 mV/cm.Oe at $\phi=0.06$ which is less than half with those obtained for the PZT/ferrite ceramic composite (115 mV/cm.Oe) [59]. Since this ME response is mainly determined by the $\phi_{\text{Terfenol-D}}$, the pre-treatment of the Terfenol-D nanoparticles, by the use of surfactants was made. The use of surfactants is usually done to improve dispersibility and dispersion stability of nanoparticles [60-61] in different kind of matrices. In the case of PZT/ferrite ceramic composite, surfactants increase the percolation threshold.

This experimental change has two consequences:

i) the maximum magnetostrictive filler concentration allowed in the ME nanocomposites is increased ;

ii) a soft and inactive interfacial layer is induced in the Terfenol-D nanoparticles.

Although the first consequence is extremely positive since it allows higher magnetostrictive content in the ME composite, the second produces a negative effect on both the piezo and ME response of the nanocomposites [62]. Further improvement in the ME response of this MF composites lies in increasing the $\phi_{\text{Terfenol-D}}$ and simultaneously ensuring a good interface contact between phases by the optimization of the nanocomposites processing. In view of this fact, theoretical calculations were performed on the mechanical boundary conditions influence in the ME properties, based on the Green´s function technique [52, 63]. Three different mechanical boundary conditions were considered:

i) completely mechanical clamped boundary condition;

ii) completely mechanical free boundary condition;

iii) completely mechanical clamped in the zz direction and free in the transverse direction.

For the composite with ϕ=0.06, the maximum α_{33} values were 117, 362 and 62 mV/cm.Oe for situations i), ii) and iii), respectively. The same calculations also revealed that the PZT particles polarization and the inactive PZT/PVDF interface have a significant effect on the ME properties of the nanocomposites. Random orientations of the polarization in the PZT particles result in the disappearance of piezoelectricity in the composites, thereby the disappearance of the extrinsic ME effect. Although the thin interface layer with the same elastic constants as the polymer matrix has only a slight effect on the effective magnetostriction of the composites, the piezoelectric effect is strongly influenced by the interface layer surrounding the PZT particles [58].

The influence of different polymers in the ME response of the same kind of MF nanocomposites was recently investigated [64]. Polymer electrolyte Polyethylene oxide (PEO) and Lithium perchlorate-doped PEO (PEO Li$^+$-PEO) and Poly(methyl methacrylate) (PMMA) were mixed separately with Terfenol-D and PZT particles aiming to evaluate the significance of the polymer matrix conductivity in the ME response of the samples. The obtained α_{31} were 1.3, 3.2, and 4.8 mV/cm.Oe respectively for the Li$^+$-PEO, PEO and PMMA polymer matrix. Those results confirm that samples with higher conductivity exhibit lower ME responses [57].

Although the flexibility, structure, simple fabrication and easy shaping of the *polymer as a binder* ME materials provide attractive advantages in possible ME applications

those added features ate limited since all of them are worse when compared with the particulate nanocomposites.

1.4.4.3 Laminated composites

In the three-phase PZT/PVDF/Terfenol-D particulate composites of the previous section, the $\varphi_{\text{Terfenol-D}}$ allowed in the nanocomposites is quite low, which strongly limits the ME response of the MF nanocomposites. To eliminate this limitation, a different class of ME material has been developed: laminated composites. MF laminated composites consisting on one PVDF/Terfenol-D particulate composite layer sandwiched between two PZT/PVDF particulate layers prepared by hot-molding technique has been reported [65]. The polymer phase PVDF is used just as a binder, with no influence on the ME properties of the laminated composite. Experiments show that with $\varphi_{\text{PVDF}} \leq 0.3$, the low concentration of PVDF leads to low quality of the composites as the connection between the three phases is poor, leading to low ME performance. The ME properties were improved in the intermediate φ_{PVDF} concentration range ($0.3 \leq \varphi_{\text{PVDF}} \leq 0.5$) and as φ_{PVDF} further increases ($\varphi_{\text{PVDF}} > 0.5$), high concentration of inert PVDF causes weak dielectric, magnetostrictive, piezo and ME activity of the three-phase laminated PVDF/Terfenol-D/PZT composites. A maximum value for α_{33} of 80mV/cm.Oe was obtained at 1 kHz, 0.4T and $f_{PVDF} = 0.5$. The maximum ME sensitivity of such laminated composites can reach up to 3V/cm.Oe at the resonance frequency of around 100 kHz [66]. The difference in the longitudinal (α_{33}) and transversal (α_{31}) ME sensitivity, 3V/cm.Oe and 3.8V/cm.Oe respectively is fully attributed to the anisotropy of the laminated ME samples. At high bias, magnetostriction gets saturated faster under in-plane bias than in out-of-plane bias producing a nearly constant electric field in the PZT, thereby decreasing α_{31} with increasing bias.

Novel laminated conformations of the ME samples, consisting on a PZT/PVDF particulate layer sandwiched between two PVDF/Terfenol-D particulate composite layers [67] were investigated. With this conformation, the maximum ME sensitivity α_{33} was improved to 300mV/cm.Oe at a frequency below 50 kHz and about 6V/cm.Oe at the resonance frequency of around 80 kHz. The ME response of such composites is also strongly dependent on the applied bias and on the thickness ratio (t_p/L) between the PVDF/Terfenol-D layers and the PZT/PVDF layer. Keeping the thickness of the composite (L) equal to ≈ 2.5 mm, the t_p/L ratio was varied from 1/7 to 5/7 by increasing

the thickness of the PZT/PVDF particulate layer (t_p) The α values of the composites first increase with t_p/L until a 2/7 ratio, which could be attributed to the increase in the effective piezoelectric effect. However, with further increasing t_p/L, the ME sensitivity declines after a maximum value, which is due to the reduction in magnetostrictively induced strain of the laminated composites with increasing tp/L [68].

Finally, three-phase Terfenol-D/PZT/binder composites were fabricated by substituting PVDF by Spurr epoxy (Polysciences Inc., USA) [69]. The ME properties of such materials were investigated experimentally and theoretically confirmed by the use of the equivalent circuit approach [70]. Samples with a $\varphi_{Terfenol-D}$=0.5 in the Terfenol-D/Spurr epoxy laminates with two different PZT concentrations (φ_{PZT}=0.6 and φ_{PZT}=0.75)   in the PZT/Spurr epoxy laminate were measured. At a frequency of 10 kHz and 504 Oe field, the obtained value for α_{31} was ~ 0.3 and 0.4 V/cm.Oe, respectively for the φ_{PZT}=0.6 and φ_{PZT}=0.75 samples. When the frequency is changed to the resonance ($\approx$55 kHz), the α increases up to 10 V/cm.Oe in the case of the φ_{PZT}=0.6 and 11 V/cm.Oe in the case of the φ_{PZT}=0.75 composite. The increase of α with increasing φ_{PZT} is expected, due to the increase of the piezoelectric phase. It is nevertheless to notice that the improvement of the ME response is accompanied by a decrease of the flexibility and strength of the composite.

A similar ME composite concept uses PU to increase the ME coupling between the piezoelectric PVDF and the magnetostrictive material (Fe_3O_4 and Terfenol-D) [71]. It was reported a ME in bi and trilayered composites consisting in on layer PVDF and one or two layers of PU filled with Fe_3O_4 or Terfenol-D particles, modelled by a driven damped oscillation system [72-73], with a highest α_{33} obtained for the trilayered sample of PE+2wt.% Fe_3O_4/PVDF/ PE+2wt.% Fe_3O_4 with a value of 753mV/cm.Oe at -2000 Oe.

Further, ME laminates of Vinyl ester resin (VER)-bonded Terfenol-D magnetostrictive layer ($\varphi_{Terfenol-D}$ from 0.16 to 0.48) and a PZT piezoelectric layer glued together with a conductive epoxy [74], show α_{31} values increasing gradually with increasing $\varphi_{Terfenol-D}$ in the magnetostrictive layer reaching a saturation for $\varphi_{Terfenol-D}$>0.4 due to the increasing elastic modulus and piezomagnetic coefficient of the magnetostrictive phase. A maximum value of 2.7 V/cm.Oe was obtained at H_{DC}=666 Oe. with $\varphi_{Terfenol-D}$ in the magnetostrictive layer equal to 0.48.

 A bilayer disk prepared by bonding a PZT disk with Terfenol-D/low viscosity epoxy disk [75] show at a bias of 0.3T three resonance peaks with α_{33} values of 2.79 V/cm.Oe

at 35 kHz, 0.924 V/cm.Oe at 100 kHz and 1.31 V/cm.Oe at 122 kHz respectively [76]. The resonance peak at 122 kHz is attributed to the transversal resonance [77-78], which is present in many sandwich laminated composites [65, 79]. The observation of three ME resonance peaks in laminated composites was for the first time reported in this work.

Thin, flexible ME laminates (Figure 1.6a) composites were fabricated following similar approaches but with different magnetostrictive layers, as for example, PVDF/Metglas unimorph (Figure 1.6b) and threelayer (Figure 1.6c) sandwich configurations [80].
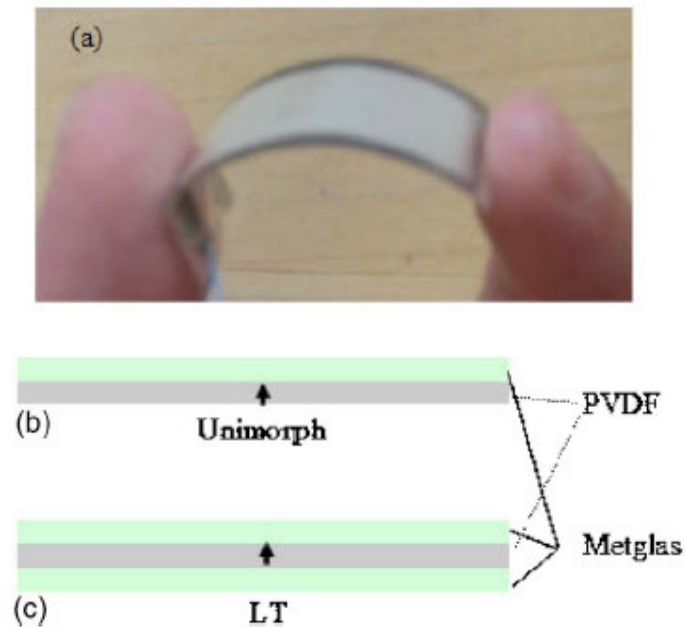
Figure 1.6 − (a) Picture of the flexible PVDF/Metglas unimorph laminate; (b) Unimorph configuration, and (c) the threelayer laminate.

Those laminates required an H_{DC} of only 8 Oe in order to achieve a maximum ME response, 1/50th than the ones required for the previous ME laminates. These small magnetic field ME laminates have giant ME voltage coefficients and excellent sensitivity to small variations in both H_{AC} and H_{DC}. The Metglas layer and PVDF layers are glued together using an epoxy and both laminate types were found to have a strong ME enhancement: three-layer composites: α_{31}=238 V/cm.Oe; unimorph composites: α_{31}=310 V/cm.Oe, both near the longitudinal resonance frequency at 50 kHz. At lower frequencies a maximum value of 7.2 V/cm.Oe was obtained for both geometries. Although the magnetostriction of Metglas SA1 was only 42 ppm which is far smaller

than the giant magnetostriction of Terfenol-D, the maximum value of its effective piezomagnetic coefficient $d_{33m}=4\times10^{-6}$ Oe^{-1} is three to four times larger than the one for Terfenol-D $d_{33m}=1.2\times10^{-6}$ Oe^{-1} due to the small saturation field [81]. This extremely low H$_{DC}$ requirement is an important advantage of PVDF/Metglas laminates over other previously reported types, offering huge potential in practical applications.

After the first works on PVDF/Metglas laminate nanocomposites [80], several works were devoted to these promising ME material. For example, taking advantage of the magnetic flux concentration effect of Metglas as a function of its sheet aspect ratio values of α_{31} = 21.46 V/cm.Oe were obtained in a PVDF/Metglas 2605SA1 laminate composite at a non resonance frequency of 20 Hz and at H$_{DC}$=3Oe [82].

By taking advantage of the anisotropy of PVDF/Metglas-SA1-MP4010XGDC laminates it was demonstrated the ability of such composites to be used as an ultra-sensitivity detection device of weak H$_{DC}$ (1×10^{-9} Oe) [83]. This high sensitivity is due to the:

i) large piezoelectric voltage coefficient of PVDF that indicates a high output voltage in response to a small variation of strain;

ii) high piezomagnetic coefficient of the Metglas-SA1-MP4010XGDC alloy;

iii) relatively small demagnetization factor of the Metglas-SA1-MP4010XGDC alloy.

Since α is proportional to the piezomagnetic and piezoelectric voltage coefficients and inversely proportional to the demagnetization factor, a high sensitivity is characteristic of the PVDF/Metglas composites. The maximum α_{31} value obtained in the PVDF/Metglas-SA1-MP4010XGDC laminate was 400 mV/cm.Oe at 1 kHz frequency and H$_{DC}$=3 Oe.

Further, as it was found that the depolarization effect is prone to occur in polymers such as PVDF, the effect of two types of poling processes were investigated in the ME properties of PVDF hexafluoropropylene (PVDF-HPFP)/Metglas laminates [84]. After applying the so-called "conventional poling", usually used in the poling of piezoelectric polymers [85] or "cycling poling" [86]. In the first, a DC electric field ranging from 100 to 300 MV/m was applied to the sample during 300 s at room temperature. Regarding the second poling method, starting at low electric fields, the sample is cycled through many "loops" until a consistent behaviour is indicated. Higher fields are then utilized until the desired stable polarization is achieved. Comparing both methods, it was verified a shift of the ME peak (α vs H$_{DC}$) of one method with respect to the other, attributed to the variation of the boundary conditions of the magnetostriction of the

Metglas. Since the maximum peak is related to the piezomagnetic coefficient of Metglas, the variation of magnetostrictive vibration will result in the variation of the magnetostrictive coefficient as well in a shift of the piezomagnetic coefficient peak. In this case, variation in the maximum of the α values with different poling processes is due to the fact that conventional poling uses DC electric field, while cyclic poling employs an AC electric field, which produces different orientation stresses in the dielectric polymer. The highest α_{31} obtained was 12V/cm.Oe at 5 Oe and is lower than the values obtained for the previously discussed PVDF/Metglas laminates, however it has the advantage of allowing the change of the H_{DC} at witch is obtained through modifications in the poling process (electric field strength and type of poling).

A novel approach to high performance ME polymer composites was presented with the chain-end cross-linked ferroelectric P(VDF-TrFE)/Metglas 2605 SA1 composites [87]. The performance improvement was due to the introduction of chain-end cross-linking and polysilsesquioxane structures into the P(VDF-TrFE) matrix which leads to the formation of larger crystalline samples and consequently better piezoelectric response in comparison to those of pristine P(VDF-TrFE) copolymers. With better piezoelectric properties a higher α was expected. For the cross-linked P(VDF-TrFE)/Metglas laminate *an* α_{31} value of 17.7 V/cm.Oe was achieved under a H_{DC}=3.79 Oe at 20 Hz, whereas the value obtained for the pristine P(VDF-TrFE)/Metglas under the same conditions is α_{31}= 6.9 V/cm.Oe. The α_{31} values for cross-linked P(VDF-TrFE)/Metglas laminates can be further improved to 383 V/cm.Oe at the resonance frequency of 65 kHz.

The later laminate composite not only shows the largest value of α in polymer based ME materials but also points to a way to improve the piezoelectric properties of the piezoelectric layer and hence the ME response.

Leaving behind the ME PVDF based/Metglas composites, this laminated polymeric ME materials section is concluded with the large ME response from mechanically mediated magnetic field-induced strain effect in PVDF/$Ni_{50}Mn_{29}Ga_{21}$ single crystal [88]. $Ni_{50}Mn_{29}Ga_{21}$ single crystal shows giant H_{DC} induced strains of 6-10% in the tetragonal and orthorhombic martensitic phases, which has attracted interest for ME applications [89]. Showing obvious differences from the traditional magnetostrictive phases (Terfenol-D, ferrites or Metglas), the mechanism of the giant magnetic field-induced strains was due to the reorientation of the martensitic twin variants under an applied magnetic field as a result of magnetocrystalline anisotropy [90-91].

PVDF/Ni$_{50}$Mn$_{29}$Ga$_{21}$ single crystal bilayered composites were produced by adhering one layer of the ferromagnetic shape memory alloy to one layer of the piezoelectric polymer with a conductive silver epoxy. The largest value α_{33} of 1.24 V/cm.Oe obtained at 1 kHz and at an optimal magnetic field of 0.51T was experimentally and theoretically confirmed [15, 92-93].

This investigation not only reported a different constitution in ME laminates but also created a distinct physical mechanism for realizing such effect.

An alternative concept in ME polymer laminated composites is based on thermal mediation [94]. This kind of MF material uses the large magnetocaloric effect (MCE), i.e., a temperature change induced in the ferromagnetic Gd crystal by a magnetic field and a large pyroelectric response in the ferroelectric P(VDF-TrFE) (68/32 mol%). Composites were prepared by bonding a Gd crystal plate to the P(VDF-TrFE) with a silver conductive adhesive epoxy to ensure a good thermal contact between the layers. An α value of 0.5V/cm.Oe was obtained at 293 K in an H$_{AC}$= 120 Oe with 2.4 Hz. The α was further enhanced to 0.9 V/cm.Oe by exploiting the magnetic flux concentration effect [95].

As a conclusion from this section, the results obtained for the main polymer based ME material are shown in Table 1.2 ordered by composite type.

Table 1.2 – Comparison of the different polymeric ME α.

Type	Constitution	$H_{DC-Max.\alpha}$ (Oe)	Ref.	α (mv/cm.Oe)	$\alpha_{resonance}$ (mv/cm.Oe)
Nanocomposite	PE/Fe$_3$O$_4$	0	[44]	11.4	-
	PE/Nickel	0	[44]	6	-
	P(VDF-TrFE)/ CoFe$_2$O$_4$	2000	[53]	-	40
Polymer *as a binder* composites	PVDF/Terfenol-D/ PZT	2000	[57]	42	-
	PEO/Terfenol-D/PZT	1400	[64]	1.3	-
	Li$^+$-PEO/TerfenolD/ PZT			3.2	-
	PMMA/TerfenolD/ PZT			4.8	-
Laminate	PVDF/TerfenolD/ PZT	4000	[66]	80	3000
	PVDF/TerfenolD/ PZT	4000	[67]	300	6000
	Spurr epoxy/Terfenol-D/PZT	504	[70]	400	1100
	PE /PVDF/ Fe$_3$O$_4$	2000	[71]	753	-
	VER/Terfenol-D/PZT	666	[74]	2700	-
	PZT/TerfenolD/ epoxy	3000	[76]	1310	2790
	Gd crystal/P(VDF-TrFE)/silver conductive epoxy	200	[94]	500	-
	PVDF/Metglas unimorph	8	[80]	7200	238000
	PVDF/Metglas three-layer				310000
	PVDF/Metglas	8	[82]	21460	-

PVDF/Metglas	3	[83]	400	-
PVDF-HPFP/Metglas	5	[84]	12000	-
Cross-linked P(VDF-TrFE)/Metglas 2605	4	[87]	17700	383000
PVDF/Ni$_{50}$Mn$_{29}$Ga$_{21}$	5100	[88]	1240	-

1.4.5   Applications

Based on the previous sections it is concluded that ME materials are ready for technological applications. Promising applications include magnetic field sensors, transducers, filters, oscillators, phase shifters, memory devices and biomedical materials, among others [22, 37]. In some of these applications polymeric based ME materials, as the one to be developed in this work, due to the polymers unique characteristics such as flexibility, lightweight, versatility, low cost and in some cases biocompatibility can be taken to advantage. Some of these applications include:

1.4.5.1   Four state-memory

To meet the intense demand of multimedia storage many efforts are being made to develop storage technologies with higher storage speed and density [96-97]. In the traditional two state (0 and 1) memories, the memory element is a magnetic tunnel junction that consists on an insulating tunnel barrier sandwiched by two magnetic electrodes [98]. The resistance of such junction strongly depends on the relative orientation of the magnetic moments, which is used to determine the memory state (0 or 1) from the two magnetic electrodes [99]. The coded magnetic bits can then be read out non destructively by detecting such resistance changes, however, in the writing process, the magnetic bits are usually encoded by the use of high magnetic fields which is a process relatively slow and energetically expensive [21]. These problems can be solved with the manipulation of the magnetization direction by the use of an electric field [100], taking advantage of the ME effect. For this kind of multi-state memory the multiferroicity is the essential factor for the information storage while the ME or the magnetodielectric effect [101] is the mechanism for the reading and writing procedure [102].

Pedro Martins

Contrary to what happened a few decades ago, when polymers were just used as a binder in memories [103-104], memories based on polymeric materials are now a interesting topic due to their simplicity, good scability, low-cost, 3D stacking capability and large capacity for data-storage [105-106]. This electroactive polymers are usually deposited by ink-jet printing, spin-coating or vacuum evaporation on a variety of substrates for the fabrication of memories [107]. In this way, polymers, may also acquire in the near future a more central status in the memories market due to the polymeric four-state ME memories.

1.4.5.2 Energy harvesting

The ever decreasing power requirement of electronic sensors and devices [108] has attracted attention to the energy harvesting technologies [109]. In particular there has been significant interest in the area of the vibration energy based on piezoelectric and magnetic harvesters [110-113].

As described in the previous section of this review, there has been significant advances in improving the magnitude of ME coefficient of laminate composites, which will improve the ME energy harvesting efficiency. Knowing that the next generation of energy-harvesting applications, such as wearable energy-harvesting systems, may require the piezoelectric materials to be flexible, lightweight, and even biocompatible [114], ME materials based on piezoelectric polymers may be an interesting approach to those requirements due to their flexibility, versatility and low cost [115].

1.4.5.3 Magnetic field sensor

Magnetic sensors have been in use for well over 2000 years. Early applications were for direction finding in navigation [116]. Today, magnetic sensors are also used in navigation but many more uses have evolved. The technology for sensing magnetic fields has also evolved driven by the need for improved sensitivity, smaller size, and compatibility with electronic systems [117]. Traditional magnetic sensors like Hall or magnetoresistive sensors need power supply, which raises some limitations. In this context, self-powered magnetic field sensors that directly transfer magnetic energy into electric signals are of large interest and can be realized thanks to the ME effect [118].

Most of the MEs tested for magnetic field sensor applications are based on PZT [118-119] but the low flexibility, cost and fragility of PZT [120-121] do not meet

the challenges of future sensor applications [122-123], therefore MF and ME polymer based composites are possible successful alternatives for the more traditional ceramic based ME magnetic sensors [39].

1.4.5.4   Other applications

ME magnetic sensors also have enormous potential as by-products related to magnetic sensors: electric current sensors , speed sensors, angular sensors, electronic steering, throttle control, battery management, vehicle transmission, digital compasses and GPS [112] are just some examples and many of them are already being studied [117, 124-125].

As a conclusion, polymer based ME materials are a promising research field with large interest for applications that certainly will appear soon. Analysing the results obtained from the different approaches for preparing such composites (Table 1.2) it is verified that the highest ME voltage coefficients are obtained to the laminate samples, but another evidence is well demonstrated by the Table 1.2: the lack of studies regarding the polymer based ME nanocomposites, which is the main objective of the present investigation.

1.5 References

1. Spaldin, N.A., *Multiferroics Magnetic Materials*. 2010: Cambridge University Press.
2. Martin, L.W. and B. University of California, *Engineering Multiferroic Materials and New Functionalities in Materials*. 2008: University of California, Berkeley.
3. Rabe, K.M., C.H. Ahn, and J.M. Triscone, *Physics of Ferroelectrics: A Modern Perspective*. 2007: Springer.
4. Lines, M.E. and A.M. Glass, *Principles and Applications of Ferroelectrics and Related Materials*. 1977: Clarendon Press.
5. McCurrie, R.A., *Ferromagnetic materials: structure and properties*. 1994: Academic.
6. Chikazumi, S. and C.D. Graham, *Physics of Ferromagnetism*. 1997: Clarendon Press.
7. Voss, D.J., *Ferroelasticity in Synthetic Leucites*. 1984: Pennsylvania State University.
8. Mehta, K., *Ferroelasticity in Lead Zirconate Titanate Ceramics*. 1997: Department of Materials Science and Engineering, University of Utah.
9. Taylor, G.W., *Piezoelectricity*. 1985: Gordon and Breach Science Publishers.
10. Townsend, R.L., *Piezomagnetism: Macroscopic and Microscopic Studies*. 1969: Department of Electrical Engineering, Stanford University.
11. Berktan, T., *Piezomagnetism and Fatigue*. 1998: Illinois Institute of Technology.
12. Kay, H.F., *Electrostriction*. 1955: Physical Society.
13. Ding, E., *Measurement techniques for studying electrostriction of polymer films*. 1997: University of Wisconsin--Madison.
14. Du Tremolet de Lacheisserie, É., *Magnetostriction: theory and applications of magnetoelasticity*. 1993: CRC Press.
15. Engdahl, G., *Handbook of Giant Magnetostrictive Materials*. 2000: Academic Press.
16. Momeni, S., *Determination of Piezomagnetic Properties for a Magnetostriction-based EMAT*. 2008: University of Toronto (Canada).
17. Fiebig, M., V.V. Eremenko, and I.E. Chupis, *Magnetoelectric Interaction Phenomena In Crystals*. 2004: Kluwer Academic Publishers.
18. O'Dell, T.H., *The electrodynamics of magneto-electric media*. 1970: North-Holland Pub. Co.
19. Landau, L.D., *Electrodynamics of continuous media / by L.D. Landau and E.M. Lifshitz ; translated from the Russian by J.B. Skyes and J.S. Bell*. Course of theoretical physics ; v. 8., ed. E.M. Lifshitz. 1960, Oxford : Reading, Mass. :: Pergamon Press ; Addison-Wesley.
20. Srinivasan, G., *Magnetoelectric Composites*, in *Annual Review of Materials Research, Vol 40*, D.R.R.M.Z.F. Clarke, Editor. 2010. p. 153-178.
21. Eerenstein, W., N.D. Mathur, and J.F. Scott, *Multiferroic and magnetoelectric materials*. Nature, 2006. **442**(7104): p. 759-765.
22. Nan, C.-W., et al., *Multiferroic magnetoelectric composites: Historical perspective, status, and future directions*. Journal of Applied Physics, 2008. **103**(3).
23. Ma, J., et al., *Recent Progress in Multiferroic Magnetoelectric Composites: from Bulk to Thin Films*. Advanced Materials, 2011. **23**(9): p. 1062-1087.

24. Fiebig, M., *Revival of the magnetoelectric effect.* Journal of Physics D-Applied Physics, 2005. **38**(8): p. R123-R152.

25. Katsura, H., N. Nagaosa, and A.V. Balatsky, *Spin current and magnetoelectric effect in noncollinear magnets.* Physical Review Letters, 2005. **95**(5).

26. Chu, Y.-H., et al., *Electric-field control of local ferromagnetism using a magnetoelectric multiferroic.* Nature Materials, 2008. **7**(6): p. 478-482.

27. Röntgen, W.C., *Dielectricums hervorgerufene electrodynamische Kraft.* Ann. Phys., 1888. **35**: p. 264-270.

28. Wilson, H.A., *On the electric effect of rotating a dielectric in a magnetic field.* Philosophical Transactions of the Royal Society of London Series a-Containing Papers of a Mathematical or Physical Character, 1905. **204**: p. 121-137.

29. Curie, P., *ur la symétrie dans les phénomènes physiques. Symétrie d'un champ électrique d'un champ magnétique.* Journal de Physique, 1894. **3**: p. 393–416.

30. Debye, P., *Remark to some new trials on a magneto-electrical direct effect.* Zeitschrift Fur Physik, 1926. **36**(4): p. 300-301.

31. Dzyaloshinskii, I.E., *On the magnetoelectric effect in antiferromagnets.* Soviet Physics Jetp-Ussr, 1960. **10**(3): p. 628-629.

32. Astrov, D.N., *The magnetoelectric effect in antiferromagnets.* Soviet Physics Jetp-Ussr, 1960. **11**(3): p. 708-709.

33. Ascher, E., et al., *Some Properties of Ferromagnetoelectric Nickel-Iodine Boracite, Ni3B7O13I.* Journal of Applied Physics, 1966. **37**(3): p. 1404-&.

34. Santoro, R.P.N., Robert E., *Survey of Magnetoelectric Materials.* 1966: Massachusetts Institute of Technology.

35. Buschow, K.H.J., *Handbook of Magnetic Materials.* Vol. 20. 2011, Amsterdam: Elsevier Science.

36. Schmid, H., *Magnetic ferroelectric materials.* Bulletin of Materials Science, 1994. **17**(7): p. 1411-1414.

37. Scott, J.F., *Applications of magnetoelectrics.* Journal of Materials Chemistry, 2012. **22**(11): p. 4567-4574.

38. Ryu, J., et al., *Magnetoelectric effect in composites of magnetostrictive and piezoelectric materials.* Journal of Electroceramics, 2002. **8**(2): p. 107-119.

39. Roy, S., B. Biswas, and S.B. Majumder, *Investigations on Flexible Multiferroic Composites*, in *Mesoscopic, Nanoscopic, and Macroscopic Materials*, S.M.B.S.N.R.B.K. Bose, Editor. 2008. p. 276-289.

40. van Suchtelen, J., *Product properties: a new application of composite materials.* Philips Research Reports, 1972. **27**(1): p. 28-37.

41. Loh, K.J. and D. Chang, *Zinc oxide nanoparticle-polymeric thin films for dynamic strain sensing.* Journal of Materials Science, 2011. **46**(1): p. 228-237.

42. Jiansirisomboon, S., et al., *Mechanical properties and crack growth behavior in poled ferroelectric PMN-PZT ceramics.* Current Applied Physics, 2006. **6**(3): p. 299-302.

43. Kepler, R.G. and R.A. Anderson, *Piezoelectricity and pyroelectricity in polyvinylidene fluoride.* Journal of Applied Physics, 1978. **49**(8): p. 4490-4494.

44. Guyomar, D., et al., *Two-phase magnetoelectric nanopowder/polyurethane composites.* Journal of Applied Physics, 2008. **104**(7).

45. Jiles, D.C., et al., *Barkhausen effect and discontinuous magnetostriction in Terfenol-D.* Journal of Applied Physics, 1988. **64**(10): p. 5417-5418.

46. Guyomar, D., et al., *Magnetoelectricity in polyurethane films loaded with different magnetic particles.* Materials Letters, 2009. **63**(6-7): p. 611-613.

Pedro Martins

47.   Li, Y.J., et al., *Multiphase Structure of a Segmented Polyurethane: Effects of Temperature and Annealing.* Macromolecules, 1992. **25**(26): p. 7365-7372.

48.   Guiffard, B., et al., *Enhanced electric field-induced strain in non-percolative carbon nanopowder/polyurethane composites.* Journal of Physics D-Applied Physics, 2006. **39**(14): p. 3053-3057.

49.   Yuse, K., et al., *Polymer nanocomposites for microactuation and magneto-electric transduction.* Frontiers of Mechanical Engineering in China, 2009. **4**(3): p. 350-354.

50.   Liu, W.O.a.T., *A Review: Carbon Nanotube-Based Piezoresistive Strain Sensors.* Journal of Sensors, 2012. **2012**: p. 15.

51.   Nan, C.W., M. Li, and J.H. Huang, *Calculations of giant magnetoelectric effects in ferroic composites of rare-earth-iron alloys and ferroelectric polymers.* Physical Review B, 2001. **63**(14).

52.   Nan, C.W., et al., *Possible giant magnetoelectric effect of ferromagnetic rare-earth-iron-alloys-filled ferroelectric polymers.* Applied Physics Letters, 2001. **78**(17): p. 2527-2529.

53.   Zhang, J.X., et al., *The effect of magnetic nanoparticles on the morphology, ferroelectric, and magnetoelectric behaviors of CFO/P(VDF-TrFE) 0-3 nanocomposites.* Journal of Applied Physics, 2009. **105**(5).

54.   Wong, C.K. and F.G. Shin, *Effect of inclusion deformation on the magnetoelectric effect of particulate magnetostrictive/piezoelectric composites.* Journal of Applied Physics, 2007. **102**(6).

55.   Zhou, Y. and F.G. Shin, *Magnetoelectric effect of mildly conducting magnetostrictive/piezoelectric particulate composites.* Journal of Applied Physics, 2006. **100**(4).

56.   Prahakaran, T. and J. Hemalatha, *Synthesis and Characterization of Magnetoelectric Polymer Nanocomposites.* Journal of Polymer Science Part B-Polymer Physics, 2008. **46**(22): p. 2418-2422.

57.   Nan, C.W., et al., *A three-phase magnetoelectric composite of piezoelectric ceramics, rare-earth iron alloys, and polymer.* Applied Physics Letters, 2002. **81**(20): p. 3831-3833.

58.   Shi, Z., et al., *Influence of mechanical boundary conditions and microstructural features on magnetoelectric behavior in a three-phase multiferroic particulate composite.* Physical Review B, 2004. **70**(13).

59.   Ryu, J., et al., *Piezoelectric and magnetoelectric properties of Lead Zirconate Titanate/Ni-Ferrite particulate composites.* Journal of Electroceramics, 2001. **7**(1): p. 17-24.

60.   Hilding, J., et al., *Dispersion of carbon nanotubes in liquids.* Journal of Dispersion Science and Technology, 2003. **24**(1): p. 1-41.

61.   Pyun, J., *Nanocomposite Materials from Functional Polymers and Magnetic Colloids.* Polymer Reviews, 2007. **47**(2): p. 231-263.

62.   Nan, C.W., et al., *Coupled magnetic-electric properties and critical behavior in multiferroic particulate composites.* Journal of Applied Physics, 2003. **94**(9): p. 5930-5936.

63.   Kirchner, H.O.K. and V.I. Alshits, *Elastically anisotropic angularly inhomogeneous media .2. The Green's function for piezoelectric, piezomagnetic and magnetoelectric media.* Philosophical Magazine a-Physics of Condensed Matter Structure Defects and Mechanical Properties, 1996. **74**(4): p. 861-885.

64. Chau, K.H., Y.W. Wong, and F.G. Shin, *Magnetoelectric effect of polymer electrolyte composites with Terfenol-D and lead zirconate titanate inclusions.* Applied Physics Letters, 2009. **94**(20).

65. Cai, N., et al., *Dielectric, ferroelectric, magnetic, and magnetoelectric properties of multiferroic laminated composites.* Physical Review B, 2003. **68**(22).

66. Cai, N., et al., *Large high-frequency magnetoelectric response in laminated composites of piezoelectric ceramics, rare-earth iron alloys and polymer.* Applied Physics Letters, 2004. **84**(18): p. 3516-3518.

67. Nan, C.W., et al., *Large magnetoelectric response in multiferroic polymer-based composites.* Physical Review B, 2005. **71**(1).

68. Lin, Y.H., et al., *Giant magnetoelectric effect in multiferroic laminated composites.* Physical Review B, 2005. **72**(1).

69. Cai, N., et al., *Dynamic magnetoelectric effect in polymer-based laminate composite.* Journal of Alloys and Compounds, 2008. **448**(1-2): p. 89-95.

70. Wan, H., R.F. Shen, and X.Z. Wu, *A theoretical study on symmetrical magnetostrictive/piezoelectric laminated composite.* Acta Physica Sinica, 2005. **54**(3): p. 1426-1430.

71. Belouadah, R., et al., *Phase switching phenomenon in magnetoelectric laminate polymer composites: Experiments and modeling.* Physica B-Condensed Matter, 2011. **406**(14): p. 2821-2826.

72. Li, L., et al., *Frequency-dependent magnetoelectric coefficient in a magnetostrictive-piezoelectric composite as a complex quantity.* Journal of Physics D-Applied Physics, 2008. **41**(12).

73. Zhai, J., et al., *Large magnetoelectric susceptibility: The fundamental property of piezoelectric and magnetostrictive laminated composites.* Journal of Applied Physics, 2007. **101**(1).

74. Nersessian, N., S.W. Or, and G.P. Carman, *Magnetoelectric behavior of Terfenol-D composite and lead zirconate titanate ceramic laminates.* Ieee Transactions on Magnetics, 2004. **40**(4): p. 2646-2648.

75. Shi, Z., et al., *Magnetoelectric resonance behavior of simple bilayered Pb(Zr,Ti)O-3-(Tb,Dy)Fe-2/epoxy composites.* Journal of Applied Physics, 2007. **101**(4).

76. Shi, Z., J. Ma, and C.-W. Nan, *A new magnetoelectric resonance mode in bilayer structure composite of PZT layer and Terfenol-D/epoxy layer.* Journal of Electroceramics, 2008. **21**(1-4): p. 390-393.

77. Zeng, M., et al., *Resonance magnetoelectric effect in bulk composites of lead zirconate titanate and nickel ferrite.* Journal of Applied Physics, 2004. **95**(12): p. 8069-8073.

78. Dong, S.X., et al., *Enhanced magnetoelectric effects in laminate composites of Terfenol-D/Pb(Zr,Ti)O-3 under resonant drive.* Applied Physics Letters, 2003. **83**(23): p. 4812-4814.

79. Bichurin, M.I., et al., *Resonance magnetoelectric effects in layered magnetostrictive-piezoelectric composites.* Physical Review B, 2003. **68**(13).

80. Zhai, J., et al., *Giant magnetoelectric effect in Metglas/polyvinylidene-fluoride laminates.* Applied Physics Letters, 2006. **89**(8).

81. Dong, S., et al., *Push-pull mode magnetostrictive/piezoelectric laminate composite with an enhanced magnetoelectric voltage coefficient.* Applied Physics Letters, 2005. **87**(6).

Pedro Martins

82. Fang, Z., et al., *Enhancing the magnetoelectric response of Metglas/polyvinylidene fluoride laminates by exploiting the flux concentration effect.* Applied Physics Letters, 2009. **95**(11).

83. Dong, X.W., et al., *Ultra-sensitive detection of magnetic field and its direction using bilayer PVDF/Metglas laminate.* Sensors and Actuators a-Physical, 2009. **153**(1): p. 64-68.

84. Lu, S.G., et al., *Large magnetoelectric coupling coefficient in poly(vinylidene fluoride-hexafluoropropylene)/Metglas laminates.* Journal of Applied Physics, 2011. **110**(10).

85. Kunstler, W., et al., *Preparation and assessment of piezo- and pyroelectric poly (vinylidene fluoride-hexafluoropropylene) copolymer films.* Applied Physics a-Materials Science & Processing, 2001. **73**(5): p. 641-645.

86. Bauer, F., *PVDF shock sensors: Applications to polar materials and high explosives.* Ieee Transactions on Ultrasonics Ferroelectrics and Frequency Control, 2000. **47**(6): p. 1448-1454.

87. Jin, J., et al., *Multiferroic Polymer Composites with Greatly Enhanced Magnetoelectric Effect under a Low Magnetic Bias.* Advanced Materials, 2011. **23**(33): p. 3853-+.

88. Zeng, M., S.W. Or, and H.L.W. Chan, *Large magnetoelectric effect from mechanically mediated magnetic field-induced strain effect in Ni-Mn-Ga single crystal and piezoelectric effect in PVDF polymer.* Journal of Alloys and Compounds, 2010. **490**(1-2): p. L5-L8.

89. Sozinov, A., et al., *Giant magnetic-field-induced strain in NiMnGa seven-layered martensitic phase.* Applied Physics Letters, 2002. **80**(10): p. 1746-1748.

90. Ullakko, K., *Magnetically controlled shape memory alloys: A new class of actuator materials.* Journal of Materials Engineering and Performance, 1996. **5**(3): p. 405-409.

91. Chopra, H.D., C.H. Ji, and V.V. Kokorin, *Magnetic-field-induced twin boundary motion in magnetic shape-memory alloys.* Physical Review B, 2000. **61**(22): p. 14913-14915.

92. Ding, H.J., Chenbuo, and Liangjian, *General solutions for coupled equations for piezoelectric media.* International Journal of Solids and Structures, 1996. **33**(16): p. 2283-2298.

93. *IEEE Standard on Piezoelectricity.* ANSI/IEEE Std 176-1987, 1988: p. 0_1.

94. Lu, S.G., et al., *Thermally mediated multiferroic composites for the magnetoelectric materials.* Applied Physics Letters, 2010. **96**(10).

95. Spichkin, Y.I., et al., *Thermodynamic features of magnetization and magnetocaloric effect near the magnetic ordering temperature of Gd.* Journal of Magnetism and Magnetic Materials, 2007. **316**(2): p. E555-E557.

96. Karedla, R., J.S. Love, and B.G. Wherry, *Caching Strategies to Improve Disk System Performance.* Computer, 1994. **27**(3): p. 38-46.

97. Burrell, K.H., et al., *Improved charge coupled device detectors for the edge charge exchange spectroscopy system on the DIII-D tokamak.* Review of Scientific Instruments, 2001. **72**(1): p. 1028-1033.

98. Zhu, J.-G., *Magnetoresistive Random Access Memory: The Path to Competitiveness and Scalability.* Proceedings of the Ieee, 2008. **96**(11): p. 1786-1798.

99. Julliere, M., *Tunneling between ferromagnetic films.* Physics Letters A, 1975. **54**(3): p. 225-226.

100. Hu, J.-M., et al., *Electric-field control of strain-mediated magnetoelectric random access memory.* Journal of Applied Physics, 2010. **107**(9).

101. Guo, Y., et al., *Giant Magnetodielectric Effect in 0-3 Ni0.5Zn0.5Fe2O4-Poly(vinylidene-fluoride) Nanocomposite Films.* Journal of Physical Chemistry C, 2010. **114**(32): p. 13861-13866.

102. Shi, Z., et al., *A four-state memory cell based on magnetoelectric composite.* Chinese Science Bulletin, 2008. **53**(14): p. 2135-2138.

103. Koster, E., *TRENDS IN MAGNETIC RECORDING MEDIA.* Journal of Magnetism and Magnetic Materials, 1993. **120**(1-3): p. 1-10.

104. Nakamae, K., et al., *Lifetime expectancy of polyurethane binder as magnetic recording media.* International Journal of Adhesion and Adhesives, 1996. **16**(4): p. 277-283.

105. Li, L., et al., *A flexible polymer memory device.* Organic Electronics, 2007. **8**(4): p. 401-406.

106. Stikeman, A., *Upstream - Spotlight on a hot technology to watch - Systems biology - Researchers look for a better model of diseases.* Technology Review, 2002. **105**(2): p. 31-31.

107. Ouyang, J.Y., et al., *Programmable polymer thin film and non-volatile memory device.* Nature Materials, 2004. **3**(12): p. 918-922.

108. Piguet, C., *Low-Power Electronics Design.* 2004: CRC Press.

109. Priya, S. and D.J. Inman, *Energy Harvesting Technologies.* 2009: Springer.

110. Beeby, S.P., M.J. Tudor, and N.M. White, *Energy harvesting vibration sources for microsystems applications.* Measurement Science & Technology, 2006. **17**(12): p. R175-R195.

111. Roundy, S., *On the effectiveness of vibration-based energy harvesting.* Journal of Intelligent Material Systems and Structures, 2005. **16**(10): p. 809-823.

112. Adhikari, S., M.I. Friswell, and D.J. Inman, *Piezoelectric energy harvesting from broadband random vibrations.* Smart Materials & Structures, 2009. **18**(11).

113. Arnold, D.P., *Review of microscale magnetic power generation.* Ieee Transactions on Magnetics, 2007. **43**(11): p. 3940-3951.

114. Qi, Y., et al., *Piezoelectric Ribbons Printed onto Rubber for Flexible Energy Conversion.* Nano Letters, 2010. **10**(2): p. 524-528.

115. Ducharme, S., et al., *Ferroelectric polymer Langmuir-Blodgett films for nonvolatile memory applications.* Ieee Transactions on Device and Materials Reliability, 2005. **5**(4): p. 720-735.

116. MarketWatch, *Global Magnetic Field Sensors Market by Product (Angular, Revolution, Current, Position) by Technology (Hall Effect, Magneto Resistive & Inductive, Fluxgate, Squid), & Applications (Consumer, Automotive, Industrial, Aerospace & Defense) 2011 - 2016.* 2011.

117. M.J. Caruso, T.B., C.H. Smith, and R. Schneider, *A New Perspective on Magnetic Field Sensing technical report.* 1998, Honeywell, Inc.

118. Giang, D.T.H. and N.H. Duc, *Magnetoelectric sensor for microtesla magnetic-fields based on (Fe80Co20)(78)Si12B10/PZT laminates.* Sensors and Actuators a-Physical, 2009. **149**(2): p. 229-232.

119. Bichurin, M.I., et al., *Magnetoelectric sensor of magnetic field.* Ferroelectrics, 2002. **280**: p. 365-368.

120. Auciello, O., *A critical comparative review of PZT and SBT-based science and technology for non-volatile ferroelectric memories.* Integrated Ferroelectrics, 1997. **15**(1-4): p. 211-220.

Pedro Martins

121. Aoyagi, M., S.P. Beeby, and N.M. White, *A novel multi-degree-of-freedom thick-film ultrasonic motor.* Ieee Transactions on Ultrasonics Ferroelectrics and Frequency Control, 2002. **49**(2): p. 151-158.

122. Frank, R., *Pressure sensors merge micromachining and microelectronics.* Sensors and Actuators a-Physical, 1991. **28**(2): p. 93-103.

133. Yurish, S.Y., *Forecasts and Modern Sensors Market: Today's Revolution Changes.* Sensors & Transducers Magazine, 2004. **41**(3): p. 170 - 173.

124. Lo, C.Y., et al., *Magnetoelectric effect in lead-free BNKLBT ceramic/terfenol-D continue fiber composite laminates.* Journal of Applied Physics, 2010. **107**(9).

125. Myers, R., et al., *Magnetoelectric laminate composite based tachometer for harsh environment applications.* Applied Physics Letters, 2007. **91**(12).

2 Nucleation of electroactive β-PVDF with CoFe₂O₄ and NiFe₂O₄ nanofillers: a new method for the preparation of multiferroic nanocomposites
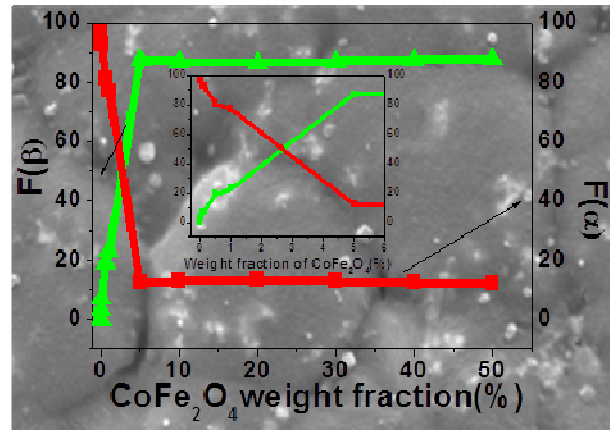
Multiferroic (MF) and magnetoelectric (ME) materials show enormous potential for technological developments. MF composites are more attractive for applications due to their enhanced properties with respect to single-phase multiferroic materials. In this paper we report on the nucleation of the electroactive β-phase of poly(vinylidene fluoride), PVDF, by the addition of $CoFe_2O_4$ and $NiFe_2O_4$ nanoparticles in order to prepare) PVDF/ferrite nanocomposite for MF and ME applications. The dispersed ferrite nanoparticles strongly enhance the nucleation of the β-PVDF. In this way, ME polymer nanocomposites can be processed avoiding the usual α to β phase transformation by stretching of the polymer matrix.

2.1   Introduction

MFs have invigorated interest in the fields of ferroelectric, ferromagnetic and multifunctional materials as they provide large potential applications in multifunctional devices, transducer, actuators, and sensors [1-3]. Such materials, which simultaneously display ferroelectricity and ferromagnetism are known as MFs [4]. The ME effect in such materials is due to the strain induced in the ferrite phase by an applied magnetic field, which in turn gives rise to an electric voltage in the ferroelectric phase [5].

The ME effect was first observed in single crystals, but the use of single-phase materials on device applications has not been successful due to the fact that these materials normally show weak ME effect [6]. One way to overcome these limitations is to use composite materials [7]. In this paper we focus on PVDF/ferrite composite for ME and MF applications, as the ME effect is larger in polymer composites from PVDF than in other polymer materials. For ME applications, the polymer must be in the electroactive phase, which, is obtained by a stretching process. In this work, it is reported and discussed the nucleation of the polar β-phase in PVDF films processed with the addition of nanometric ferrite particles.

PVDF is a semi-crystalline polymer which shows four crystal polymorphs referred to as α, β, γ and δ [8]. The α and β polymorphs are most common, but melt processing usually results in the α-phase [9]. The polar phase, β, is technologically the most interesting one, it shows an all-trans conformation comprising fluorine atoms and hydrogen atoms on opposite sides of the polymer backbone, resulting in a net non-zero dipole moment, consequently, this phase is ferroelectric, exhibits large piezoelectric and pyroelectric coefficients and a high dielectric constant [10]. The β-phase of PVDF can be obtained from the α-phase by uniaxial or biaxial stretching of PVDF film and by solution crystallization at adequate temperature conditions [11] among others [12]. Until recently, this phase was exclusively obtained by mechanical stretching of films originally in the non-polar α-phase [13]. This process results in films mostly in the β phase, but with a small percentage of α-phase. Further, this method is not appropriate for the preparation of composites, as the stretching process leads to non-controlled reconfiguration of the fillers, as well as to their agglomeration. Furthermore, the maximum α to β-phase transformation occurs for deformations larger that 400%, which is not possible for large filler contents as the material becomes fragile [10]. It is also possible to obtain films in the β-phase directly by solution but this material presents a

high porosity leading to an opaque appearance and a decrease of the electrical and mechanical properties. Further, the films cannot be oriented by stretching due to their fragility [14].

Nucleation of the polar PVDF β-phase has been reported, taking advantage of addition of nanoparticles such as silicates and clays [15-18]. Andrew *et al.* also showed that by adding the oxidic spinel Ni–Zn ferrite nanoparticles into PVDF, the β and γ-phase, containing longer trans sequences, were enhanced in the composite electrospun fibers [19, 20].

Oxidic spinels used as the ferromagnetic phase in our work are interesting both for fundamental studies and for technological applications [21-23]. In particular, ferrite spinels such as $CoFe_2O_4$ and $NiFe_2O_4$ exhibit combined electrical and magnetic properties that have found numerous applications in high-frequency devices, memory cores and magnetic recording media. Nanometre size ferrites are under intense investigation due to the broad range of magnetic behaviour that is used for the preparation of tailored composites and structures [24].

As mentioned before, the ME effect is larger in polymer composites from PVDF than in other materials, but the polymer must be in the electroactive phase, which is obtained by a stretching process. Due to this process, particulate composites loose ME efficiency and need large filler contents, therefore, just laminate composites seem to be of applied interest. Laminate composites are, on the other hand, more difficult to fabricate in an up-scaled process. In this paper we demonstrate the possibility of nucleating the electroactive phase of PVDF with nanosized ferrite spinels, giving rise to particulate ME polymer composites.

2.2   Experimental

Ferrite nanoparticles were purchased from Nanoamor, $CoFe_2O_4$ and $NiFe_2O_4$ powders have dimensions between 35-55 and 20-30 nm respectively. *N*,*N*-dimethylformamide (DMF), pure grade was supplied by Fluka and PVDF (Solef 1010) was supplied by Solvay. All the chemicals and nanoparticles were used as received from the suppliers. The initial concentration of solution was 0.2 g of PVDF for 1 ml of DMF. In order to obtain a good dispersion of the ferrite nanoparticles within the polymeric matrix, the following procedure was applied: first, the desired amount of nanoparticles was added to 12 ml of DMF and then placed in an ultrasound bath during 6 h, to ensure that

nanoparticles were well dispersed in the solution and also to avoid loose aggregates; then 3g of PVDF were subsequently added and the obtained mixture was placed in a Teflon mechanical stirrer for complete dissolution of the polymer during 1h. Flexible films of ~30 μm were obtained by spreading the solution on a clean glass substrate.

Solvent evaporation and polymer crystallization were obtained inside an oven at controlled temperature. The samples were maintained inside the oven for 10 min at 210 ºC to ensure the complete melting of the nanocomposite. After this process, samples are crystallized by cooling down to room temperature. The wt.% of ferrite nanoparticles varied from 0.001 to 50 in the case of PVDF/CoFe$_2$O$_4$ and 5 to 50 in the case of PVDF/NiFe$_2$O$_4$ composites.

Fourier transformed infrared spectroscopy (FTIR) spectra of the films were recorded on a Perkin-Elmer Spectrum 100 in Attenuated Total Reflectance (ATR) mode over a range of 650-1150cm^{-1} with a resolution of 4 cm^{-1}. 32 scans were performed to each sample.

DSC studies were performed using a Perkin-Elmer Diamond DSC. During the DSC analysis the samples were ramped from -70°C to 200°C under a dry N$_2$ environment at a rate of 10°C/min, then maintained at isothermal conditions for 5 min at 200°C. The specimens were then cooled at a rate of 10°C/min to -70°C. Nominal melting temperature (T$_m$) was defined as the peak of the melting endotherm during the heating from -70°C to 200°C and the crystallization temperature, T$_c$, was defined as the peak of the crystallization exothermic upon cooling from 200°C to -70°C.

SEM was carried out at a resolution of 20 μm in a Leica Cambridge S360 apparatus.

2.3   Results and discussion

FTIR has been proved to be suitable to identify and quantify phase content in PVDF [25, 26]. In particular specific bands such as 766 and 840 cm^{-1} have been identified to correspond to the α and β-phase respectively. These specific bands have been used for identification and quantification of the phases in the present work.

A comparison of the FTIR spectra (Figure 2.1a and Figure 2.2a) of CoFe$_2$O$_4$ and NiFe$_2$O$_4$ nanocomposites shows that as the weight fraction of CoFe$_2$O$_4$ increases from 0.01 wt.% up to 1 wt.% the bands corresponding to the α-phase of the polymer decrease, almost disappearing for the 5% content composites.
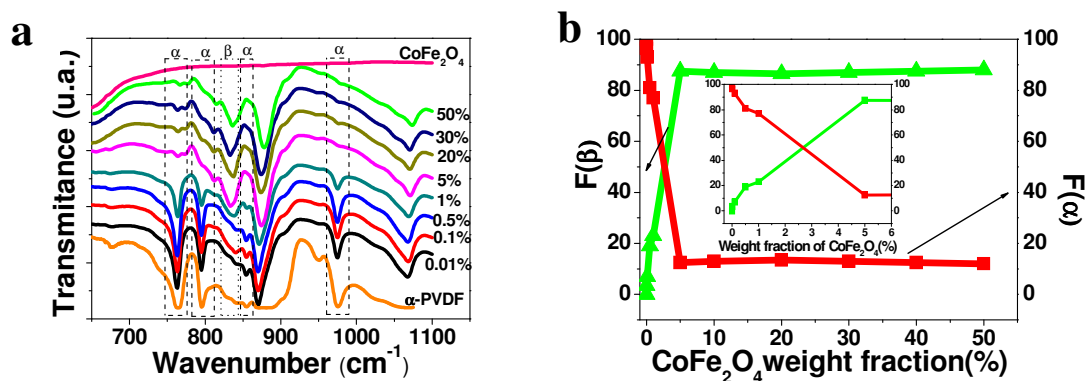
Figure 2.1 − (a) Infrared transmittance vs. wavenumber for PVDF nanocomposites with Cobalt ferrite nanoparticles with weight concentrations going from 0.01% until 50%. (b) Evolution of α into β-phase transformation for $CoFe_2O_4$.

The β-phase band at 840 cm^{-1} increases reaching the minimum transmittance value at 5 wt.%. For higher concentrations than 5% no differences are detected in the characteristic bands of the different phases.
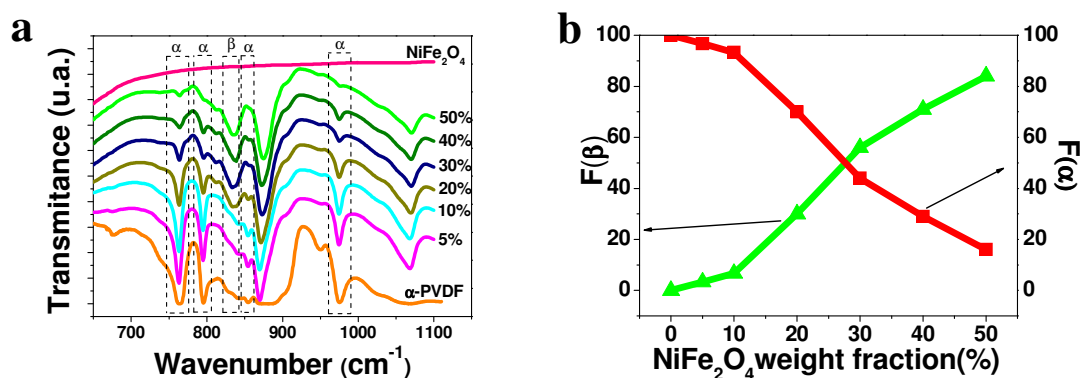
Figure 2.2 − (a) Infrared transmittance vs. wavenumber for PVDF nanocomposites with Nickel ferrite nanoparticles with weight concentrations from 5% until 50%. (b) Evolution of α into β-phase transformation for $NiFe_2O_4$.

As the wt.% of $NiFe_2O_4$ increases from 5 up to 40 wt.%, the α-phase bands decrease, almost disappearing for 50% content. At the same time, the β-phase band at 840 cm^{-1} increases reaching the minimum transmittance value at 50 wt.%. This phase evolution with ferrite concentration is also proven by X-ray diffraction (XRD) measurements (not shown).

Pedro Martins

The relative amount β phase ($F(\beta)$) present in the different samples was calculated applying equation 2.1 [26]:

$$F(\beta) = \frac{X_\beta}{X_\alpha + X_\beta} = \frac{A_\beta}{(K_\beta / K_\alpha)A_\alpha + A_\beta} \qquad \textbf{(2.1)}$$

Here, $F(\beta)$ represents the β-phase content; A_α and A_β the absorbencies at 766 and 840 cm^{-1}, corresponding to the α and β phase material; K_α and K_β are the absorption coefficients at the respective wave number and X_α and X_β the degree of crystallinity of each phase. The value of K_α is 6.1×10^4 and K_β is 7.7×10^4 cm^2/mol. A similar procedure was used for the calculation of the α-phase content [26].

The evolution of the α and β phase content with ferrite concentration is observed in Figure 2.1b and in Figure 2.2b. The β-phase increases and correspondingly the α-phase content decreases with increasing nanoparticle concentration. For $CoFe_2O_4$ composites the full phase nucleation of the β-phase occurs for much lower concentrations than for $NiFe_2O_4$ composites.

In the case of cobalt ferrite, the full nucleation of the β-phase has been already achieved for 5 wt.%. In the case of nickel ferrite, the maximum β-phase content is obtained for 50 wt.%.

These results are not in agreement with the theory presented by Andrew and Clarke [20], once they proposed that nanoparticles promote the phase nucleation when their radius was less than the Radius of gyration (R_g) of the polymer. The R_g value for PVDF is 27,5 nm, and the average radius of nanoparticles is 45 nm for $CoFe_2O_4$ and 25 nm for $NiFe_2O_4$.

The fact that the β-phase of PVDF forms preferentially in PVDF/ferrite nanocomposites suggests one of two phenomena, either the ferrite nanoparticles are nucleating β-phase epitaxially on their surfaces or they are interrupting the chain mobility during crystallization, so that more extended-chain β-phase crystals are formed [19, 20].

DSC analysis of pure α-PVDF and the ferrite nanocomposites were conducted to analyze the effect of nanoparticles on the X_c.

Table 2.1 − Thermal analysis for PVDF nanocomposites with ferrite nanoparticles.

Sample	X_c^m (%)	T_m (ºC)	ΔS (J/g ºC)	X_c^C (%)	T_c (ºC)	ΔT (ºC)
0.01% CoFe$_2$O$_4$	55.67	173.29	0.3	53.50	141.52	32
0.1% CoFe$_2$O$_4$	49.50	172.3	0.27	51.72	141.7	31
0.5% CoFe$_2$O$_4$	45.43	169.95	0.25	51.09	140.86	29
1% CoFe$_2$O$_4$	42.15	174.81	0.23	50.45	143.7	31
5% CoFe$_2$O$_4$	35.09	174.53	0.21	39.63	143.9	31
10% CoFe$_2$O$_4$	35.42	174.6	0.21	36.81	144.24	30
20% CoFe$_2$O$_4$	24.86	176	0.14	26.78	145.23	31
30% CoFe$_2$O$_4$	18.64	178.84	0.11	22.50	144.38	34
40% CoFe$_2$O$_4$	15.11	178.7	0.086	15.75	145.05	34
50% CoFe$_2$O$_4$	8.38	177	0.048	9.99	143.33	34
5% NiFe$_2$O$_4$	44.09	172.3	0.24	45.62	144.37	28
10% NiFe$_2$O$_4$	51.03	173	0.28	47.51	143.69	29
20% NiFe$_2$O$_4$	35.35	174	0.20	28.18	143.99	30
30% NiFe$_2$O$_4$	16.71	176	0.094	20.92	145.21	31
40% NiFe$_2$O$_4$	10.64	177	0.060	13.38	143.03	34
50% NiFe$_2$O$_4$	6.95	184	0.038	7.81	142.94	41

The DSC results for $CoFe_2O_4$ and $NiFe_2O_4$ samples are presented on Table 2.1 and Figure 2.3. The melting and crystallization enthalpies, ΔH_m and ΔH_c, data obtained for nanocomposite samples were corrected due to the presence of ferrite nanoparticles, i.e. considering just the wt.% of the polymer phase.
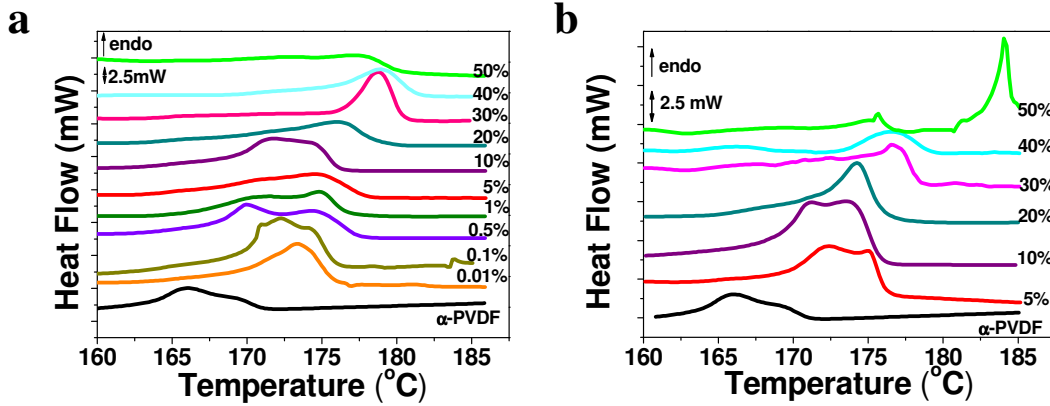
Figure 2.3 − (a) DSC thermogram (heating) for $CoFe_2O_4$ nanocomposites. (b) DSC thermogram (heating) for $NiFe_2O_4$ nanocomposites.

The degree of crystallinity of α-PVDF and PVDF nanocomposites, based on either the melting (X_c^m) or crystallization (X_c^c) DSC scans, can be obtained from equation 2.2:

$$X_c^{m/c} = \frac{\Delta H_{m/c} \times 100}{x(\Delta H_{100\%crystalline})_\alpha + y(\Delta H_{100\%crystalline})_\beta} \qquad \textbf{(2.2)}$$

Here, x is the weight fraction of the α phase, y is the weight fraction of the β phase, $(\Delta H_{100\%crystalline})_\alpha$ is the enthalpy of pure crystalline α-PVDF and $(\Delta H_{100\%crystalline})_\beta$ is the enthalpy of pure crystalline β-PVDF: 93.04 J/g and 103.4 J/g respectively [27].

The degree of supercooling can be obtained from ΔT, the difference between T_c and T_m, obtained from the cooling and heating DSC scans peaks, respectively [28],

$$\Delta T = T_m - T_c \qquad \textbf{(2.3)}$$

ΔT in $CoFe_2O_4$ ferrite remains practically unchanged and in $NiFe_2O_4$ ferrites increases with increasing filler concentration, accompanying the α to β-phase transformation. This fact indicates an increasing degree of supercooling.

The entropy, ΔS, of the melting process is calculated by equation 2.4, with ΔG, the Gibbs free energy, being zero:

$$\Delta S = \frac{\Delta H_m - \Delta G}{T_m} \qquad\qquad (2.4)$$

According to the DSC scans and results summarized in Table 2.1, the addition of nanoparticles has the effect of increasing of the melting temperature. The increase in the melting temperature results in higher thermal stability. In addition ΔS of the polymer decrease with increasing filler content.

The degree of crystallinity of the α-phase is 45% [10]. For the lower concentrations of ferrite nanoparticles the degree of crystallinity is higher than 45%, decreasing for increasing ferrite nanoparticle content. This fact is in agreement with the nanoparticles acting as nucleating agents [20, 29]. The enhancement in the nucleation efficiency of the PVDF leads to more nucleation centers, smaller spherulites and decreasing crystallinity with increasing concentration of ferrite nanoparticles, as illustrated also by SEM images of α-PVDF and PVDF/ferrite nanocomposites crystallized at the same temperatures.
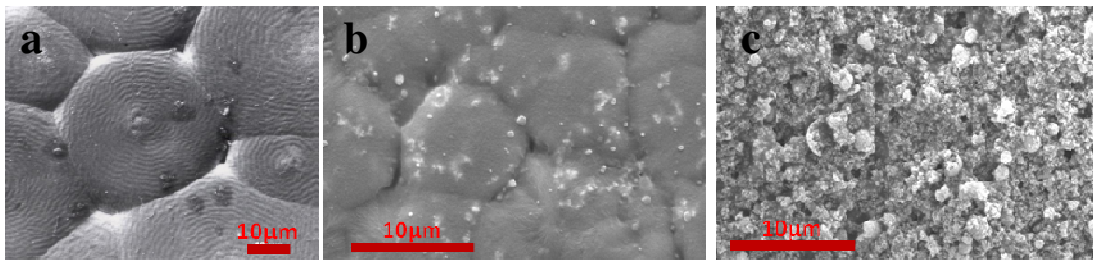
Figure 2.4 – SEM images from α-PVDF (a) and PVDF/CoFe$_2$O$_4$ nanocomposites with wt.% concentrations of 5 (b) and 50% (c), respectively.

α-PVDF, Figure 2.4a, presents a typical spherulitic structure. By adding cobalt ferrite nanoparticles the amount of spherulites increases (Figure 3.4b) and its sizes decreases from 30 μm in α-PVDF to 10 μm in PVDF with 5 wt% of CoFe$_2$O$_4$. Similar results were already observed in PVDF/clay nanocomposites [29]. A great number of nucleus generated from the nucleation agents simultaneously grow in a limited space and lead to smaller spherulites. On the other hand, the large number of nucleation centers will also cause more crystal defects, leading to a lower crystallinity, which is consistent with our DSC measurements. For high ferrite concentrations, Figure 2.4c, no spherulitic structures are detected.

2.4 Conclusions

In conclusion, it is demonstrated that it is possible to prepare PVDF/ferrite nanocomposites in the electroactive β-phase of the polymer by melt processing, with great potential for the preparation of ME composites. Two different ferrites, $CoFe_2O_4$ and $NiFe_2O_4$, were used to promote the β-phase crystallization of the PVDF composites. The crystallization of the β-phase of PVDF was observed for both ferrite nanofillers, although the β-phase content increases with increasing ferrite concentration in a different way. It was verified that composites with more that 90% of the crystalline phase in the β-phase are obtained for 5 wt.% of $CoFe_2O_4$ and 50 wt.% of $NiFe_2O_4$.

2.5 References

1. Ma, J., Z. Shi, and C.-W. Nan, *Magnetoelectric properties of composites of single Pb(Zr,Ti)O-3 rods and Terfenol-D/epoxy with a single-period of 1-3-type structure.* Advanced Materials, 2007. **19**(18): p. 2571-+.

2. Fiebig, M., *Revival of the magnetoelectric effect.* Journal of Physics D-Applied Physics, 2005. **38**(8): p. R123-R152.

3. Eerenstein, W., N.D. Mathur, and J.F. Scott, *Multiferroic and magnetoelectric materials.* Nature, 2006. **442**(7104): p. 759-765.

4. Chen, Y., et al., *Giant magnetoelectric coupling and E-field tunability in a laminated Ni(2)MnGa/lead-magnesium-niobate-lead titanate multiferroic heterostructure.* Applied Physics Letters, 2008. **93**(11).

5. Devan, R.S. and B.K. Chougule, *Magnetic properties and dielectric behavior in ferrite/ferroelectric particulate composites.* Physica B-Condensed Matter, 2007. **393**(1-2): p. 161-166.

6. Patil, D.R., et al., *Magnetoelectric properties of ME particulate composites.* Journal of Materials Science, 2008. **43**(8): p. 2708-2712.

7. Spaldin, N.A. and M. Fiebig, *The renaissance of magnetoelectric multiferroics.* Science, 2005. **309**(5733): p. 391-392.

8. Kang, S.J., et al., *Localized pressure-induced ferroelectric pattern arrays of semicrystalline poly(vinylidene fluoride) by microimprinting.* Advanced Materials, 2007. **19**(4): p. 581-+.

9. Gregorio, R. and M. Cestari, *Effect of crystallization temperature on the crystalline phase content and morphology of poly(vinylidene fluoride).* Journal of Polymer Science Part B-Polymer Physics, 1994. **32**(5): p. 859-870.

10. Sencadas, V., R. Gregorio, Jr., and S. Lanceros-Mendez, *alpha to beta Phase Transformation and Microestructural Changes of PVDF Films Induced by Uniaxial Stretch.* Journal of Macromolecular Science Part B-Physics, 2009. **48**(3): p. 514-525.

11. Gregorio, R. and N. Nociti, *Effect of PMMA addition on the solution crystallization of the alpha-phase and beta-phase of poly(vinylidene fluoride) (PVDF).* Journal of Physics D-Applied Physics, 1995. **28**(2): p. 432-436.

12. Scheinbeim, J., et al., *High-pressure crystallization of poly(vinylidene fluoride).* Journal of Applied Physics, 1979. **50**(6): p. 4399-4405.

13. Lovinger, A.J., *Crystallization of the beta-phase of poly(vinylidene fluoride) from the melt.* Polymer, 1981. **22**(3): p. 412-413.

14. Sencadas, V., R. Gregorio Filho, and S. Lanceros-Mendez, *Processing and characterization of a novel nonporous poly(vinilidene fluoride) films in the β phase.* Journal of Non-Crystalline Solids, 2006. **352**(21-22): p. 2226-2229.

15. Priya, L. and J.P. Jog, *Poly(vinylidene fluoride)/clay nanocomposites prepared by melt intercalation: Crystallization and dynamic mechanical behavior studies.* Journal of Polymer Science Part B-Polymer Physics, 2002. **40**(15): p. 1682-1689.

16. Dillon, D.R., et al., *On the structure and morphology of polyvinylidene fluoride-nanoclay nanocomposites.* Polymer, 2006. **47**(5): p. 1678-1688.

17. Cebe, P. and S.Y. Chung, *Tensile behavior of blends of poly(vinylidene fluoride) with poly(methyl methacrylate).* Journal of Materials Science, 1990. **25**(5): p. 2367-2378.

18. Ramasundaram, S., et al., *Preferential Formation of Electroactive Crystalline Phases in Poly(vinylidene fluoride)/Organically Modified Silicate*

Nanocomposites. Journal of Polymer Science Part B-Polymer Physics, 2008. **46**(20): p. 2173-2187.

19. Andrew, J.S., J.J. Mack, and D.R. Clarke, *Electrospinning of polyvinylidene difluoride-based nanocomposite fibers.* Journal of Materials Research, 2008. **23**(1): p. 105-114.

20. Andrew, J.S. and D.R. Clarke, *Enhanced ferroelectric phase content of polyvinylidene difluoride fibers with the addition of magnetic nanoparticles.* Langmuir, 2008. **24**(16): p. 8435-8438.

21. Hu, J.T., et al., *Linearly polarized emission from colloidal semiconductor quantum rods.* Science, 2001. **292**(5524): p. 2060-2063.

22. Sloczynski, J., et al., *Catalytic activity of chromium spinels in SCR of NO with NH3.* Applied Catalysis B-Environmental, 2000. **24**(1): p. 45-60.

23. Pena, M.A. and J.L.G. Fierro, *Chemical structures and performance of perovskite oxides.* Chemical Reviews, 2001. **101**(7): p. 1981-2017.

24. Papaefthymiou, G.C., S.R. Ahmed, and P. Kofinas, *Magnetic and structural characterization of CoFe2O4 nanoparticles encapsulated within block copolymer films.* Reviews on Advanced Materials Science, 2005. **10**(4): p. 306-313.

25. Kobayashi, M., K. Tashiro, and H. Tadokoro, *Molecular Vibrations of 3 Crystal Forms of Poly(Vinylidene Fluoride).* Macromolecules, 1975. **8**(2): p. 158-171.

26. Miranda, D., et al., *Influence of Silver Nanoparticles Concentration on the alpha- to beta-Phase Transformation and the Physical Properties of Silver Nanoparticles Doped Poly(vinylidene fluoride) Nanocomposites.* Journal of Nanoscience and Nanotechnology, 2009. **9**(5): p. 2910-2916.

27. Bassett, D.C., *Developments in crystalline polymers*. 1982: Applied Science Publishers.

28. Vidhate, S., et al., *Crystallization, Mechanical, and Rheological Behavior of Polyvinylidene Fluoride/Carbon Nanofiber Composites.* Journal of Applied Polymer Science, 2009. **112**(1): p. 254-260.

29. Shah, D., et al., *Dramatic enhancements in toughness of polyvinylidene fluoride nanocomposites via nanoclay-directed crystal structure and morphology.* Advanced Materials, 2004. **16**(14): p. 1173-+.

3 Influence of ferrite nanoparticle type and content on the crystallization kinetics and electroactive phase nucleation of PVDF
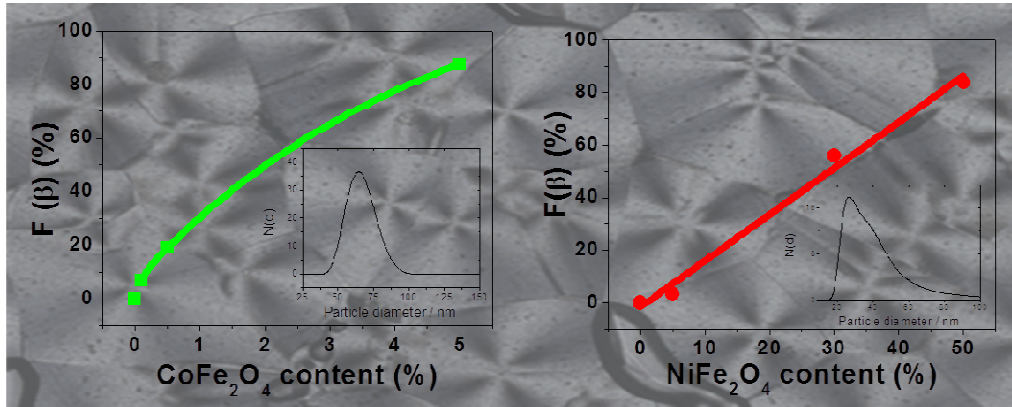
This work reports on the nucleation of the β-phase of Poly(vinylidene fluoride), PVDF, by incorporating $CoFe_2O_4$ and $NiFe_2O_4$ nanoparticles, leading in this way, to the preparation of magnetoelectric composites. The fraction of filler nanoparticles needed to produce the same β to α-phase ratio in crystallized PVDF is one order of magnitude lower in the $CoFe_2O_4$. The interaction between nanoparticles and PVDF chains induce the *all trans* conformation in PVDF segments and this structure then propagates in crystal growth. The nucleation kinetics is enhanced by the presence of nanoparticles, as corroborated by the increasing number of spherulites with increasing nanoparticle content and by the variations of the Avrami's exponent. Further, the decrease of the crystalline fraction of PVDF with increasing nanoparticles content indicates that an important fraction of polymer chains are confined in interphases with the filler particle.

3.1   Introduction

Polymer nanocomposites represent a class of materials with improved performance. Compared with traditional filled grades of polymers, nanocomposites show property improvements at lower loadings of the inorganic fillers [1].

Among the electroactive polymers, PVDF and its copolymers, represent the family of polymers with the best electroactive performance [2-3]. PVDF shows typically a degree of crystallinity around 50% and can appear in four different crystalline phases known has α, β, γ and δ, depending on the processing conditions [4]. The α and β-phases are the most important crystalline polymorphs. The α-phase is non-polar and has a trans-gauche bond (TGTG') conformation, being most commonly obtained directly cooling from the melt or by solvent cast at solvent evaporation temperatures above 120 ºC [5-7]. The β-phase, with an *"all-trans"* conformation (TTT) comprising fluorine and hydrogen atoms on opposite sides of the polymer chain, resulting in a net non-zero dipole moment, which results in the most polar phase, being extensively applied in technological applications involving the electroactive properties of the material [3, 8].

Typically, the β-PVDF is obtained by stretching the α-phase t temperatures below 100 ºC with a draw ratio between 3 and 5 [3, 6]. Unoriented β-phase may also be obtained by solvent casting, when the material is crystallized at temperatures below 70 ºC, but the samples obtained by this procedure presents high porosity [6]. Solvent evaporation at higher temperatures results in a mixture of the α and β-phase, with the α-phase fraction increasing with increasing temperature [3, 6]. A method to remove the porosity of such samples was developed by Sencadas *et al.* by applying a uniaxial compression force at temperatures above 140 ºC [6]. Due to the high porosity of the samples, the material has very poor mechanical and electrical properties, what reduce the applicability of these materials as sensors and actuators.

Consequently, some other methods were introduced to improve the way in which the β-PVDF phase is obtained. Among them, crystallization under high pressure or the use of copolymers such as P(VDF-TrFE) resulting from the copolymerization of vinylidene fluoride with trifluorethylene are examples of such efforts [9]. Other method to develop a β-PVDF is based on the incorporation of nanoclay into PVDF [1, 10].

Most recently, ferrite nanoparticles were added to PVDF with the intention of nucleate the electroactive phase of the polymer [11-12]. These ferrite nanoparticles are usually used as the ferromagnetic phase in ME composites and are interesting both for

fundamental studies and technological applications [13]. Nanometre size ferrites are under intense investigation due to the broad range of magnetic behaviour that is used for the preparation of tailored composites and structures [14].

The physical properties of PVDF depend upon the processing conditions and can also be strongly influenced by the presence of nanoparticles, which affect the crystallization behaviour and the resulting polymer morphology [15]. Additionally, the presence of nanoparticles also has influence on crystallization kinetics [16].

Despite crystallization behaviour of the α-phase PVDF has been already studied [17] the effect of nanoparticles in the polymer crystallization remains vaguely discussed [16, 18].

Recent publications reveal that addition of nanoparticles into PVDF matrix shift the crystallization peak to higher temperatures and smaller spherulites are created [12, 16]. This suggests that the faster crystallization rate of PVDF observed in the blends is due to the nucleating ability of nanoparticles.

In a general way, the subject of polymer crystallization has been of great interest for several decades and can be carried out under isothermal or non-isothermal conditions [19]. Studies on the overall crystallization rate under isothermal conditions are usually accomplished in the scope of the Avrami formalism [20-22] which is valid at least for the early stages of the process [17, 23].

Non-isothermal crystallization of polymers, on the other hand, is not easy to be modelled. This difficulty has been overcome by assuming the non-isothermal process as an approximation of infinitesimally small isothermal stages, so that it can be described by models based on modifications of the initial Avrami equation [17, 23-24].

The non-isothermal crystallization kinetics of several polymeric nanocomposites has been discussed. Xu *et al*. [25] reported that the crystallization of Polypropylene/Montmorillonite nanocomposites was faster than the pure Polypropylene at a given cooling rate. The addition of Montmorillonite accelerates then the overall non-isothermal crystallization and reduces the activation energy. Qian *et al*. [26] showed that the crystallization rate of HDPE/nano-SiO2 nanocomposite was faster than that of pure high-density polyethylene (HDPE) and that the activation energies of the composites increased with the increasing SiO_2 loading.

The nucleation activities of silica nanoparticles were also investigated by Kim *et al*. [27]. The addition of nano–sized silica nanoparticles shift the crystallization peaks to higher temperatures compared with the pure Poly(ethylene 2,6-naphthalate) (PEN), and the

overall crystallization time was reduced. On the other hand, the degree of crystallinity of PEN nanocomposites was increased.

More recently, Kim *et al*. and Manna *et al*. took advantage of carbon nanotubes and silver nanoparticles respectively to act as nuclei in the crystallization process of the piezoelectric β-phase of the polymer PVDF [28-29]. It was found that melting temperature and enthalpy of fusion of PVDF increased slightly in the PVDF/silver nanoparticles; however, with increasing Ag nanoparticle content they gradually decreased. The crystallization studies on cooling from the melt indicated that silver nanoparticles acted as nucleating agents for crystallization of PVDF.

Regarding isothermal crystallization kinetics of polymer nanocomposites, Chen *et al* [30], using the Avrami analysis, demonstrated that adding organo-attapulgite (ATT) into Poly(butylene terephthalate) accelerate the crystallization kinetics of PBT. Similar results were found by Zhang *et al* [31] when Carbon black (CB) nanoparticles were added into Poly(ethylene terephthalate (PET). The crystallization temperature decreased from 393 to 373 K with increasing CB content from 0 to 12.5 wt.%. Avrami exponents *n* were evaluated to be in the range 2.1—2.6 for neat PET and the composites. Carbon black nanoparticles acting as nucleating agent in the composites accelerated the crystallization rate, and the crystallinity of the composites was improved largely by addition of CB.

Concerning the isothermal crystallization, Raka *et al* [32] reported the effect of organo-modified clay (Cloisite 93A) nanoparticles on the isothermal crystallization behaviour of isotactic polypropylene (iPP) in iPP/clay nanocomposites. Results indicated that higher nanoparticle clay loading promotes the formation of the β-phase crystallites. Analysis of the isothermal crystallization showed that the Polypropylene (PP) nanocomposite (1% C93A) exhibited higher crystallization rates than the neat PP and that the activation energy decreased with the incorporation of clay nanoparticles into the matrix, which in turn indicates that the nucleation process is facilitated by the presence of clay.

In present work, ferrite nanoparticles were added into PVDF via solution blending with different concentrations to obtain PVDF/ferrite ME composites. The used ferrites ($CoFe_2O_4$ and $NiFe_2O_4$) have the ability to nucleate the ferroelectric phase of the polymer, but they do it at a tailored concentration rate. Further, the crystallization dynamic has been studied in order to shed some light on the influence of the nanoparticles in the crystallization in the different phases of the polymer. Finally, this study is relevant as allows the preparation of ME composites taking advantage of the

piezoelectric properties of the β-phase of PVDF and the magnetostriction of the ferrite nanoparticles.

3.2 Experimental

3.2.1 Sample preparation and characterization

Ferrite nanoparticles were purchased from *Nanoamor*. $CoFe_2O_4$ and $NiFe_2O_4$ powders have dimensions between 35-55 and 20-30 nm, respectively. The size distribution of the nanoparticles was further determined by DLS (inset of Figures 3.1 (c-d)). DMF (pure grade) was obtained from *Fluka* and PVDF (Solef 1010) was supplied by *Solvay*. All the chemicals and nanoparticles were used as received from the suppliers. The initial concentration of the solution was 0.2 g of PVDF for 1ml of DMF. In order to obtain a good dispersion of the ferrite nanoparticles within the polymeric matrix, the following procedure was applied: first, the desired amount of nanoparticles was added to 12 ml of DMF and then placed in ultrasound bath during 6 h, to ensure that nanoparticles were well dispersed in the solution and to avoid loose aggregates; then 3 g of PVDF were subsequently added. Finally, the mixture was placed in a Teflon mechanical stirrer for complete dissolution of the polymer. Flexible films were obtained by spreading the solution on a clean glass substrate.

Solvent evaporation and polymer crystallization were obtained inside an oven at controlled temperature. The samples were maintained inside the oven for 10 min at 210 ºC to ensure the complete melting of the nanocomposite and solvent evaporation. After this process, samples are crystallized by cooling down to room temperature. The wt.% of ferrite nanoparticles varied from 0.1 to 5% in the case of cobalt ferrite and from 5 to 50% in the case of nickel ferrite.

Infrared measurements were performed in order to determine and characterize the presence of the different PVDF crystalline phases. A Perkin-Elmer Spectrum 100 apparatus was used in ATR mode from 4000 to 650 cm^{-1}. FTIR spectra were collected with 32 scans and a resolution of 4 cm^{-1}.

DLS was performed with a Zetasizer Nano ZS (Malvern instruments), provided by a He/Ne laser of 633 nm wavelength. The nanoparticles dispersion was analyzed in a polystyrene cell for size distribution.

3.2.2 Crystallization kinetics

Crystallization kinetics of PVDF was measured by means of isothermal experiments and cooling scans using a differential scanning calorimetre Pyris (Perkin-Elmer, Waltham, MA, USA). Dry nitrogen gas was let through the DSC cell with a flow rate of 20 mL.min^{-1}. A single sample of each material, around 2 mg weight, directly cut from the film was used for all isothermal experiments. All the samples had approximately the same weight (2 mg) and the same thickness, around 50 μm. The calibration of the DSC was made using the 4-cyano-40-octyloxybiphenyl (M24) transition from smectic to nematic phase, T_{s-n}, measured at different temperature rates on cooling and heating runs and the melting point of indium measured at different heating rates. The measurements were conducted with the standard calibration of the DSC and the temperature scale was then corrected by software taking into account the rate dependence of T_{s-n} and the indium melting.

Images of spherulitic growth during the crystallization of PVDF were obtained by Optical microscopy with polarized light (OMPL) (Leica DM2500M, Portugal) provided with a Leica DFC-280 camera (Portugal).

3.3 Results

3.3.1 Polymer phase content within the composite

As already reported in other works, the inclusion of nanofillers like carbon nanotubes or silver nanoparticles changes the crystallization behaviour of the polymeric matrix [33-34].

In this work, PVDF nanocomposites were prepared with two different ferrites ($CoFe_2O_4$ and $NiFe_2O_4$) and different concentration of the filler in the polymeric matrix in order to understand the effect of the filler in the crystallization behaviour of the nanocomposite and the ability of the ferrites in induce crystallization of the β-PVDF directly from the melt.

The infrared measurements for the samples with different filler types and contents are presented in Figure 3.1. It is observed that, when cooled from the melt, the pure polymer crystallizes directly in the α-PVDF crystalline phase. For the nanocomposite samples the FTIR measurements shows that α and β crystalline phases coexist in the polymer matrix, with increasing amount of β-PVDF with increasing ferrite filler content.
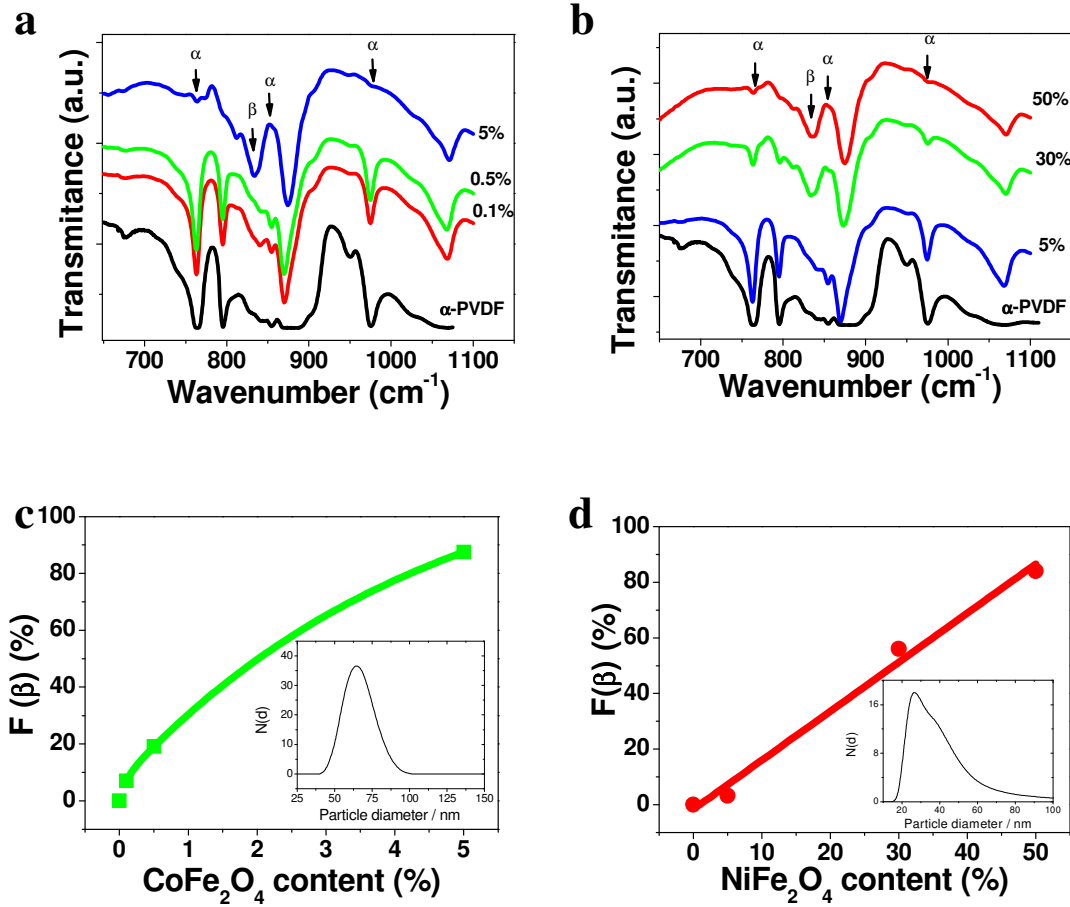
Figure 3.1 – Infrared spectra for the PVDF nanocomposites with increasing filler contents: (a) CoFe2O4, (b) NiFe2O4. Evolution of the β-phase content with increasing filler concentration for the (c) $CoFe_2O_4$, (d) $NiFe_2O_4$ nanocomposite samples. Inset of figures (c) and (d): size distribution of the $CoFe_2O_4$ and $NiFe_2O_4$ nanoparticles as obtained by DLS.

The β-phase content present in each sample was calculated from the infrared absorption bands at 764 cm^{-1} and 840 cm^{-1}, characteristic of the α and β-phases of PVDF, respectively, with a procedure similar to the one presented in [3]. Assuming that the infrared absorption follows the Lambert-Beer law, for a system containing α and β-phases, the relative fraction of the β-phase, F(β), can be calculated applying equation (3.1):

$$F(\beta) = \frac{X_\beta}{X_\alpha + X_\beta} = \frac{A_\beta}{\left(K_\beta/K_\alpha\right)A_\alpha + A_\beta} \tag{3.1}$$

Pedro Martins

For the nanocomposite samples, the variation of the relative fraction of the β-phase with increasing amount of $CoFe_2O_4$ and $NiFe_2O_4$ ferrite fillers is presented in Figures 3.1c and Figure 3.1d. For $CoFe_2O_4$, even a small amount of nanoparticles induces the crystallization of the polymer matrix and the co-existence of the α and β-phases of PVDF. Figure 3.1c shows that a maximum of 88% of β-phase is obtained for 5% of $CoFe_2O_4$ content. On the other hand, for the $NiFe_2O_4$ co-existence of α and β -phases is observed for small filler content, too, but to obtain the highest amount of β-phase 84%, it is necessary to add as much as 50 wt.% $NiFe_2O_4$ nanoparticles. It is to notice that the densities of $CoFe_2O_4$ (5.3 g/cm^3) and $NiFe_2O_4$ (5.4 g/cm^3) are quite similar, representing therefore similar volume content for the same mass content.

3.3.2   Composite microstructural morphology

The morphology of the samples during polymer crystallization was observed by (Polarized optical microscopy) POM a technique that evidences that the crystalline morphology of PVDF is highly influenced by the presence of ferrite nanoparticles. Figure 3.2 shows the spherulitic structure of the semi-crystalline α-PVDF (Figure 3.2a), PVDF filled with Cobalt (Figures 3.2b and 3.2c) and Nickel ferrite nanocomposites (Figure 3.2d). The spherulites of PVDF present a compact and well-defined structure with Maltese-cross texture (Figure 3.2), as it was shown in a previous paper [17]. The addition of even the smallest amount of Cobalt ferrite nanoparticles, 0.1 wt.%, increases the number of the spherulites while spherulite size decreases strongly (Figure 3.2b), but the samples reveal almost the same spherulitic microstructure as for the α-phase of the PVDF. This is a clear evidence that nanoparticles act as nucleation points. Nevertheless it is worth note that the increase in the number of spherulites is orders of magnitude smaller than the number of nanoparticles. Only some of them initiate growing of a spherulite while the rest are embedded in the growing crystalline structure. With increasing $CoFe_2O_4$ nanoparticle content, the number of nucleation points grows so much that spherulites cannot be formed. In fact, the sample containing 5 wt.% $CoFe_2O_4$ (Figure 3.2c) shows no texture in the polarized light microscope in spite that, as will be shown by the DSC results, below, its crystalline fraction is nearly the same than in pure PVDF. In the case of $NiFe_2O_4$ nanocomposites it was impossible to observe the crystalline structure except in the sample with the smallest nanoparticles content since the higher particles

concentration of the other two turned the samples almost opaque (Figure 3.2d). Nanocomposites with 5 wt.% $NiFe_2O_4$ show a large number of very small spherulites proving that these particles are also able to nucleate PVDF.
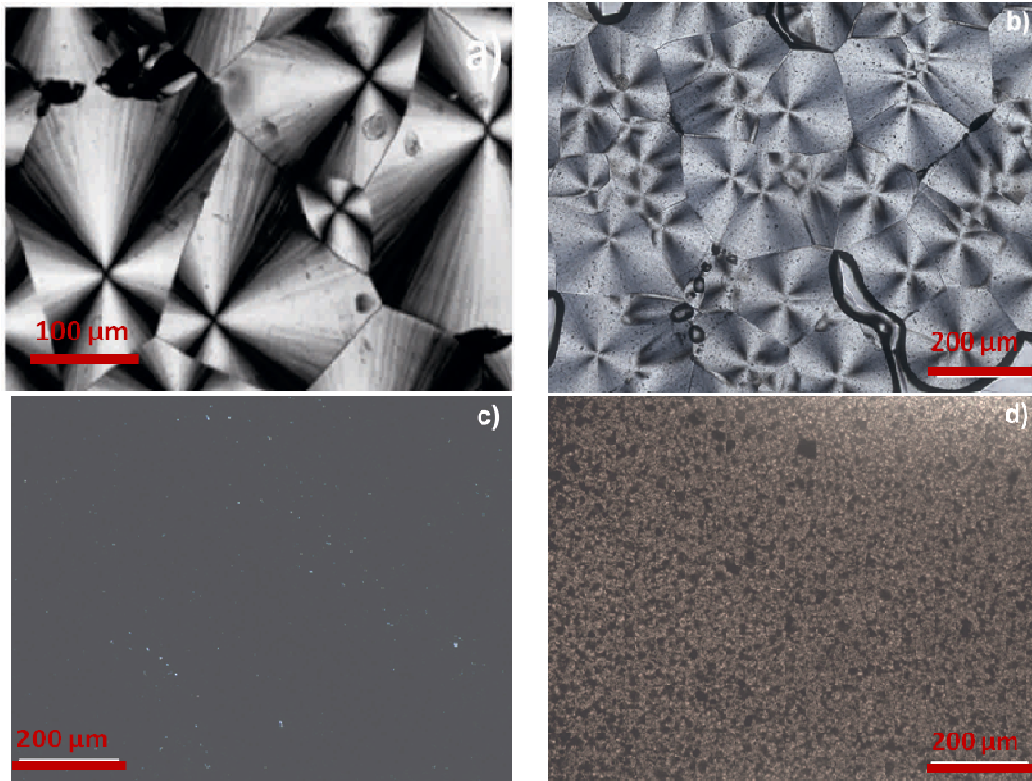
Figure 3.2 – Spherulitic structure of the samples crystallized at 155 ºC: (a) pure PVDF, (b) 0.1% of $CoFe_2O_4$, (c) 5% of $CoFe_2O_4$ and (d) 5% of $NiFe_2O_4$.

3.3.3   Crystallization kinetics

All the crystallization experiments were conducted on a single sample that was not removed from the sample holder of the DSC at any time. In this way, after the first melting, reproducibility is excellent, for instance the uncertainty in the exothermal peak position is smaller than 0.5% while the uncertainty in the crystalline fraction determined by integration of the peak was smaller than 1%. Reproducibility in the case of a series of different samples was tested by encapsulating 3 samples of the same nanocomposite composition and subjecting them to melting and subsequent isothermal crystallization. Uncertainty is still smaller than 1% in peak position and smaller than 2% in the crystalline fraction. This fact is also an indication of the good dispersion of the nanoparticles in the nanocomposite.

Typical DSC thermograms of pure PVDF and the nanocomposites with different ferrite content are presented in Figure 3.3.
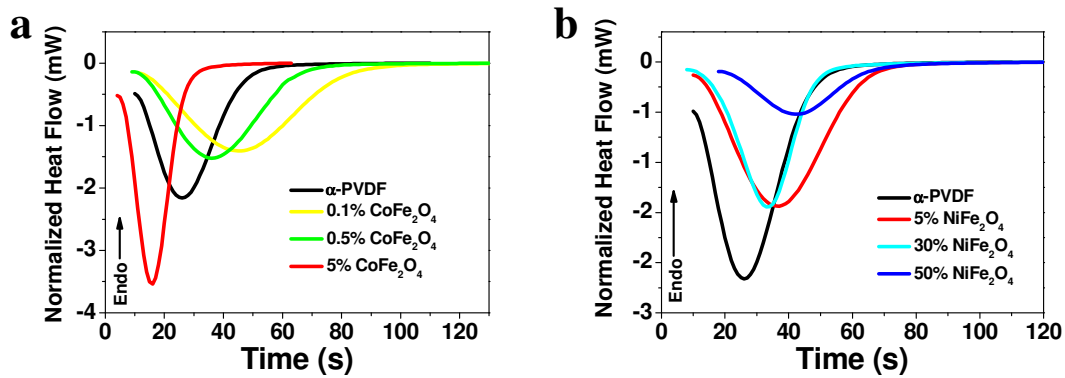
Figure 3.3 – Crystallization thermograms at 145ºC for PVDF/ferrite composites with different ferrite concentration: (a) $CoFe_2O_4$ and (b) $NiFe_2O_4$.

Figure 3.3 shows the complex effect of the presence of nanoparticles on PVDF crystallization. In the case of the 145 ºC crystallization isotherms of the nanocomposites containing $NiFe_2O_4$ nanoparticles (Figure 3.3b) the maximum of the exothermic peak shifts towards longer times as nanoparticle content increases. Nevertheless, this behaviour is not the same at higher temperatures, where the peak shifts to longer times for low particles content but then to shorter times for further filler content increase. For instance, at 155 ºC the exothermic peak for the sample containing 50 wt.%. $NiFe_2O_4$ nanoparticles is situated at the same crystallization time than the one observed in pure PVDF (results not shown). The crystalline fraction was calculated from the area of the exotherms, assuming a value for the melting enthalpy of the 100% crystalline α-PVDF is 93.07 J/g [35]. The crystalline fraction slightly decreases with increasing crystallization temperature. Table 3.1 collects the values corresponding to 145 and 155 ºC. The crystalline PVDF fraction in the sample clearly decreases as the $NiFe_2O_4$ nanoparticles increases. The behaviour of the nanocomposites containing $CoFe_2O_4$ particles is quite different: the melting enthalpy with the smallest amount of particles increases with respect to pure PVDF decreasing for further increasing nanoparticle content to reach values slightly below that of pure PVDF for the sample containing 5 wt.% of $CoFe_2O_4$.

Table 3.1 – Evolution of the polymer matrix enthalpy for the PVDF nanocomposites.

Sample	ΔH_m at 145ºC (J/g)	ΔH_m at 155ºC (J/g)
PVDF	0.58	0.52
0.1% $CoFe_2O_4$	0.67	0.57
0.5% $CoFe_2O_4$	0.56	0.49
5% $CoFe_2O_4$	0.55	0.50
5% $NiFe_2O_4$	0.53	0.48
30% $NiFe_2O_4$	0.48	0.34
50% $NiFe_2O_4$	0.36	0.25

The position of the exothermic crystallization peak of the 0.1 wt.% $CoFe_2O_4$ sample at 145 ºC shifts towards longer times and then monotonously shifts towards shorter times as the nanoparticles content increases (Figure 3.3a). As for the $NiFe_2O_4$ nanocomposites, this behaviour varies with increasing crystallization temperatures.

The interpretation of the peak shift in isothermal crystallization is not straightforward. Further, the correlation between the position of the peak and its broadness makes difficult to analyze changes in the shape of the thermogram with nanocomposite composition or temperature. In the case of nanocomposites, mass crystallization kinetics depends on nucleation, interaction between polymer chains and nanoparticles surfaces, possible distortion of spherulite growth due to the presence of particles, co-existence of two crystalline phases with possibly different nucleation and crystal growth rates.

The bell form of the peaks suggests a primary crystallization with no obvious secondary crystallization happening at later stages of isothermal crystallization process. Additionally, it can be observed that the crystallization isotherms show the typical sigmoid shape [17].

The crystallization kinetics has been frequently analyzed using Avrami model [20-21]. The theoretical background of the model relies on the probability of a given point of the polymer mass to be occupies by growing crystals, considered as spheres whose diameters growth at a given rate and that start growing with a given time dependence. In this way, the theory does not allow accounting for all the subtle details involved in nucleation and growth in a multicomponent system like the nanocomposites and thus it is difficult to correlate the values of the equation parameters with the nanocomposite structure. Nevertheless, it has been shown that it is a very convenient phenomenological equation to

describe isothermal crystallization and it will be used in this work to understand the complex nanoparticles content dependence of the crystallization thermograms. The X_t as a function of crystallization temperature T_c, can be defined as [20-21] :

$$X_t = \frac{\int_0^t \left(\frac{\partial H}{\partial t}\right)\partial t}{\int_0^\infty \left(\frac{\partial H}{\partial t}\right)\partial t} \qquad \textbf{(3.2)}$$

where $\frac{\partial H}{\partial t}$ is the DSC heat flow. The numerator represents the enthalpy at a given time t and the denominator is the total exothermal enthalpy. The Avrami equation is stated as:

$$1 - X_t = \exp(-Kt^n)$$

$$\textbf{(3.3)}$$

n in pure polymers has been correlated to the nature of the nucleation and growth geometry of the crystals), and K is a rate constant involving both nucleation and growth rate parameters [20-21]. Equation 3.3 is applicable only if the nucleation and growth conditions do not change during the crystallization [20-21, 36].

The Avrami exponent can be easily determined if equation (3.3) is linearized

$$\ln[-\ln(1 - X_t)] = \ln K + n \ln t \qquad \textbf{(3.4)}$$

Equation 3.4 shows that n is the slope of the plot of $\ln[-\ln(1 - X_t)]$ against lnt. Figure 3.4 shows this representation for PVDF (Figure3.4a) and the nanocomposite containing 50 wt.% of $NiFe_2O_4$ (Figure 3.4b). Interestingly, the temperature dependence of the slope of these curves is quite different in both materials: while in PVDF it increases slightly at low crystallization temperatures and then stabilizes, in the nanocomposite it clearly decreases with temperature after going through a maximum. The values of the Avrami index n are shown in Figure 3.4 for each temperature.
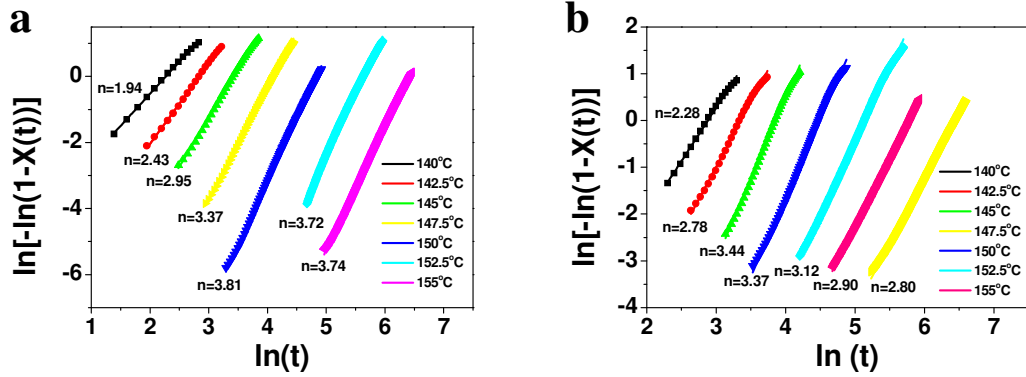
Figure 3.4 – Plots of $\ln\left[-\ln(1 - X_t)\right]$ against $\ln t$ performed in the (a) CoFe2O4 and (b) NiFe$_2$O$_4$ samples crystallized at different temperatures (indicated in the plots) to calculate the Avrami exponent from the fitting with equation 3.4.

Nevertheless, linearization of equation 3.3 with the double logarithmic expression of equation 3.4 gives different statistical weight to the different parts of the thermogram [37]. Non-linear least squares fitting of the measured thermograms were proposed in previous papers to determine both K and n in equation 3.3. The heat flow per unit mass, taking into account equation 3.2, can be expressed as:

$$q(t) = \phi_c^{\infty} \frac{\rho_c}{\rho} \Delta H_m \frac{\partial X_t}{\partial t} \tag{3.5}$$

where ρ_c and ρ are the density of the crystalline phase and the whole sample, respectively, ϕ_c^{∞} the maximum volume fraction of the crystalline phase obtained in the isothermal crystallization process [17].

The substitution of equation 3.3 into equation 3.5 gives an equation that can be compared with an experimental thermogram for a pair of parameter values (K, n) and thus K and n can be determined using a non-linear least-squares search routine.

The fitting results generated for the isothermal crystallization are shown in Figure 3.5. It can be observed that for the 145 ℃ isotherm, the fitting procedure can adjust the experimental data with high accuracy.
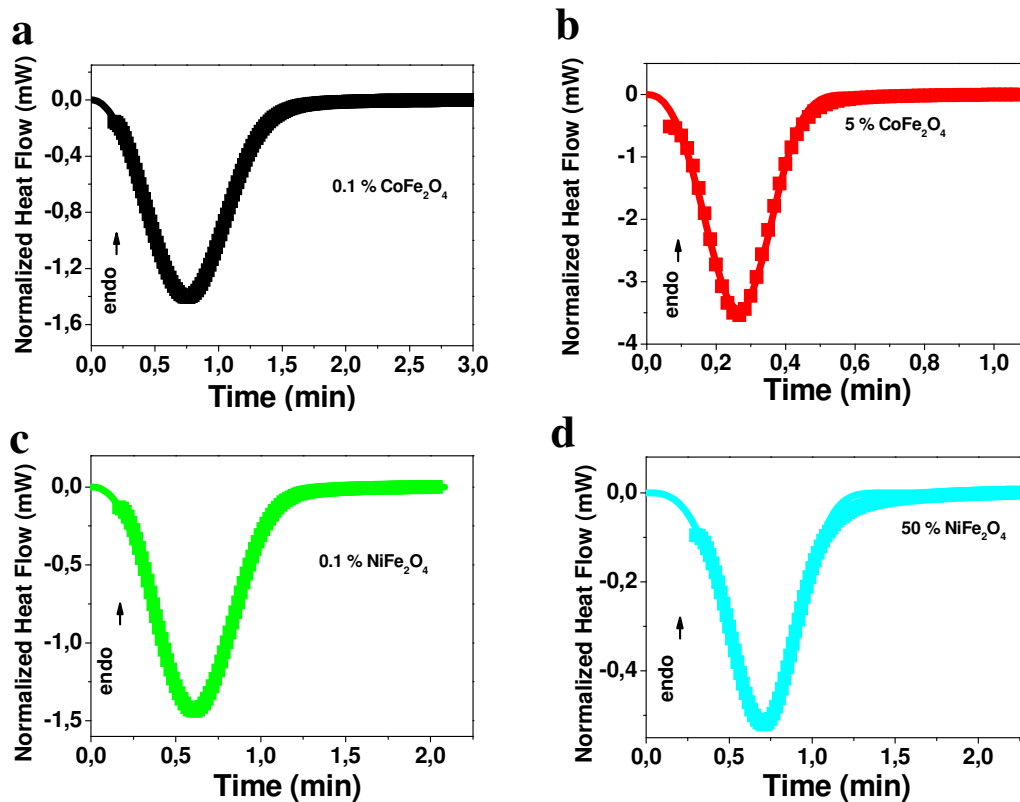
Figure 3.5 – Avrami fitting results for the PVDF samples with: (a) 0.1% CoFe$_2$O$_4$, (b) 5% CoFe$_2$O$_4$, (c) 5% NiFe$_2$O$_4$ and (d) 50% NiFe$_2$O$_4$. The dots correspond to the experimental data and the lines to the fitting at 145 ºC.

The results of the fitting procedure allow verifying the influence of the nanoparticles in the crystallization behaviour of PVDF (Figure 3.6). Figure 3.6 confirms that the crystallization kinetics of the pure α-PVDF polymer is quite different from the nanocomposite samples. The *n* parameter for PVDF is quite similar for all experimental temperatures higher than 145 ºC and has a value of approximately 3, already observed by other authors [17, 36]. The *n* value shows that the pure PVDF crystallizes in a spherulitic growth with athermal nucleation, characterized by the fact that all crystallization nuclei are already formed when the crystallization process starts. This fact is confirmed by optical microscopy by the fact that the intersections between most of the spherulites are straight lines (Figure 3.2).
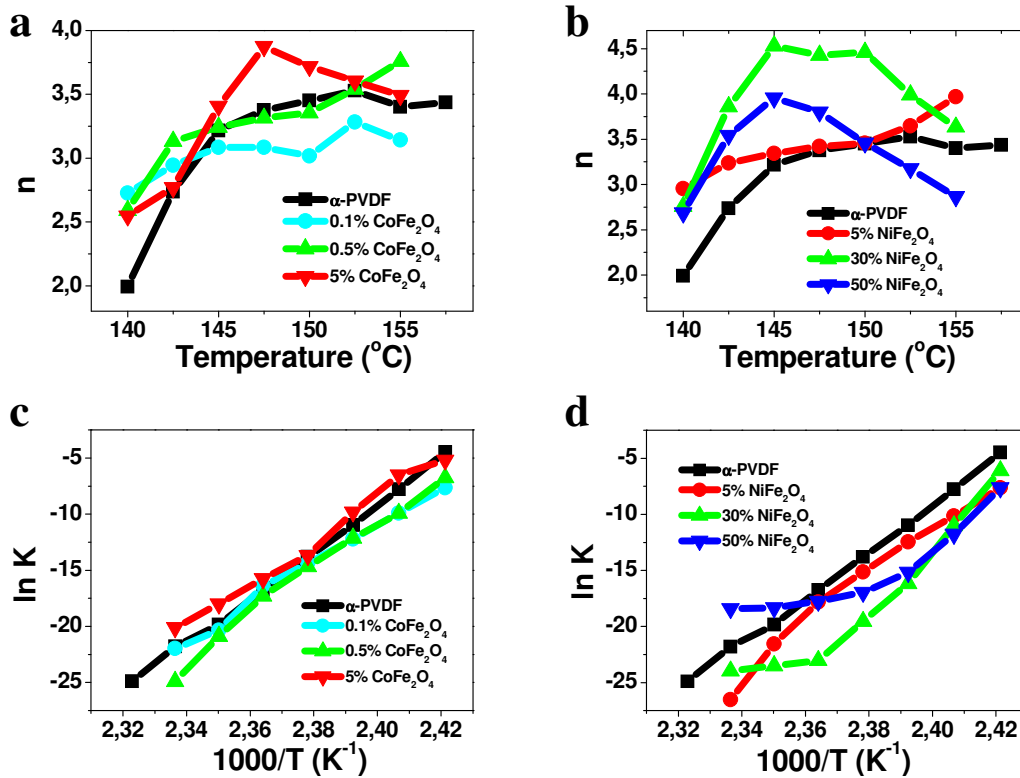
Figure 3.6 – Evolution of the Avrami parameters with the crystallization temperature for: (a) and (c) PVDF/CoFe$_2$O$_4$ and (b) and (d) PVDF/NiFe$_2$O$_4$, composites.

On the other hand, the temperature dependence of the Avrami exponent of the nanocomposites with low β-phase content is similar to that of pure α-PVDF, while in those in which a high fraction β-phase is forming (PVDF with 5 wt.% CoFe$_2$O$_4$ and with 30 and 50 wt.% NiFe$_2$O$_4$) the index n after going through a maximum around 147.5 ºC, clearly decreases with temperature. Changes in the temperature dependence of the kinetic constant from low to high β-phase contents in the nanocomposite can also be observed, in particular in Figure 3.6d, where the phase transformation is observed for larger nanoparticle contents.

Further, the t$_{1/2}$, defined as the time at which the extent of crystallization is 50% completed, can be obtained by equation 3.6:

$$t_{\frac{1}{2}} = \left(\frac{ln2}{k}\right)^{\frac{1}{n}} \tag{3.6}$$

Reciprocal half-time crystallization ($^1/_{t_{1/2}}$) can be considered approximately proportional to the crystallization growth rate (*G*).

Figure 3.7 shows the evolution of the $t_{1/2}$ for the pure polymer and for the nanocomposites samples with $CoFe_2O_4$ and $NiFe_2O_4$ both as a function of crystallization temperature and concentration for several temperatures.
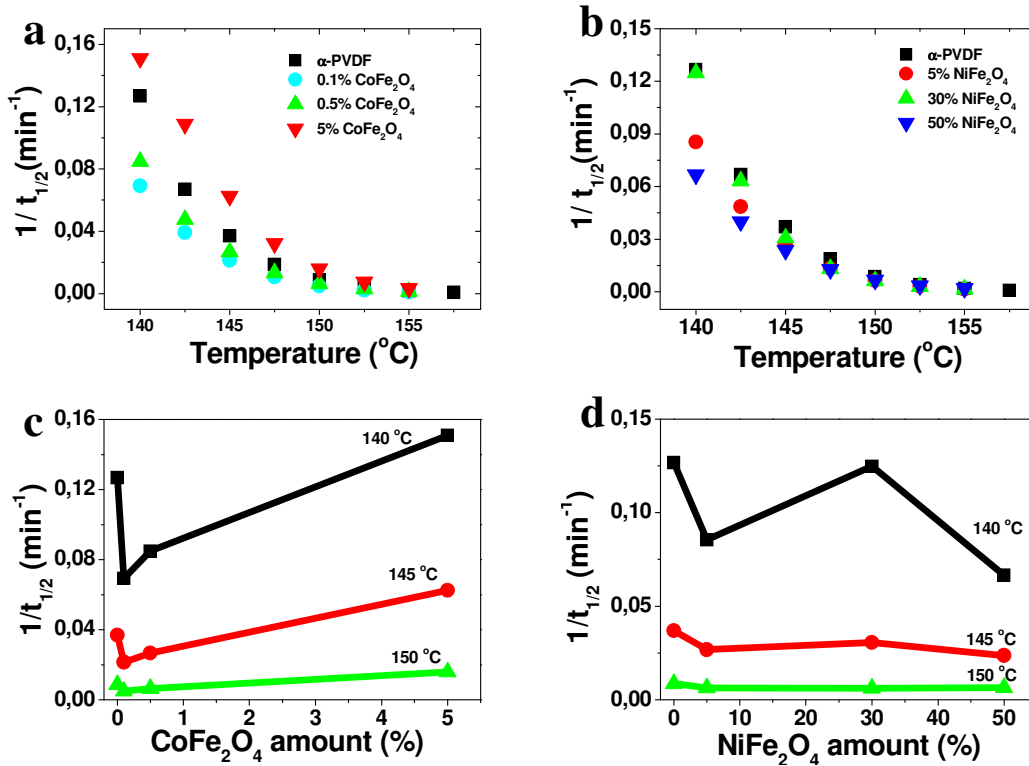
Figure 3.7 – Reciprocal half-time of the crystallization as a function of the crystallization temperature (above) and nanoparticle concentration for several crystallization temperatures (below) for the: PVDF/$CoFe_2O_4$ (a and c) and PVDF/$NiFe_2O_4$ (b and d) nanocomposites.

From the obtained values of $t_{1/2}$ it seems that the inclusion of the nanoparticles affect the overall crystallization rate of the nanocomposites when compared to the crystallization rate of the α-PVDF. For the $CoFe_2O_4$ nanocomposites with higher amount of nanoparticles (F(β) = 87%) the crystallization rate is higher than for the pure PVDF, suggesting that the overall crystallization rate of the nanocomposite samples is affected by the crystalline phase of the polymeric matrix. Same result is observed for the samples with $NiFe_2O_4$ nanoparticles.

3.4   Discussion

The presence of $CoFe_2O_4$ and $NiFe_2O_4$ nanoparticles induce PVDF crystallization in β-phase but the fraction of filler nanoparticles needed to produce the same β- to α-phase ratio in crystallized PVDF is one order of magnitude higher in the case of $NiFe_2O_4$ particles than in $CoFe_2O_4$. This phenomenon was not shown by nanoparticles with other chemical structure such as Ag [34] and $Pb(Zr_{0.53}Ti_{0.47})O_3$ [38]. Obviously interaction between nanoparticles and PVDF chains induce the *all trans* conformation in PVDF segments and this structure then propagates in crystal growth. Thus, induction of morphology changes in PVDF crystallization must be some way related to crystal nucleation. In this work, in addition to demonstrate by FTIR the progressive change of crystalline morphology with the presence of a fraction of these nanoparticles, we looked for changes in physical properties related to nucleation kinetics. That nucleation is enhanced by the presence of nanoparticles is clear from the polarized light microscopy that shows an increasing number of spherulites (and thus of crystallization nuclei) as the fraction of nanoparticles increases. It is interesting to observe that as for the ratio of β to α-phases, to obtain the same effect, i.e., the same increase in spherulite number, a larger fraction of $NiFe_2O_4$ particles than of $CoFe_2O_4$ ones is required (Figures 3.2c and 3.2d). This feature still supports the role of nucleation in β-phase generation. On the other hand nucleation plays an important role in the kinetics of mass crystal growth that was determined by DSC. In principle, for the same crystal growth rate, mass growth rate should increase for increasing nucleation at least in the first period of crystallization when spherulites still do not touch each other. But this is not what the DSC results show. It is clearly observed in the case of $NiFe_2O_4$ particles that in spite of the increase of nucleation shown by light microscopy, mass crystallization rates decrease with nanoparticle contents as shown in Figure 3.3b. A deeper analysis at the light of the Avrami equation shows that an important change in Avrami's exponent occurs, that at 145ºC goes from around 3 in PVDF to 4.5 in the nanocomposites with $NiFe_2O_4$ particles, with a simultaneous changes in the kinetic constant K. Trying to correlate these dependence of the macroscopic parameters of the Avrami equation with microscopic characteristics of nanoparticle-polymer chain interaction will be few more than speculation because both nucleation kinetics and interaction of the growing crystals with the nanoparticles (note the high number of particles per unit volume in these nanocomposites) can produce changes in kinetic parameters that can have opposite effects of crystal growth rate. Nevertheless, the

Pedro Martins

results show how important is the effect of the presence of nanoparticles. Another interesting point is the important decrease of crystalline fraction of PVDF with increasing $NiFe_2O_4$ nanoparticles content. This means that an important fraction of polymer chains are confined in interphases with the filler particle and are impossible to diffuse to incorporate to the growing crystals. All these phenomena appear in the $CoFe_2O_4$ nanocomposites as well but changes both in n and in K are smaller what shows how the large amount of $NiFe_2O_4$ nanoparticles hinders polymer chain reorganizations. It is to notice at this point that the size of the nanoparticles may play an important role in this issue, being the average size of the $NiFe_2O_4$ particles one half on the size of the $CoFe_2O_4$ particles. These facts are in contrast to other fillers such as silica nanoparticles [27], carbon black [31] and vapour grown carbon nanofibers that are reported to increase polymer degree of crystallinity [33].

3.5   Conclusions

In this investigation has been proven that the presence of $Co\,Fe_2O_4$ and $NiFe_2O_4$ nanoparticles induce PVDF crystallization in β-phase but the fraction of filler nanoparticles needed to produce the same β- to α-phase ratio in crystallized PVDF is one order of magnitude higher in the case of $NiFe_2O_4$ particles than in $Co\,Fe_2O_4$. The interaction between nanoparticles and PVDF chains induce the *all trans* conformation in PVDF segments and this structure then propagates in crystal growth. In this way, ME composites taking advantage of the piezoelectric response of β-PVDF and the magnetostrictive response of the ferrite nanoparticles can be prepared. The nucleation kinetics is enhanced by the presence of nanoparticles, as there are an increasing number of spherulites with increasing nanoparticle content. A deeper analysis at the light of the Avrami equation shows that an important change in the Avrami's exponent occurs with increasing nanoparticle content. Finally, it is observed that an important decrease of crystalline fraction of PVDF with increasing nanoparticles content, indicating that an important fraction of polymer chains are confined in interphases with the filler particle and are impossible to diffuse to incorporate to the growing crystals.

3.6 References

1. Priya, L. and J.P. Jog, *Poly(vinylidene fluoride)/clay nanocomposites prepared by melt intercalation: Crystallization and dynamic mechanical behavior studies.* Journal of Polymer Science Part B: Polymer Physics, 2002. **40**(15): p. 1682-1689.

2. Murayama, N., et al., *The strong piezoelectricity in polyvinylidene fluroide (PVDF).* Ultrasonics, 1976. **14**(1): p. 15-24.

3. Sencadas, V., R. Gregorio, and S. Lanceros-Méndez, *α to β Phase Transformation and Microestructural Changes of PVDF Films Induced by Uniaxial Stretch.* Journal of Macromolecular Science, Part B: Physics, 2009. **48**(3): p. 514 - 525.

4. Fukada, E., *History and recent progress in piezoelectric polymers.* Ultrasonics, Ferroelectrics and Frequency Control, IEEE Transactions on, 2000. **47**(6): p. 1277- 1290.

5. Lovinger, A.J., *Ferroelectric Polymers.* Science, 1983. **220**(4602): p. 1115-1121.

6. Sencadas, V., R. Gregorio Filho, and S. Lanceros-Mendez, *Processing and characterization of a novel nonporous poly(vinilidene fluoride) films in the [beta] phase.* Journal of Non-Crystalline Solids, 2006. **352**(21-22): p. 2226-2229.

7. Martins, P., et al., *Local variation of the dielectric properties of poly(vinylidene fluoride) during the [alpha]- to [beta]-phase transformation.* Physics Letters A, 2009. **373**(2): p. 177-180.

8. He, L., et al., *Effect of multi-walled carbon nanotubes on crystallization, thermal, and mechanical properties of poly(vinylidene fluoride).* Polymer Composites, 2010. **31**(5): p. 921-927.

9. Koga, K., et al., *Crystallization, field-induced phase transformation, thermally induced phase transition, and piezoelectric activity in P(vinylidene fluoride-TrFE) copolymers with high molar content of vinylidene fluoride.* Journal of Applied Physics, 1990. **67**(2): p. 965-974.

10. Sadeghi, F. and A. Ajji, *Study of crystal structure of (polyvinylidene fluoride/clay) nanocomposite films: Effect of process conditions and clay type.* Polymer Engineering & Science, 2009. **49**(1): p. 200-207.

11. Andrew, J.S. and D.R. Clarke, *Enhanced Ferroelectric Phase Content of Polyvinylidene Difluoride Fibers with the Addition of Magnetic Nanoparticles.* Langmuir, 2008. **24**(16): p. 8435-8438.

12. Martins, P., C. Costa, and S. Lanceros-Mendez, *Nucleation of electroactive beta-phase poly(vinilidene fluoride) with CoFe(2)O(4) and NiFe(2)O(4) nanofillers: a new method for the preparation of multiferroic nanocomposites.* Applied Physics A: Materials Science & Processing, 2011. **103**(1): p. 233-237.

13. Hill, N.A., *Why Are There so Few Magnetic Ferroelectrics?* The Journal of Physical Chemistry B, 2000. **104**(29): p. 6694-6709.

14. G.C. Papaefthymiou, S.R. Ahmed, and P. Kofinas, *Magnetic and Structural Characterization of CoFe2O4 Nanoparticles encapsulated within Block Copolymer Films.* Reviews on advanced materials science, 2005. **10**(4): p. 306-313.

15. Dillon, D.R., et al., *On the structure and morphology of polyvinylidene fluoride-nanoclay nanocomposites.* Polymer, 2006. **47**(5): p. 1678-1688.

16. Mago, G., F.T. Fisher, and D.M. Kalyon, *Deformation-Induced Crystallization and Associated Morphology Development of Carbon Nanotube-PVDF Nanocomposites.* Journal of Nanoscience and Nanotechnology, 2009. **9**: p. 3330-3340.

17.   Silva, M.P., et al., *alpha- and gamma-PVDF: Crystallization kinetics, microstructural variations and thermal behaviour.* Materials Chemistry and Physics, 2010. **122**(1): p. 87-92.

18.   Silva, M.P., et al., *[alpha]- and [gamma]-PVDF: Crystallization kinetics, microstructural variations and thermal behaviour.* Materials Chemistry and Physics, 2010. **122**(1): p. 87-92.

19.   Di Lorenzo, M.L. and C. Silvestre, *Non-isothermal crystallization of polymers.* Progress in Polymer Science, 1999. **24**(6): p. 917-950.

20.   Avrami, M., *Kinetics of Phase Change. I General Theory.* The Journal of Chemical Physics, 1939. **7**(12): p. 1103-1112.

21.   Avrami, M., *Granulation, Phase Change, and Microstructure Kinetics of Phase Change. III.* The Journal of Chemical Physics, 1941. **9**(2): p. 177-184.

22.   Ozawa, T., *Kinetics of non-isothermal crystallization.* Polymer, 1971. **12**(3): p. 150-158.

23.   Xiu Ling Zhu, et al., *Non-isothermal Crystallization Kinetics and Nucleation Activity of Filler in Polypropylene/Microcrystalline Cellulose Composites.* Iranian Polymer Journal, 2008. **17**: p. 297.

24.   López, L.C., G.L. Wilkes, and J.F. Geibel, *Crystallization kinetics of poly(p-phenylene sulphide): the effect of branching agent content and endgroup counter-atom.* Polymer, 1989. **30**(1): p. 147-155.

25.   Xu, W., M. Ge, and P. He, *Nonisothermal crystallization kinetics of polypropylene/montmorillonite nanocomposites.* Journal of Polymer Science Part B: Polymer Physics, 2002. **40**(5): p. 408-414.

26.   Jiasheng, Q. and H. Pingsheng, *Non-isothermal crystallization of HDPE/nano-SiO$_2$; composite .* Journal of Materials Science, 2003. **38**(11): p. 2299-2304.

27.   Kim, S.H., S.H. Ahn, and T. Hirai, *Crystallization kinetics and nucleation activity of silica nanoparticle-filled poly(ethylene 2,6-naphthalate).* Polymer, 2003. **44**(19): p. 5625-5634.

28.   Manna, S., S.K. Batabyal, and A.K. Nandi, *Preparation and Characterization of Silver−Poly(vinylidene fluoride) Nanocomposites: Formation of Piezoelectric Polymorph of Poly(vinylidene fluoride).* The Journal of Physical Chemistry B, 2006. **110**(25): p. 12318-12326.

29.   Kim, G.H., S.M. Hong, and Y. Seo, *Piezoelectric properties of poly(vinylidene fluoride) and carbon nanotube blends: [small beta]-phase development.* Physical Chemistry Chemical Physics, 2009. **11**(44): p. 10506-10512.

30.   Chen, X., et al., *Isothermal crystallization kinetics of poly(butylene terephthalate)/attapulgite nanocomposites.* Journal of Polymer Science Part B: Polymer Physics, 2006. **44**(15): p. 2112-2121.

31.   Zhang, G.Q., et al., *Thermodynamics Properties and Isothermal Crystallization Kinetics of Carbon Black/Poly(ethylene terephthalate) Composites.* Journal of Composite Materials, 2007. **41**(12): p. 1477-1485.

32.   Raka, L., A. Sorrentino, and G. Bogoeva-Gaceva, *Isothermal crystallization kinetics of polypropylene latex–based nanocomposites with organo-modified clay.* Journal of Polymer Science Part B: Polymer Physics, 2010. **48**(17): p. 1927-1938.

33.   Costa, P., et al., *The effect of fibre concentration on the [alpha] to [beta]-phase transformation, degree of crystallinity and electrical properties of vapour grown carbon nanofibre/poly(vinylidene fluoride) composites.* Carbon, 2009. **47**(11): p. 2590-2599.

34.   Miranda, D., et al., *Influence of Silver Nanoparticles Concentration on the - to - Phase Transformation and the Physical Properties of Silver Nanoparticles Doped*

Poly(vinylidene fluoride) Nanocomposites. Journal of Nanoscience and Nanotechnology, 2009. **9**: p. 2910-2916.

35. Nalwa, H.S., *Ferroelectric Polymers: Physics, Chemistry and Applications.* Vol. 1. 1995, London: M. Dekker, Inc.

36. Mancarella, C. and E. Martuscelli, *Crystallization kinetics of poly(vinylidene fluoride).* Polymer, 1977. **18**(12): p. 1240-1242.

37. Strobl, G.R., *Physics of polymers: concepts for understanding theirs structures and behavior.* 1997, Berlin: Springer.

38. Costa, C.M., et al., *Influence of processing parameters on the polymer phase, microstructure and macroscopic properties of poly(vinilidene fluoride)/Pb(Zr0.53Ti0.47)O3 composites.* Journal of Non-Crystalline Solids, 2010. **356**(41-42): p. 2127-2133.

Pedro Martins

4 Correlation between crystallization kinetics and electroactive polymer phase nucleation in PVDF/ferrite magnetoelectric nanocomposites
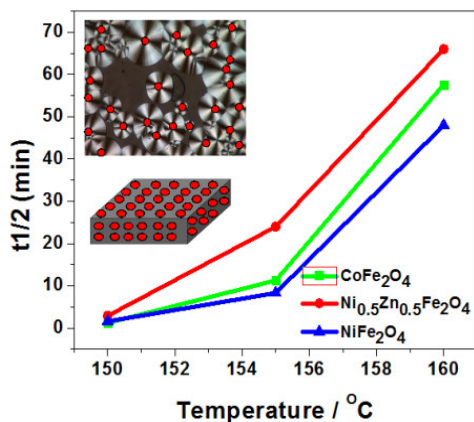
Poly(vinylidene fluoride) (PVDF) nanocomposites with different ferrite nanoparticle loadings are interesting as, depending on ferrite type and content, the electroactive β-phase of the polymer is nucleated and the magnetoelectric coupling is induced. The isothermal crystallization behaviour of PVDF/ferrite nanocomposites is studied using Polarized optical microscopy (POM) and the crystallization kinetic is analyzed by the Avrami theory in order to understand the crystallization conditions leading to the nucleation of the electroactive polymer phase. It is found that the nucleation kinetics is enhanced by the presence of ferrite nanoparticles. The crystallization velocity is intimately related to the polymer α or β−phase formation in the nanocomposites and follows the order: PVDF/$NiFe_2O_4$> PVDF/$CoFe_2O_4$>PVDF/$Ni_{0.5}Zn_{0.5}Fe_2O_4$ for a given temperature and nanoparticle loading.

4.1 Introduction

PVDF and its composites are intensively studied due to their excellent piezoelectric, pyroelectric and ferroelectric properties [1-3].

These properties combined with high elasticity and easy processability make this material interesting for numerous technological applications [4].

Also interesting in this polymer is its polymorphism, showing four different crystalline forms, named α, β, δ and γ, which appear depending on the processing conditions [5]. The α and β phases are the most studied polymorphs. The non-polar α-phase is the most common one as it is obtained when the polymer is cooled from the melt at moderated or high cooling rates and therefore is the one readily obtained in conventional processing polymer methods such as extrusion [6-8].

The ferroelectric β-phase has a non-zero dipole moment and is widely used in technological applications such as sensors, actuators, batteries and membranes due to its exceptional electroactive properties among polymer materials [9-11]. β-PVDF is usually obtained by stretching α-phase films at stretch ratios from 3 to 5 at controlled temperature between 70°C and 100°C [15].

β-phase samples can also be obtained by solvent casting methods when the material is crystallized at temperatures below 70°C, but the samples reveal high porosity [7], showing therefore poor mechanical and electrical properties and compromising the applicability of these materials.

Consequently, strong efforts are being undertaken to develop easy to process, stable and non-porous β-PVDF. Some examples of these approaches are the crystallization under high pressure, the use of copolymers such as P(VDF-TrFE) or the incorporation of nanoclays into PVDF [16-18].

A more recent and interesting approach is the nucleation of the electroactive phase of the polymer by the incorporation of ferrite nanoparticles into PVDF [19-20]. Ferrite nanoparticles are usually used as the magnetostrictive phase in ME composites and are interesting both for fundamental studies and technological applications [20-21]. In this case, nanoparticles can be used both for inducing the electroactive phase of the polymer, when low particle loadings are used, or for the preparation of ME materials, for higher nanoparticle contents [20, 22]. In this way, the physical properties of PVDF depend not only upon the processing conditions but are also strongly influenced by the presence of such nanoparticles. The presence of the nanoparticles can determine the crystallized

phase and the resulting polymer microstructure and morphology [23] through variations, among other effects, in the crystallization kinetics [24]. In this way, it also interesting to study the influence of the nanoparticles in the crystallization kinetics both in order to study the interactions responsible for the variations in the crystallization kinetics and also in order to study the origin of the β-phase nucleation.

The influence of ferrite nanoparticles in the polymer crystallization kinetics has been previously addressed by measuring the crystallization kinetics of composites by means of isothermal experiments and cooling scans using DSC. It was concluded that the nucleation kinetics is enhanced by the presence of nanoparticles, as corroborated by the increasing number of spherulites and variations of the Avrami's exponent with increasing nanoparticle content [32]. Nevertheless, for further understand the nucleation effect, the variations in the crystallization kinetics is investigated in the present work by polarized optical microscopy in three different ferrites, $CoFe_2O_4$, $NiFe_2O_4$ and $Ni_{0.5}Zn_{0.5}Fe_2O_4$, with different electroactive phase nucleation ability and analyzing spherulite and microstructure evolution over ferrite type, concentration and crystallization temperature.

The different ferrites were chosen as, together with being all suitable for the development of ME materials, all of them have the ability to fully nucleate the β-phase of PVDF but with different concentration dependence, allowing therefore a complete study, understanding and control of the relation between the PVDF β-phase nucleation process and the polymer crystallization kinetics.

4.1.1 Crystallization kinetics

The isothermal crystallization kinetics of polymers is commonly analyzed within the Avrami theory, as represented by equation 4.1 [33-34]:

$$1 - X_t = \exp(-Kt^n) \qquad \textbf{(4.1)}$$

n depends on the nature of the nucleation and growth geometry of the crystals, K is a rate constant involving both nucleation and growth rate parameters and t is the crystallization time. Equation 4.1 can be applied just when the nucleation and growth conditions do not change during the crystallization [32-33].

From images like the ones presented in Figure 4.1, obtained by POM at regular time intervals during the crystallization process the time, t, evolution of the fraction (X_t) of the

material that crystallizes can be calculated from the evolution of the crystallized area as a function of time ($\partial A/\partial t$):

$$X_t = \frac{\int_0^t (\partial A/\partial t)\partial t}{\int_0^\infty (\partial A/\partial t)\partial t} \qquad \textbf{(4.2)}$$

where the numerator represents the crystallized area at a given time and the denominator is the total area of the fully crystallized material [35].

The crystallization half-time, $t_{1/2}$, defined as the time at which the extent of crystallization is 50%, can be obtained from equation 4.3 [32]:

$$t_{\frac{1}{2}} = \left(\frac{\ln 2}{K} \right)^{\frac{1}{n}} \qquad \textbf{(4.3)}$$

Finally, the activation energy of the crystallization process is obtained by applying the Arrhenius equation to the overall crystallization rate constant K, containing contributions from both nucleation and growth rate [35]:

$$K = A^{\left(-\frac{Eact}{RT_{crystallization}} \right)} \qquad \textbf{(4.4)}$$

where A is the pre-exponential factor, E_{act} is the activation energy of the crystallization process and R the ideal gas constant ($R = 8.31$ J mol^{-1} K^{-1}) [36-37].

4.2 Experimental

CoFe$_2$O$_4$, NiFe$_2$O$_4$ and Ni$_{0.5}$Zn$_{0.5}$Fe$_2$O$_4$ nanoparticles were purchased from *Nanoamor*, having dimensions between 35-55, 20-30 and 10-30 nm, respectively [38]. DMF (pure grade) was obtained from *Fluka* and PVDF (Solef 1010) powder was supplied by *Solvay*. All the chemicals and nanoparticles were used as received from the suppliers. For the preparation of the films, the initial concentration of the solution was 0.2 g of PVDF for 1ml of DMF. Then, the MF nanocomposites were prepared by adding the desired amount of nanoparticles to 12 ml of DMF and placing them in ultrasound bath during 6 h, to ensure that nanoparticles were well dispersed in the solution and to avoid aggregates.

Chapter 4

Then PVDF was added. The wt.% of the ferrite nanoparticles was varied from 0.001% to 50% corresponding to ϕ between 3×10^{-6} and 0.25.

The mixture was then placed in a Teflon mechanical stirrer for complete dissolution of the polymer and flexible films of ~50 μm were obtained by spreading the solution on a clean glass substrate. Solvent evaporation and polymer melting were obtained inside an oven at a controlled temperature of 210 ºC for 10 min. After this process, samples were crystallized by cooling down to room temperature.

Images of spherulitic growth during the crystallization of the PVDF nanocomposites were obtained by an OMPL (Leica DM 2500M) provided with a Leica DFC-295 camera. The hot plate used was a Linkam LTS350. Samples with different wt.% and ferrite type were measured during isothermal crystallization at 150, 155 and 160 ºC until complete crystallization to study the influence of temperature, ferrite type and ferrite concentration in the spherulitic growth.

4.3   Results

Figure 4.1 shows the nanocomposite microstructure after 5200s crystallization time obtained for samples of PVDF/CoFe$_2$O$_4$ with 0.01 wt.% of nanoparticles crystallized at different temperatures.
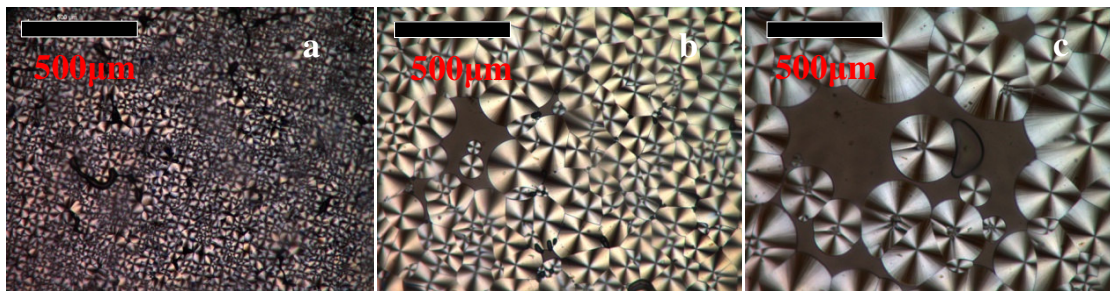
Figure 4.1 – Reciprocal Images of spherulitic growth for the PVDF/CoFe$_2$O$_4$ composite with 0.01 wt.% ferrite with 5200s crystallization time at: (a) 150 °C, (b) 155 °C and (c) 160 °C.

The sample crystallized at 150 °C shows the finest microstructure due to the faster crystallization. With increasing crystallization temperature the crystallization rate slows down and the diameter of the spherulites increases [35]. The same behaviour was found in the other PVDF/ferrite nanocomposites under investigation (images not shown).

The effect of ferrite concentration in the spherulite microstructure for a given filler concentration is shown in Figure 4.2 after 5200s crystallization time for semicrystalline

α-PVDF (Figure 4.2a) and PVDF/CoFe$_2$O$_4$ composites with cobalt ferrite loadings of 0.01 wt.% and 1 wt.%, respectively (Figure 4.2b and 4.2c) crystallized at 150 $^\circ$C.
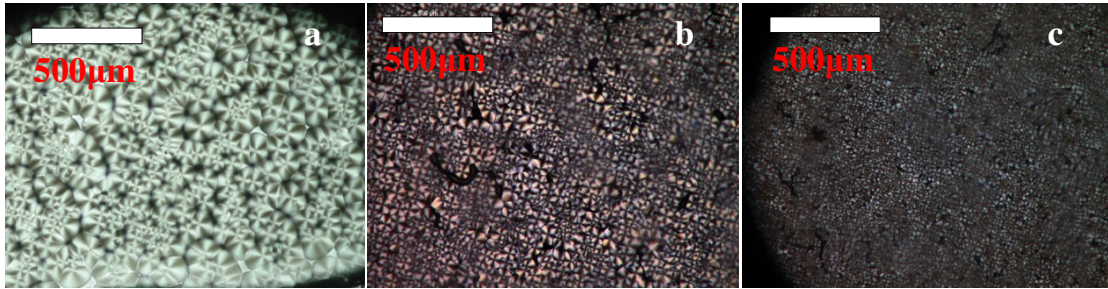
Figure 4.2 – Images of spherulitic growth for the PVDF/CoFe$_2$O$_4$ nanocomposites ferrite with 5200s crystallization time at 150 $^\circ$C with CoFe$_2$O$_4$ wt.%: (a) 0, (b) 0.01 and (c) 1.

The spherulites of PVDF present in all cases a compact and well-defined microstructure with the Maltese-cross texture typical for PVDF [32, 35]. The addition of even the smallest amount of cobalt ferrite nanoparticles increases the number of the spherulites, with the spherulite size decreasing strongly with increasing ferrite concentration for a given crystallization time and temperature (Figures 4.2b and 4.2c). These facts clearly indicate that the nanoparticles effectively act as nucleation agents. With further increasing CoFe$_2$O$_4$ nanoparticle content the number of nucleation points grows so much that spherulites cannot be formed. In fact, the sample containing 1 wt.% of CoFe$_2$O$_4$ (Figure 4.2c) shows almost no definite texture to be observed by polarized light microscopy. Higher particle concentrations turned the samples almost opaque. The results shown in Figure 4.2 are representative of all three ferrite nanocomposites (not shown).

The spherulitic microstructure of the different nanocomposites (PVDF/Ni$_{0.5}$Zn$_{0.5}$Fe$_2$O$_4$, PVDF/NiFe$_2$O$_4$ and PVDF/CoFe$_2$O$_4$) with 0.01 wt.% nanoparticle content crystallized at 160 $^\circ$C after 5200s crystallization time is represented in Figure 4.3.
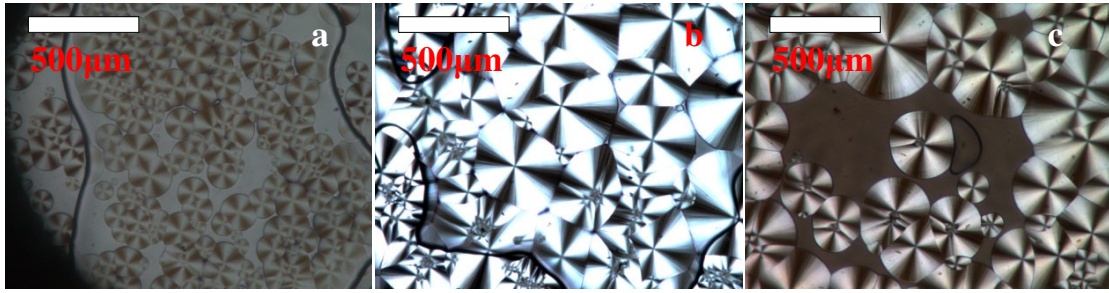
Figure 4.3 − Images of spherulitic growth for the PVDF/ferrite (0.01 wt.%) samples crystallized at 160 $^{\circ}$C with 5200s crystallization time: (a) $Ni_{0.5}Zn_{0.5}Fe_2O_4$, (b) $NiFe_2O_4$ and (c) $CoFe_2O_4$ nanoparticles.

The microstructure obtained at 160 ºC for the nanocomposite samples indicates that the PVDF/$NiFe_2O_4$ nanocomposite (Figure 4.3b) shows a higher crystallization rate than the PVDF/$Ni_{0.5}Zn_{0.5}Fe_2O_4$ and PVDF/$CoFe_2O_4$ nanocomposites (Figures 4.3a and 4.3c) once that the final microstructure is already achieved to the PVDF/$NiFe_2O_4$ nanocomposite at that crystallization time, contrary to what happens with PVDF/$Ni_{0.5}Zn_{0.5}Fe_2O_4$ and PVDF/$CoFe_2O_4$ nanocomposites.

As the crystallization rate increases, the PVDF chains change from the β to the α conformation [39-40], behaviour which is in agreement to previous studies [20, 32]. This fact suggests that the crystallization rate in the MF samples and consequently the α-phase nucleation ability follows the following order: PVDF/$NiFe_2O_4$> PVDF/$CoFe_2O_4$ > PVDF/$Ni_{0.5}Zn_{0.5}Fe_2O_4$.

The nucleation ability of the nanoparticles can be quantitatively estimated by the variation of the number of nucleus over time in the samples. This calculation was performed for the composites with 0.01 wt.% of ferrite nanoparticles for the three temperatures used in this study (Figure 4.4).
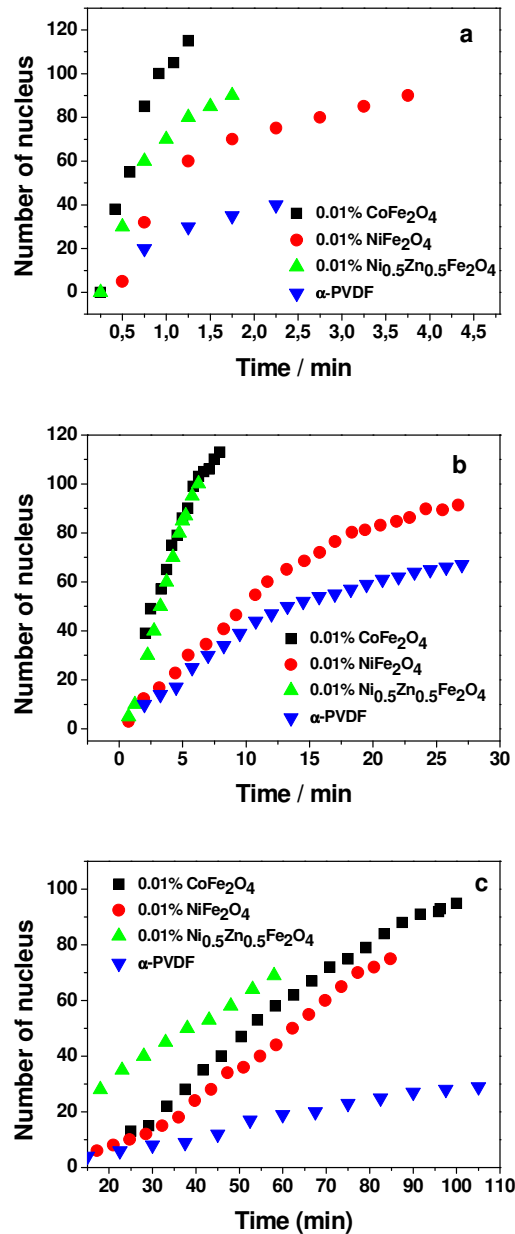
Figure 4.4 − Number of nucleus over time to PVDF /ferrite (0.01 wt.%) samples crystallized at (a) 150 °C, (b) 155 °C and (c) 160 °C.

It is observed that the addition of low nanoparticle contents abruptly increases the number of nucleus comparatively to pure α-PVDF. Further, the nucleation ability is higher in the $Ni_{0.5}Zn_{0.5}Fe_2O_4$ and $CoFe_2O_4$ nanoparticles with respect to $NiFe_2O_4$ ferrite nanoparticles, as corroborated by the larger number of nucleus in the PVDF/$Ni_{0.5}Zn_{0.5}Fe_2O_4$ and PVDF/$CoFe_2O_4$ nanocomposites. Finally, the increase in the crystallization temperature

has as a consequence the diminution in the number of nucleus generated, as observed in Figure 4.4.

4.4 Discussion

The crystallization kinetics was studied by analyzing the variation of the radius of the spherulites over time (Figure 4.5).
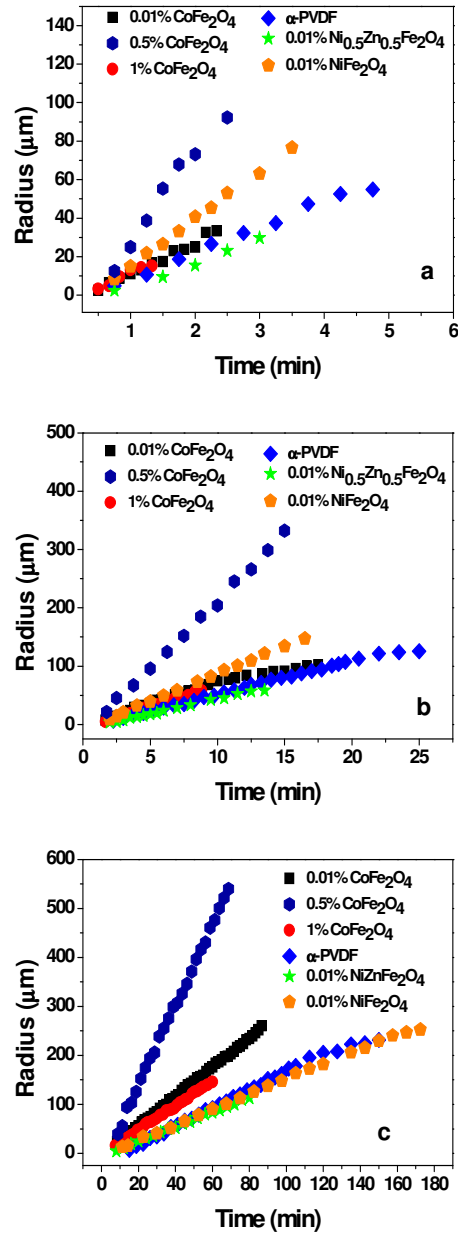
Figure 4.5 – Spherulitic growth to the different nanocomposites with crystallization temperatures: (a) 150ºC, (b) 155ºC and (c) 160ºC.

The data was evaluated during the time in which the spherulites growth independently, with no influence of the neighbouring growing spherulites.

For the lowest temperatures, the polymer crystallizes faster, giving rise to the smallest spherulites (Figure 4.1, 4.2 and 4.5). For higher temperatures, the crystallization process is slower and the diameter of the spherulites is larger [35].

The addition of $NiFe_2O_4$ and $CoFe_2O_4$ nanoparticles induces the formation of larger spherulites for a given ferrite concentration and crystallization time as compared to the incorporation of $Ni_{0.5}Zn_{0.5}Fe_2O_4$ nanoparticles in the polymer. This result is related to the higher number of nucleus found in the $PVDF/Ni_{0.5}Zn_{0.5}Fe_2O_4$ and $PVDF/CoFe_2O_4$ nanocomposites. Keeping all other parameters unchanged, higher number of nucleus implies smaller spherulites [41].

Plots of the relative crystallinity as a function of time (equation 4.2) are represented in the Figure 4.6 for different ferrite types, concentrations and crystallization temperatures.
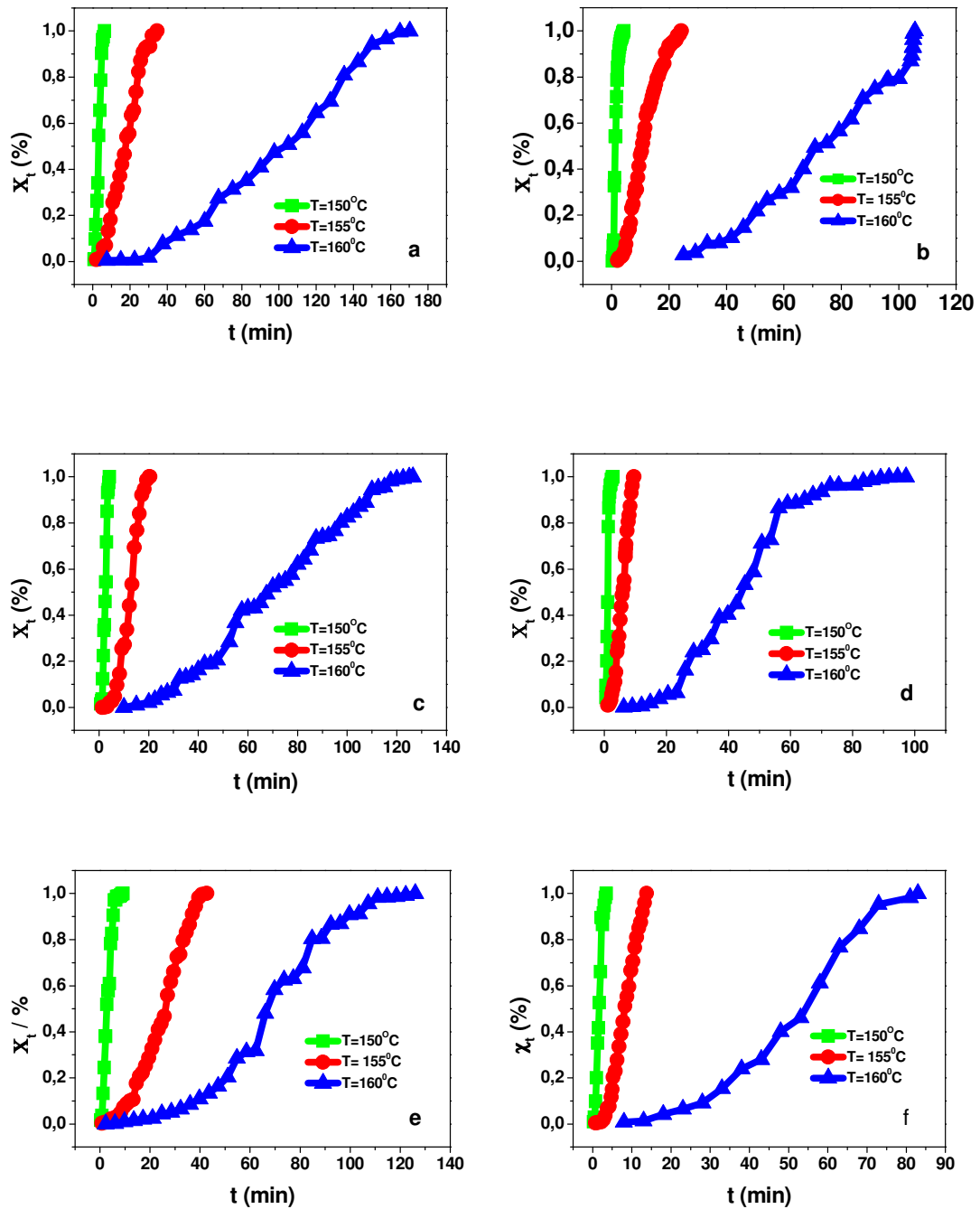
Figure 4.6 – Crystallization isotherms of the PVDF/ferrite nanocomposites for the different crystallization temperatures with: (a) α-PVDF, (b) PVDF/CoFe$_2$O$_4$ (0.01wt.%), (c) PVDF/CoFe$_2$O$_4$ (0.5wt.%), (d) PVDF/CoFe$_2$O$_4$ (1wt.%), (e) PVDF/Ni$_{0.5}$Zn$_{0.5}$Fe$_2$O$_4$ (0.01wt.%) and (f) PVDF/Ni$_{0.5}$Zn$_{0.5}$Fe$_2$O$_4$ (0.01wt.%).

All plots show the typical sigmoidal shape of the isothermal polymer crystallization [35]. Furthermore, the initial slope decreases with increasing crystallization temperature, indicating a progressively slower crystallization rate [32].

The initial slope is the highest for the $NiFe_2O_4$ nanocomposites and the lowest for the $Ni_{0.5}Zn_{0.5}Fe_2O_4$ samples. This fact confirms that the crystallization rate in the MF samples follows the following order: $PVDF/NiFe_2O_4 > PVDF/CoFe_2O_4 > PVDF/Ni_{0.5}Zn_{0.5}Fe_2O_4$.

After calculation of the relative crystallinity, Figure 4.7 displays the Avrami plots and respective fittings obtained from equation 4.5 for the nanocomposites at three different crystallization temperatures.
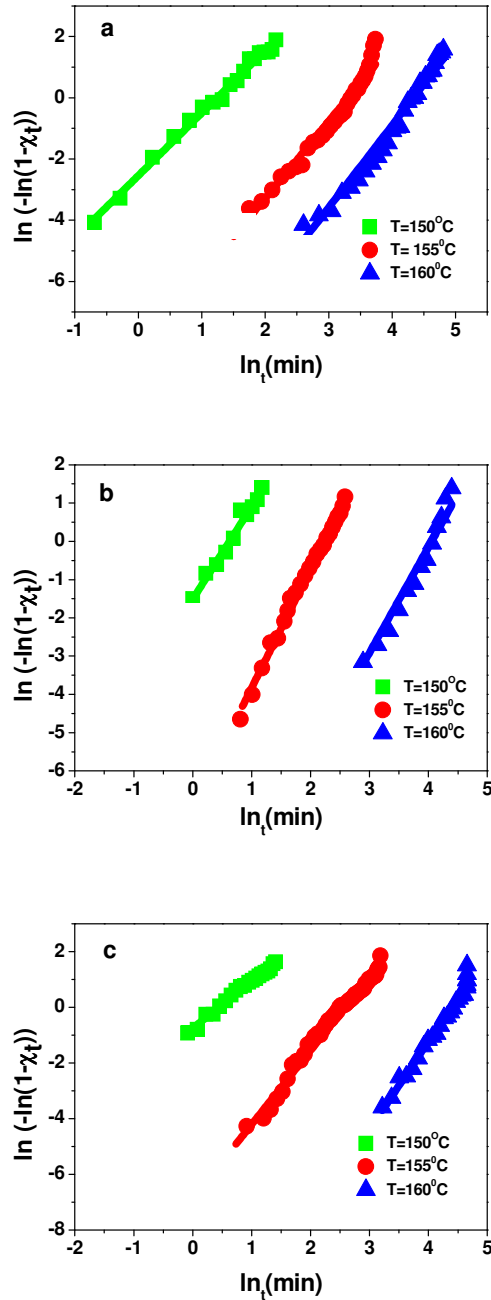
Figure 4.7 – Evolution of the crystallization rate at different temperature of the nanocomposite spherulites with: (a) $Ni_{0.5}Zn_{0.5}Fe_2O_4$, (b) $NiFe_2O_4$ and (c) $CoFe_2O_4$ nanoparticles.

The plot of

$$\ln\left[-\ln\left(1 - X_t\right)\right] = \ln K + n \ln t \qquad \textbf{(4.5)}$$

obtained by linearization of equation 4.1 produces a straight line with intercept and slope given by *ln K* and *n*, respectively. Typically, the Avrami equation represents correctly only the initial steps of polymer crystallization, characterized by a linear regime.

In the present case, the linear behaviour observed indicates that the Avrami equation properly describes the isothermal crystallization behaviour of the composite samples. All fittings show a linear fit with $R^2 > 0.99$.

Figure 4.8a shows the dependence of the Avrami exponent on crystallization temperature. In pure PVDF, a value of *n* close to 3 is obtained, which indicates that nucleation is heterogeneous and the growth of spherulites is tridimensional [42].
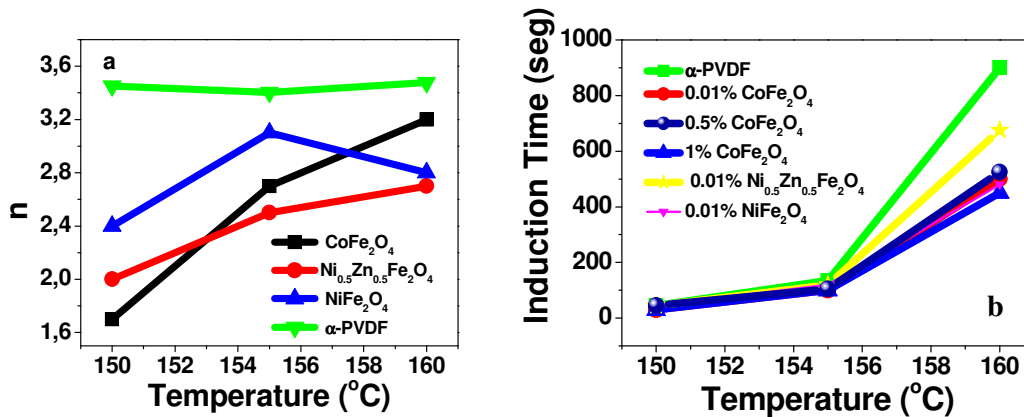
Figure 4.8 – (a) Evolution of the Avrami exponent with the crystallization temperature to PVDF/ferrite (0.01 wt.%); (b) Half-time of the crystallization as a function of the crystallization temperature.

With the addition of ferrite nanoparticles, at low crystallization temperatures *n* decreases by ~1, implying that the nucleation and growth of PVDF becomes two-dimensional [42]. The temperature dependence of the Avrami exponent in the same type of nanocomposites with higher loadings of ferrite nanoparticles has been recently reported, being approximately equal to that obtained for the α-PVDF sample [32].

Figure 4.8b shows the evolution of the induction time, defined as the period needed to form a critical nucleus during which no crystallinity is observed [43], for the pure polymer and for the ferrite nanocomposite samples as a function of the crystallization

temperature. A decrease in the induction time is observed with increasing ferrite wt.%, being this decrease more significant for the higher crystallization temperatures. The decrease of the induction time is associated to the nucleation rate, which is controlled by the availability and the concentration of the heterogeneous nuclei. As a result, ferrite nanoparticles in the polymeric matrix serve as heterogeneous nucleating sites and are more effective at higher temperatures due to the slower crystallization [44].

The decrease in the induction time with respect to the polymer matrix follows the order $PVDF/Ni_{0.5}Zn_{0.5}Fe_2O_4 > PVDF/CoFe_2O_4 > PVDF/NiFe_2O_4$.

For a pure polymer melt, the nucleation step involves the folding of polymer chains and the formation of solid surfaces that become the nuclei for crystallization [45]; the energy barrier for this process is usually very high. The existence of a foreign solid surface such as ferrite nanoparticles in the melt, as observed, anticipates the nucleation step [45].

The $t_{1/2}$ evolution with the crystallization temperature, calculated by equation 4.3, for the samples with 0.01% of ferrite content is represented in Figure 4.9.
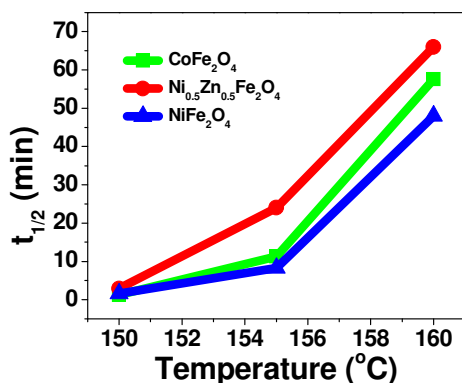
Figure 4.9 – $t_{1/2}$ vs crystallization temperature to PVDF/ferrite (0.01 wt.%) nanocomposites.

As expected, the crystallization half-time increases with increasing crystallization temperature.

Table 4.1 summarizes the crystallization parameters for the isothermal crystallization of PVDF and nanocomposites obtained from the fittings with Equation 4.1 and 4.5.

Table 4.1 – Avrami parameters obtained from the fittings with equation 4.1 and equation 4.5, describing the crystallization kinetic of PVDF nanocomposites upon isothermal crystallization from the melt.

Nanocomposite	Temperature [ºC]	n	K [min]	$t_{1/2}$ [min]	E_{act} [kJ mol^{-1}]
0.01% CoFe$_2$O$_4$	150	1.7	0.48	1.24	1.309
	155	2.7	0.001	11.28	
	160	3.2	8.87E-07	58	
0.01% NiZnFe$_2$O$_4$	150	2	0.08	2.9	1.392
	155	2.5	2.44E-04	24	
	160	2.7	8.60E-06	66	
0.01% NiFe$_2$O$_4$	150	2.4	0.22	1.6	1.473
	155	3.1	9.76E-04	8.3	
	160	2.8	1.38E-05	48	
0.5% CoFe$_2$O$_4$	150	3.5	0.03	2.5	1.509
	155	3.98	3.10E-05	12	
	160	3.1	1.50E-06	67	
1% CoFe$_2$O$_4$	150	2.93	0.49	1.12	1.838
	155	2.95	4.04E-03	5.72	
	160	3.3	2.76E-06	43	
α-PVDF	150	2.46	0.046	3	1.389
	155	2.36	8.81E-04	17	
	160	2.6	4.96E-06	95	

Although the incorporation of ferrite nanoparticles can induce heterogeneous nucleation and accelerate the isothermal crystallization of PVDF nanocomposites, nanoparticles may also restrict the movement of polymer chains, thereby making crystallization more difficult. The values of the crystallization activation energy are the combined results of the above two competing effects of nucleation and restriction [46]. The obtained value for the α-PVDF activation energy is in the same order of previous investigations [47-48]. Fine dispersion in the nanocomposite with 0.01 wt.% of $CoFe_2O_4$ was achieved and the nucleating effect of nanoparticles was most significant, thus its crystallization activation energy was the lowest. The increasing crystallization activation energy with increasing ferrite content results from the restriction of polymer chain movements caused by high ferrite loading [46].

In this way, additionally to previous investigations [32], the crystallization behaviour of the composite samples presented in this study and the obtained Avrami parameters show the higher nucleation ability and the lower crystallization velocity of the $Ni_{0.5}Zn_{0.5}Fe_2O_4$ and $CoFe_2O_4$ nanocomposites with respect to $NiFe_2O_4$ nanocomposites. This is in agreement with the PVDF β-phase nucleation ability of those three ferrites [20].

4.5   Conclusion

The isothermal crystallization behaviour from the melt and the growth kinetics of neat PVDF and ferrite nanocomposites were studied by POM.

The results indicated that the addition of ferrite nanoparticles leads to an increase of the nucleation kinetics of PVDF, which is ascribed to the nucleating effect of ferrite nanoparticles. The incorporation of ferrite nanoparticles increases the number of spherulites and thus decreases significantly the spherulite size of PVDF. The nucleation ability is higher for the $Ni_{0.5}Zn_{0.5}Fe_2O_4$ and $CoFe_2O_4$ nanoparticles with respect to $NiFe_2O_4$ nanoparticles and the crystallization rate in the MF samples was found to follow the following order: $PVDF/NiFe_2O_4$> $PVDF/CoFe_2O_4$ > $PVDF/Ni_{0.5}Zn_{0.5}Fe_2O_4$. Higher activation energies of the nanocomposites with respect to the one of neat PVDF can be attributed to the movement restriction of polymer chains caused by the presence of ferrite nanoparticles. In this way, the crystallization behaviour of the composite samples presented in this study and the obtained Avrami show the higher nucleation ability and the lower crystallization velocity of the $Ni_{0.5}Zn_{0.5}Fe_2O_4$ and $CoFe_2O_4$ nanocomposites

Pedro Martins

with respect to NiFe$_2$O$_4$ nanocomposites, which in turns results in a larger ability for the nucleation of the PVDF β-phase of those ferrites fillers.

4.6 References

1. Broadhurst, M.G. and G.T. Davis, *Physical basis for piezoelectricity in PVDF*. Ferroelectrics, 1984. **60**: p. 3-13.
2. Murayama, N., et al., *The Strong Piezoelectricity in Polyvinylidene Fluoride (PVDF)*. Ultrasonics, 1976. **14**(1): p. 15-23.
3. Lanceros-Mendez, S., et al., *FTIR and DSC studies of mechanically deformed beta-PVDF films*. Journal of Macromolecular Science-Physics, 2001. **B40**(3-4): p. 517-527.
4. Chaves, M.C.R.G.a.N., *The Polymeric Material Encyclopedia*, Boca Raton: CRC Press.
5. Kang, S.J., et al., *Localized pressure-induced ferroelectric pattern arrays of semicrystalline poly(vinylidene fluoride) by microimprinting*. Advanced Materials, 2007. **19**(4): p. 581-+.
6. Lovinger, A.J., *Ferroelectric polymers*. Science, 1983. **220**(4602): p. 1115-1121.
7. Sencadas, V., R. Gregorio, and S. Lanceros-Mendez, *Processing and characterization of a novel nonporous poly(vinilidene fluoride) films in the beta phase*. Journal of Non-Crystalline Solids, 2006. **352**(21-22): p. 2226-2229.
8. Martins, P., et al., *Local variation of the dielectric properties of poly(vinylidene fluoride) during the alpha- to beta-phase transformation*. Physics Letters A, 2009. **373**(2): p. 177-180.
9. Fukada, E., *History and recent progress in piezoelectric polymers*. IEEE Transactions and ultrasonics and Ferroelectrics and frequency Control 2000. **47**: p. 1277-1290.
10. He, L., et al., *Effect of multi-walled carbon nanotubes on crystallization, thermal, and mechanical properties of poly(vinylidene fluoride)*. Polymer Composites, 2010. **31**(5): p. 921-927.
11. Ribeiro, C., et al., *Influence of Processing Conditions on Polymorphism and Nanofiber Morphology of Electroactive Poly(vinylidene fluoride) Electrospun Membranes*. Soft Materials, 2010. **8**(3): p. 274-287.
12. Magalhaes, R., et al., *The Role of Solvent Evaporation in the Microstructure of Electroactiveβ-Poly(VinylideneFluoride) Membranes Obtained by Isothermal Crystallization*. Soft Materials, 2011. **9**(1): p. 1-14.
13. Jiang, Z., B. Carroll, and K.M. Abraham, *Studies of some poly(vinylidene fluoride) electrolytes*. Electrochimica Acta, 1997. **42**(17): p. 2667-2677.
14. Ferreira, A., et al., *Extrusion of poly(vinylidene fluoride) filaments: effect of the processing conditions and conductive inner core on the electroactive phase content and mechanical properties*. Journal of Polymer Research: p. 1-6.
15. Sencadas, V., R. Gregorio, and S. Lanceros-Méndez, *α to β Phase Transformation and Microestructural Changes of PVDF Films Induced by Uniaxial Stretch*. Journal of Macromolecular Science, Part B: Physics, 2009. **48**(3): p. 514 - 525.
16. Priya, L. and J.P. Jog, *Poly(vinylidene fluoride)/clay nanocomposites prepared by melt intercalation: Crystallization and dynamic mechanical behavior studies*. Journal of Polymer Science Part B-Polymer Physics, 2002. **40**(15): p. 1682-1689.
17. Sadeghi, F. and A. Ajji, *Study of Crystal Structure of (Polyvinylidene fluoride/Clay) Nanocomposite Films: Effect of Process Conditions and Clay Type*. Polymer Engineering and Science, 2009. **49**(1): p. 200-207.
18. Lopes, A.C., et al., *Nucleation of the Electroactive γ Phase and Enhancement of the Optical Transparency in Low Filler Content Poly(vinylidene)/Clay*

Nanocomposites. The Journal of Physical Chemistry C, 2011. **115**(37): p. 18076-18082.

19. Andrew, J.S. and D.R. Clarke, *Enhanced ferroelectric phase content of polyvinylidene difluoride fibers with the addition of magnetic nanoparticles.* Langmuir, 2008. **24**(16): p. 8435-8438.

20. Martins, P., C.M. Costa, and S. Lanceros-Mendez, *Nucleation of electroactive beta-phase poly(vinilidene fluoride) with CoFe2O4 and NiFe2O4 nanofillers: a new method for the preparation of multiferroic nanocomposites.* Applied Physics a-Materials Science & Processing, 2011. **103**(1): p. 233-237.

21. Hill, N.A., *Why Are There so Few Magnetic Ferroelectrics?* The Journal of Physical Chemistry B, 2000. **104**(29): p. 6694-6709.

22. Ramesh, R. and N.A. Spaldin, *Multiferroics: progress and prospects in thin films.* Nature Materials, 2007. **6**(1): p. 21-29.

23. Dillon, D.R., et al., *On the structure and morphology of polyvinylidene fluoride-nanoclay nanocomposites.* Polymer, 2006. **47**(5): p. 1678-1688.

24. Mago, G., F.T. Fisher, and D.M. Kalyon, *Deformation-Induced Crystallization and Associated Morphology Development of Carbon Nanotube-PVDF Nanocomposites.* Journal of Nanoscience and Nanotechnology, 2009. **9**(5): p. 3330-3340.

25. Xu, W.B., M.L. Ge, and P.S. He, *Nonisothermal crystallization kinetics of polypropylene/montmorillonite nanocomposites.* Journal of Polymer Science Part B-Polymer Physics, 2002. **40**(5): p. 408-414.

26. Qian, J.S. and P.S. He, *Non-isothermal crystallization of HDPE/nano-SiO2 composite.* Journal of Materials Science, 2003. **38**(11): p. 2299-2304.

27. Kim, S.H., S.H. Ahn, and T. Hirai, *Crystallization kinetics and nucleation activity of silica nanoparticle-filled poly(ethylene 2,6-naphthalate).* Polymer, 2003. **44**(19): p. 5625-5634.

28. Achilias, D.S., et al., *Characterization and Crystallization Kinetics of in situ Prepared Poly(propylene terephthalate)/SiO(2) Nanocomposites.* Macromolecular Chemistry and Physics, 2010. **211**(1): p. 66-79.

29. Naffakh, M., et al., *Novel melt-processable nylon-6/inorganic fullerene-like WS(2) nanocomposites: Complex isothermal crystallization kinetics and melting behaviour.* Materials Chemistry and Physics, 2011. **128**(1-2): p. 265-273.

30. Kim, G.H., S.M. Hong, and Y. Seo, *Piezoelectric properties of poly(vinylidene fluoride) and carbon nanotube blends: beta-phase development.* Physical Chemistry Chemical Physics, 2009. **11**(44): p. 10506-10512.

31. Manna, S., S.K. Batabyal, and A.K. Nandi, *Preparation and characterization of silver-poly(vinylidene fluoride) nanocomposites: Formation of piezoelectric polymorph of poly(vinylidene fluoride).* Journal of Physical Chemistry B, 2006. **110**(25): p. 12318-12326.

32. Sencadas, V., et al., *Influence of Ferrite Nanoparticle Type and Content on the Crystallization Kinetics and Electroactive Phase Nucleation of Poly(vinylidene fluoride).* Langmuir, 2011: p. null-null.

33. Avrami, M., *Kinetics of phase change I - General theory.* Journal of Chemical Physics, 1939. **7**(12): p. 1103-1112.

34. Avrami, M., *Granulation, Phase Change, and Microstructure - Kinetics of Phase Change. III.* Journal of Chemical Physics, 1941. **9**(2): p. 177-184.

35. Silva, M.P., et al., *alpha- and gamma-PVDF: Crystallization kinetics, microstructural variations and thermal behaviour.* Materials Chemistry and Physics, 2010. **122**(1): p. 87-92.

36. Long, Y., R.A. Shanks, and Z.H. Stachurski, *Kinetics of polymer crystallization.* Progress in Polymer Science, 1995. **20**(4): p. 651-701.

37. Qiu, Z.B., et al., *Miscible crystalline/crystalline polymer blends of poly(vinylidene fluoride) and poly(butylene succinate-co-butylene adipate): Spherulitic morphologies and crystallization kinetics.* Macromolecules, 2007. **40**(14): p. 5047-5053.

38. Pedro Martins, C.M.C., Maria Benelmekki, Gabriela Botelho and Senentxu Lanceros-Mendez, *On the origin of the electroactive poly(vinylidene fluoride) β– phase nucleation by ferrite nanoparticles via surface electrostatic interactions* submitted to Soft Matter 2011. SM-ART-09-2011-006671.

39. Cebe, P. and S.Y. Chung, *Tensile behavior of blends of poly(vinylidene fluoride) with poly(methyl methacrylate.* Journal of Materials Science, 1990. **25**(5): p. 2367-2378.

40. Lee, J.G. and S.H. Kim, *Structure development of PVDF/PMMA/TiO2 composite film with casting conditions.* Macromolecular Research, 2011. **19**(1): p. 72-78.

41. Tanniru, M., et al., *The determining role of calcium carbonate on surface deformation during scratching of calcium carbonate-reinforced polyethylene composites.* Materials Science and Engineering a-Structural Materials Properties Microstructure and Processing, 2005. **404**(1-2): p. 208-220.

42. Liu, Z.H., P. Marechal, and R. Jerome, *Melting and crystallization of poly(vinylidene fluoride) blended with polyamide 6.* Polymer, 1997. **38**(20): p. 5149-5153.

43. Mamun, A., et al., *Influence of thermal history on primary nucleation and crystal growth rates of isotactic polystyrene.* Polymer, 2006. **47**(15): p. 5531-5537.

44. Chae, D.W. and S.M. Hong, *Dynamic Crystallization Behavior, Morphology, and Physical Properties of Highly Concentrated Poly(vinylidene fluoride)/Silver Nanocomposites.* Journal of Polymer Science Part B-Polymer Physics, 2010. **48**(22): p. 2379-2385.

45. Xu, L. and R.A. Weiss, *Melt crystallization of bisphenol a polycarbonate in blends of polycarbonate with zinc salts of sulfonated polystyrene ionomers.* Macromolecules, 2003. **36**(24): p. 9075-9084.

46. Chen, D., et al., *Crystallization Behavior of Poly(vinylidene fluoride) Nanocomposites Containing Multiwalled Carbon Nanotubes.* Journal of Macromolecular Science Part B-Physics, 2010. **49**(6): p. 1069-1082.

47. Elashmawi, I.S., et al., *Spectroscopic and thermal investigations of poly(vinylidene fluoride) films composites with LaNi3CO2.* Crystal Research and Technology, 2007. **42**(2): p. 157-163.

48. Asai, K., M. Okamoto, and K. Tashiro, *Real-time investigation of crystallization in poly(vinylidene fluoride)-based nano-composites probed by infrared spectroscopy.* Polymer, 2008. **49**(24): p. 5186-5190.

5 On the origin of the electroactive PVDF β-phase nucleation by ferrite nanoparticles via surface electrostatic interactions
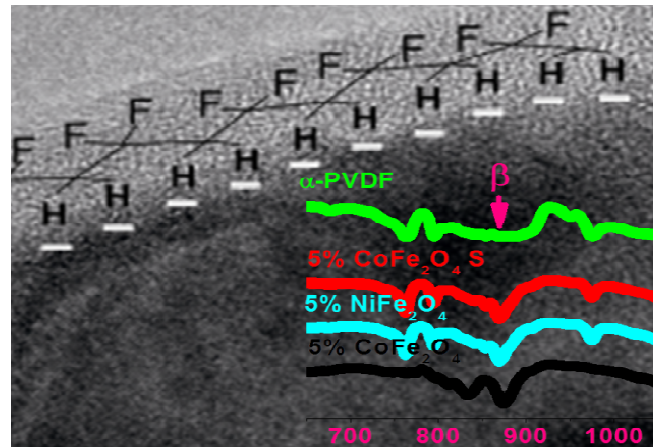
Flexible composite films, comprising $NiFe_2O_4$ and $CoFe_2O_4$ nanoparticles in a Poly(vinylidene fluoride (PVDF) matrix, have been prepared by solvent casting and melt crystallization to investigate the polymer β-phase nucleation mechanism. Infrared spectroscopy (FTIR) confirms the nucleation of the β-PVDF with the addition of both ferrites. Transmission electron microscopy (TEM) imaging and thermogravimetric analyses (TGA) indicate the formation of an interface in the nanocomposites with the β-phase nucleation. It is shown that the essential factor for the nucleation of the β-phase in the PVDF/ferrite nanocomposites is the static electric interaction between the magnetic particles with a negative zeta potential and the CH_2 groups having a positive charge density.

5.1 Introduction

PVDF is a semi-crystalline polymer which shows five crystalline forms namely α, β, γ, δ, and ε and is commonly crystallized in non-polar crystalline α-phase [1-2].

During the last decades it has found increasing applications in the areas of sensors, actuators, batteries, filters, chemical warfare protection and, more recently, in the biomedical field [3-6].

Most of the applications of the material take advantage of the properties of the polar β-phase that shows an all trans conformation comprising fluorine and hydrogen atoms on opposite sides of the polymer backbone, resulting in a net non-zero dipole moment. This molecular conformation confers to the polymer its high dielectric constant, large piezoelectric coefficients, pyroelectric and ferroelectric properties [7].

In this way, obtaining the β-phase is of primary importance for improving the technological applications of this material and, for this reason, increasing β-phase content of the polymer has always been of great concern [8].

Melt processing of the polymer results in the α-phase and traditionally the β-phase is obtained by stretching the α-phase films prepared by melt crystallization [5, 7, 9]. Such a mechanical stretching process is not suitable for the preparation of thin films directly on substrates or nanocomposites [10], which is required for micro technology applications.

In a different approach, the β-phase can be directly prepared by solution evaporation from an appropriate solvent (e.g. from dimethylformamide) below 70 °C, which facilitates film deposition directly on a desired substrate. On the other hand, the material obtained in this way shows a high porosity leading to an opaque appearance and a decrease of the electrical and mechanical properties [11].

At a solvent evaporation temperature above 110 °C the porous structure can be avoided [8], but the nonpolar α-phase becomes the predominant crystalline structure.

Some methods have been proposed for nucleating the electroactive β-phase at evaporation temperatures above 110 °C, such as the use of $BaTiO_3$ ceramic filler [12], blending clay [13-15], hydrated ionic salt [16], PMMA [17], TiO_2 [8] or ferrite nanoparticles [18] with PVDF.

Previous studies have shown that adding these type of nanofillers into the polymer matrix also leads to significant modification of the breakdown field, charge transport, and charge distribution of the dielectric materials due to the interfacial effects [19-20].

In a previous work [12] it was reported that the electroactive β-phase of PVDF is nucleated by the presence of the $BaTiO_3$ ceramic filler, being this effect strongly dependent on filler size and almost independent on filler content. The nucleation of the ferroelectric phase should be strongly influenced both by geometrical factors due to the nanosize of the fillers and, in particular, by the interactions in the interface between the local electric field and PVDF dipoles. These local field-dipole interactions can have different nature such as ion-dipole and dipole-dipole, among others, being different for the different nanofillers [21].

In this way, understanding interfaces in nanocomposites is an important issue for the design of nanocomposite materials with tailored properties [22-23]. Double-layer or three-layer interface models have been proposed to understand the interfaces in the nanocomposites [24-25], nevertheless, there is a need to understand the specific nature of the interfaces and its role in the nucleation of the polar β-PVDF, as both size effects but, in particular, dipolar interactions can play an important role. Further, this issue gains special relevance when the material is doped with ferrite nanoparticles as, together to the nucleation of the electroactive phase, a ME effect is also present in the composite, leading to strong potential applications [26].

It has been reported that ferrite nanoparticles affected the nucleation kinetics, as corroborated by the increasing number of spherulites with increasing nanoparticle content and by the variations of the Avrami's exponent. Further, the observed decrease of the crystalline fraction of PVDF with increasing nanoparticle content indicates that an important fraction of polymer chains are confined in interphases with the filler particle [27].

In this paper, $CoFe_2O_4$ and $NiFe_2O_4$ nanoparticles were incorporated into the PVDF matrix and the interface properties and their effect in the nucleation of the β-phase of the polymer has been addressed.

5.2   Experimental

5.2.1   Preparation of the nanocomposites

$CoFe_2O_4$ and $NiFe_2O_4$ nanoparticles were purchased from Nanoamor. The ferrite dimensions are between 35-55 and 20-30 nm for $CoFe_2O_4$ and $NiFe_2O_4$, respectively. DMF (pure grade) was supplied by Fluka and PVDF (Solef 1010) was supplied by Solvay. All the chemicals and nanoparticles were used as received from the suppliers.

For composite preparation, the initial concentration of solution was 0.2 g of PVDF for 1 ml of DMF. The desired amounts of nanoparticles were then mixed with ultrasound in DMF for 6 h. After that, PVDF powder was added to the mixture and placed in a Teflon mechanical stirrer with ultrasound during 1h for complete dissolution of the polymer. After the nanoparticles were dispersed in the polymer solution, flexible films were obtained by spreading the solution on a clean glass substrate.

Solvent evaporation was performed inside the oven for 10 min at 210 ℃ to ensure the complete melting of the nanocomposite and solvent evaporation. Crystallization was then achieved by cooling down to room temperature.

In order to modify the nanoparticle surface interaction, some nanoparticles were added to the polymer after a surfactation process. Surfactation was achieved by mixing 2 g of nanoparticles with 65 ml of an aqueous solution of citric acid (0,02g/ml). Then the pH value of the mixture during the adsorption step was adjusted to 5.2 with concentrated ammonia and rigorously stirred during 2 h. After that, the mixture was allowed to cool down to room temperature. The nanoparticles were then suspended merely by rising up the pH value of the mixture to 10. The suspension was then vacuum-filtered and washed with water to remove any agglomerated particles. Finally, the surfactated nanoparticles were vacuum-filtered and washed with DMF.

5.2.2   *Characterization of the nanocomposites*

FTIR spectra of the films were recorded on a PERKIN-ELMER SPECTRUM 100 in ATR mode from 650 to 1150 cm^{-1} with a resolution of 4 cm^{-1}. 32 scans were performed to each sample. FTIR was used to identify and quantify phase content in PVDF.

The polymer/nanoparticle interface was investigated by Transmission electron microscopy (TEM) imaging using a JEOL JEM-1210 electron microscope operating at 200 keV. The samples were embedded in an epoxy resin and cut into thin films of about 100 nm using a Leica Ultracut UCT Ultramicrotome.

Thermogravimetric analyses (TGA) was carried out under nitrogen atmosphere supplied at a constant 50 mL min^{-1} flow rate using a Pyris 1 TGA – Perkin-Elmer device. The sample holders were ceramic crucibles with a capacity of 60 µL. The samples were subjected to a heating rate of 10 ± 0.2℃.min^{-1} between 50 and 850 ℃ in order to evaluate the influence of the nanoparticles in the degradation of the polymer.

Zeta potential measurements were used to determine the surface charge of the

nanoparticles and were performed with a Zetasizer Nano ZS (Malvern instruments) provided with a He/Ne laser of 633 nm wavelength.

5.3 Results and Discussion

FTIR has been proved to be suitable to identify and quantify phase content in PVDF. In particular specific bands such as 766 and 840 cm^{-1} have been identified to correspond to the α- and β-phase respectively [28-29]. These specific bands have been used for identification and quantification of the phases in the present work [18].

Assuming that the infrared absorption follows the Lambert-Beer law, for a system containing α and β-phases the relative β-phase fraction, F(β), can be determined using equation 5.1:

$$F(\beta) = \frac{X_\beta}{X_\alpha + X_\beta} = \frac{A_\beta}{\left(K_\beta / K_\alpha\right) A_\alpha + A_\beta} \tag{5.1}$$

where $K_\beta = 7.7 \times 10^4$ cm^2/mol and $K_\alpha = 6.1 \times 10^4$ cm^2/mol [1, 6, 11, 18].

For the nanocomposite samples, typical spectra and the variation of the relative fraction of the β-phase with increasing amount of ferrite fillers are presented in Figure 5.1. The β-phase evolution with ferrite concentration was also confirmed by XRD measurements (not shown).
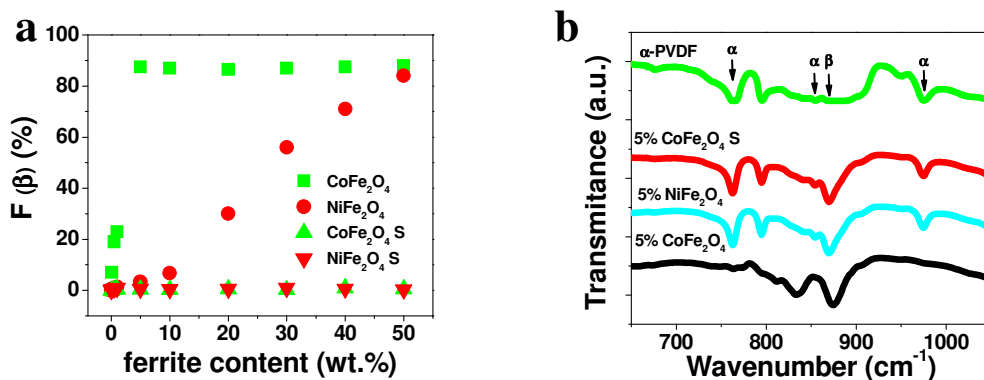
Figure 5.1 – (a) Evolution of the β-phase content with increasing filler concentration for the PVDF/CoFe$_2$O$_4$ and PVDF/NiFe$_2$O$_4$ nanocomposite samples calculated from the infrared spectra (b) for the nanocomposites with 5 wt.% filler content. "*S*" represents the samples prepared with surfactated nanoparticles.

For cobalt ferrite samples, even at small amount of nanoparticles induce the crystallization of the polymer matrix in the β-phase. On the other hand, to obtain the highest amount of β-phase in the Ni ferrite nanocomposites, it is necessary to add as much as 50 wt.% $NiFe_2O_4$ nanoparticles.

In this way, it is demonstrated that specific interactions near the PVDF/ferrite interfaces can effectively induce the nucleation of the polar (ferroelectric) phase of PVDF. However, at locations far away from these polar interfaces, non-polar α-phase grows, as expected for the processing conditions without nanoparticles, leading to the co-existence of both phases within the composites. In this way, the induced amount of ferroelectric phase depends on the ferrite content, and, as demonstrated in Figure 5.1a, on the ferrite type.

Figure 5.1a also reveals the critical role of the surface interactions and not just the size effects: not only the different ferrites nucleate different amounts of electroactive phase for the same concentration, but also the surface modification of the nanoparticle through the surfactation procedure has as a consequence the loss of the β-phase nucleation ability, indicating that this process suppresses the surface interaction responsible for the nucleation of the *β*-phase of the polymer.

A specific study on the nanoparticle surface and interphase characteristics responsible for the nucleation of the polar phase of the polymer was performed in composites with ferrite wt.% of 5% (ɸ=2%), since this is the concentration with the most significant difference on the relative fraction of the β-phase nucleated by $CoFe_2O_4$ nanoparticles, $CoFe_2O_4$ surfactated nanoparticles and $NiFe_2O_4$ nanoparticles. The FTIR spectra of those specific samples are represented in Figure 5.1b.

The nanoparticle/polymer interface as observed by TEM in the three PVDF/ferrite (95/5 wt.%) composites is represented in Figure 5.2.
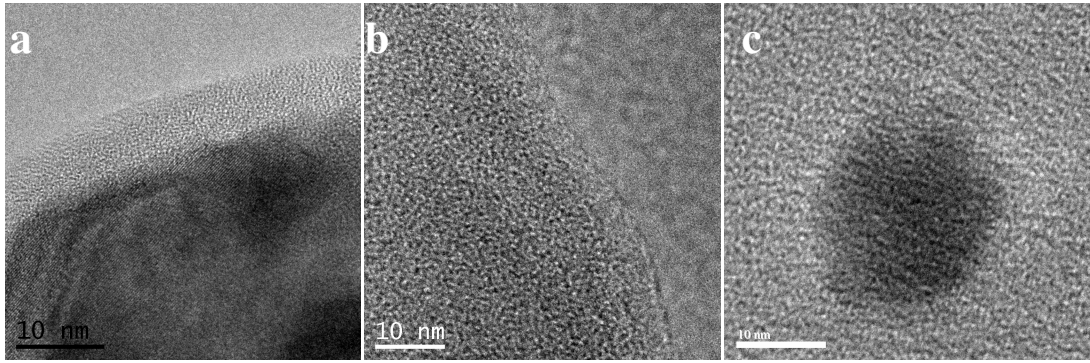
Figure 5.2 – TEM images of PVDF/ferrite (95/5 wt.%) nanocomposites with: (a) $CoFe_2O_4$ nanoparticles; (b) $CoFe_2O_4$ surfactated nanoparticles and (c) $NiFe_2O_4$ nanoparticles.

Figure 5.2 reveals a substantial difference between all composites: whereas there is a distinguished interface between the ferrite nanoparticle and the polymer for the PVDF/$CoFe_2O_4$ nanocomposites (a), that interface is not observed in the PVDF/$NiFe_2O_4$ nanocomposites (c). In the case of surfactated nanoparticles, this interface is also not observed (b). This result is consistent with the results presented in Figure 5.1 since the nucleation of the electroactive β-phase in PVDF/$NiFe_2O_4$ nanocomposites starts from the 5 wt.% and does not occur for the surfactated nanoparticles.

Further insight about the existence of the polymer interface was obtained by studying the thermal stability of the nanocomposites by TGA (Figure 5.3).
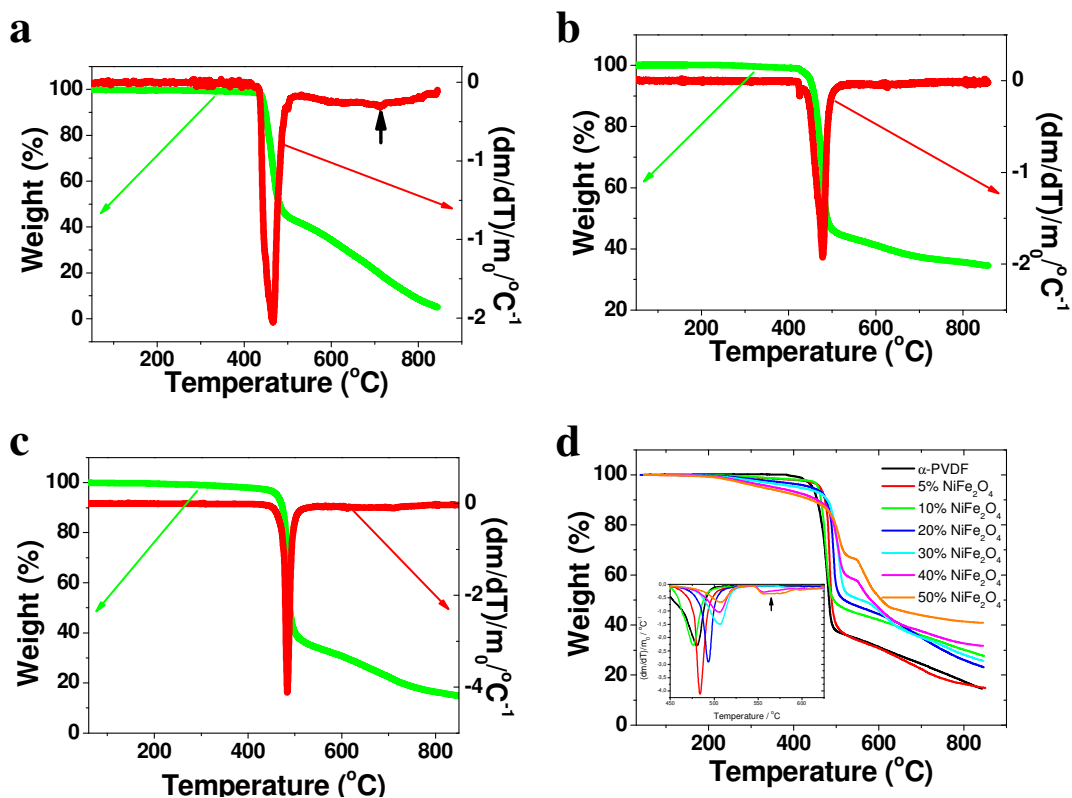
Figure 5.3 − TGA plots of PVDF/ferrite (95/5 wt.%) nanocomposites with: (a) $CoFe_2O_4$ nanoparticles; (b) $CoFe_2O_4$ surfactated nanoparticles and (c) $NiFe_2O_4$ nanoparticles. (d) Evolution of TGA plots of PVDF/$NiFe_2O_4$ with increasing ferrite concentration.

Figure 5.3 shows that the samples that do not show the polymer/particle interface show identical TGA spectra with a single degradation step (Figure 5.3 b and 5.3 c) at 420 °C. On the other hand, non surfactated PVDF/$CoFe_2O_4$ nanocomposites (Figure 5.3a) exhibits two-step degradation: the first one occurs at 420 °C, and the second one occurs at 540 °C, as better observed by the derivative of the TGA curves (black arrow) (Figure 5.3 a-c).

The restrained state of PVDF chains due to the interaction between the chains and the nanoparticle surface is an important factor to induce the observed additional step in the thermal behaviour of the nanocomposites [30], providing larger thermal stability to the polymer chains closer to the ferrite surface [31].

Pedro Martins

It is to notice that with increasing ferrite concentration the peak area corresponding to the second degradation step at 540º, which should be proportional to the interface volume, follows the same behaviour than the evolution of the β-phase content represented in Figure 5.1: it does not appear for the composites with surfactated nanoparticles, it increases abruptly in the PVDF/CoFe$_2$O$_4$ nanocomposites and increases progressively in the PVDF/NiFe$_2$O$_4$ nanocomposites (Figure 5.3d). This suggest a close relation between the nucleation of the β-phase, the existence of an interface and the change in the degradation temperature of the surrounding polymer molecules due to the strong polymer/ferrite interaction [32].

Once the existence of the polymer/ferrite interface is proven to exist in the nanocomposites nucleated in the electroactive phase of the polymer by TEM and TGA, it is necessary to study the origin of this interaction. Previous studies propose the existence of strong electrostatic between the negative charged nanofillers surface and the positive density of change of the CH$_2$ on the PVDF chains [21, 32-34].

Zeta potential analysis was used to evaluate the electrostatic charge on the surface of ferrite nanoparticles [35] and correlate it with the β-phase nucleation.
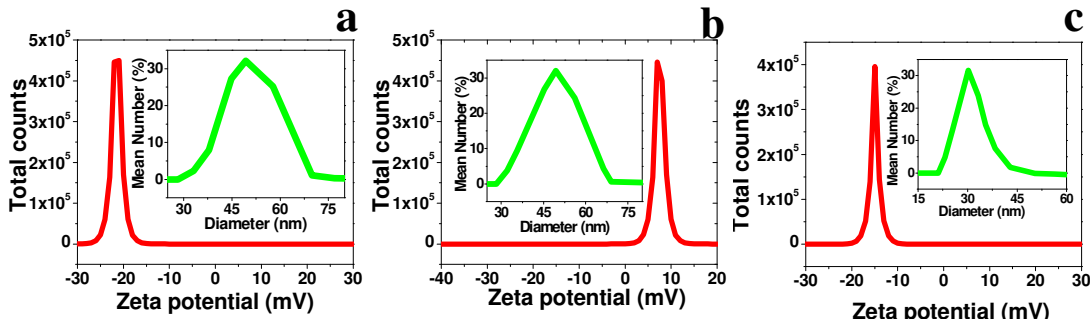
Figure 5.4 – Zeta potential and size distribution of the different ferrite nanoparticles (a) CoFe$_2$O$_4$ nanoparticles; (b) CoFe$_2$O$_4$ surfactated nanoparticles and (c) NiFe$_2$O$_4$ nanoparticles.

The obtained results for the three different particles are represented in Figure 5.4 and Table 5.1. The inset on Figure 5.4 shows the experimental size of nanoparticles determined by DLS.

Table 5.1 – Zeta potential, density and size values of the different nanoparticles.

Ferrite	Zeta potential (mV)	Density (g/cm^3)	Size* (nm)	Experimental size (nm)
CoFe$_2$O$_4$	-22±5	5.3	35-55	30-70
CoFe$_2$O$_4$ surfactated	+9±4	5.3	35-55	30-70
NiFe$_2$O$_4$	-15±5	5.4	20-30	20-60

*provided by Nanoamor

Since the surface charge depends strongly on the pH of the suspension, the Zeta potential of the nanoparticles was determined at the same pH of the PVDF/ferrite mixture (pH≈6) used during sample preparation. As observed in Figure 5.4 and Table 5.1 ferrite nanoparticles show negative Z-potentials, whereas the surfactated nanoparticles change the Z-potential to positive values. In this way, the nucleation of the electroactive β-phase occurs in the surface of the negative charged nanoparticles (note that the nucleation in PVDF/NiFe$_2$O$_4$ nanocomposites also occurs for low concentrations, only that this nucleation is less efficient than for the PVDF/CoFe$_2$O$_4$ for the 5 wt.% filler content (Figure 5.1a).

The positive CH$_2$ charge density of the PVDF chains suffer in this way strong interactions with the negatively charged surface ferrites that lead the polymer chains to align on the surface of the nanoparticle (Figure 5.5) in the extended TTTT conformation and therefore resulting in the β- phase [33, 36].
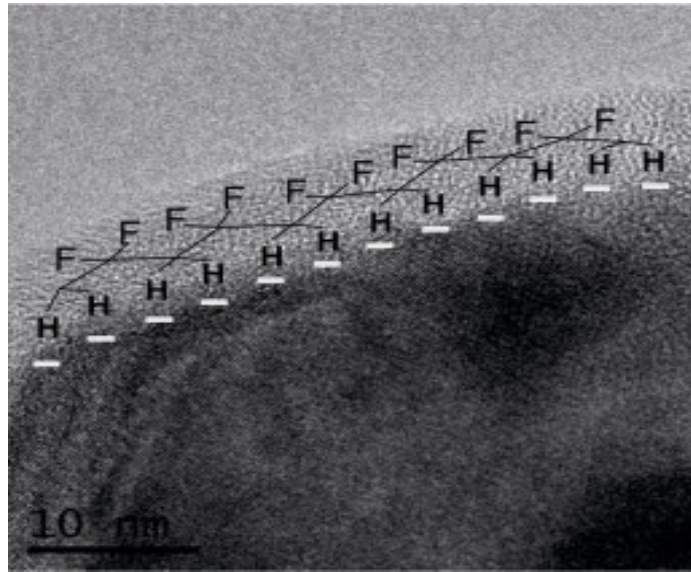
Figure 5.5 – Schematic representation of the interaction between $CoFe_2O_4$ nanoparticles and PVDF chains in the nanocomposite: the partially positive C–H bonds of the polymer are attracted by the negatively charged ferrite surface due to the static electric force. This leads to the all-trans conformation of the polymer phase.

The surfactation process, on the other hand, promotes the change in the electric charge of the surface of the nanoparticle from negative to positive and in this way the interaction with the positive CH_2 charge density on the PVDF chains essential to the nucleation of the electroactive β-phase is repulsive.

Finally, by comparing both used ferrites, it is observed that whereas the highest amount of β-phase (≈90%) is obtained for 5 wt.% for the $CoFe_2O_4$ ferrites (ф=2%), 50% is necessary for the $NiFe_2O_4$ nanoparticles (ф=25%). The origin of this effect has to be found in the differences obtained in the Zeta potential, density and size values of both ferrites (Table 5.1), as they are at the ground of the described interactions. Since the surface of the $CoFe_2O_4$ nanoparticles is more negatively charged than the $NiFe_2O_4$ ones, the electrostatic interactions will be stronger in the PVDF/$CoFe_2O_4$ nanocomposites [37]. This will lead to a larger interaction volume and a larger nucleation effect all along the sample. In this way, the different size is a minor factor in the determination of the phase nucleation, as smaller particles show a larger interfacial interaction area and should therefore promote larger nucleation efficiencies. This is not the case for the sizes under consideration, and therefore, the interaction strength fully accounts for the observed effects: as the interaction strength is lower for Ni-ferrites, they have to be

closer in order to be able to nucleate all the polymer phase.

5.4 Conclusions

The crystal polymorphism of PVDF/ferrite nanocomposites prepared by solvent casting and melt crystallization method has been investigated.

Crystallization of the β-phase of PVDF was observed for $CoFe_2O_4$ and $NiFe_2O_4$ ferrite nanofillers, although the β-phase content increases with increasing ferrite concentration in a different way: composites with more that 90% of electroactive β-phase are obtained for 5 wt.% of $CoFe_2O_4$, whereas 50 wt.% of $NiFe_2O_4$ is needed to obtain similar polymer phase contents in the composites. Further, the ability of the nanoparticles to nucleate the electroactive β-phase of the polymer is lost by the surface modifications of the nanoparticles through a surfactation process.

The nucleation is attributed to the negative electrostatic charge of the ferrites nanoparticles at the working pH and the positive charge density of the CH_2 groups. The strong interaction between the partially positive CH_2 bonds of the PVDF chains and the negatively charged ferrites surface induces the polymer chains to align on the surface of the nanoparticles in a extended TTTT conformation and results in formation of the β-PVDF crystallographic phase. The different nucleation efficiency in both nanoparticles is fully ascribed to the interaction strength, which is larger for the $CoFe_2O_4$ nanoparticles.

5.5   References

1.   Salimi, A. and A.A. Yousefi, *Conformational changes and phase transformation mechanisms in PVDF solution-cast films.* Journal of Polymer Science Part B-Polymer Physics, 2004. **42**(18): p. 3487-3495.

2.   Lovinger, A.J., *Ferroelectroc Polymers.* Science, 1983. **220**(4602): p. 1115-1121.

3.   Martins, P., et al., *Local variation of the dielectric properties of poly(vinylidene fluoride) during the alpha- to beta-phase transformation.* Physics Letters A, 2009. **373**(2): p. 177-180.

4.   Ribeiro, C., et al., *Influence of Processing Conditions on Polymorphism and Nanofiber Morphology of Electroactive Poly(vinylidene fluoride) Electrospun Membranes.* Soft Materials, 2010. **8**(3): p. 274-287.

5.   Lanceros-Mendez, S., et al., *FTIR and DSC studies of mechanically deformed beta-PVDF films.* Journal of Macromolecular Science-Physics, 2001. **B40**(3-4): p. 517-527.

6.   Foster, F.S., E.A. Harasiewicz, and M.D. Sherar, *A history of medical and biological imaging with polyvinylidene fluoride (PVDF) transducers.* Ieee Transactions on Ultrasonics Ferroelectrics and Frequency Control, 2000. **47**(6): p. 1363-1371.

7.   Gregorio, R. and M. Cestari, *Effect of crystallization temperature on the crystalline phase content and morphology of poly(vinylidene fluoride). Journal* of Polymer Science Part B-Polymer Physics, 1994. **32**(5): p. 859-870.

8.   An, N.L., et al., *Preparation and electroactive properties of a PVDF/nano-TiO2 composite film.* Applied Surface Science, 2011. **257**(9): p. 3831-3835.

9.   Sencadas, V., et al., *alpha-to-beta transformation on PVDF films obtained by uniaxial stretch.* Advanced Materials Forum Iii, Pts 1 and 2, 2006. **514-516**: p. 872-876.

10.   He, X.J., K. Yao, and B.K. Gan, *Ferroelectric poly(vinylidene fluoride-hexafluoropropylene) thin films on silicon substrates.* Sensors and Actuators a-Physical, 2007. **139**(1-2): p. 158-161.

11.   Sencadas, V., R. Gregorio, and S. Lanceros-Mendez, *Processing and characterization of a novel nonporous poly(vinilidene fluoride) films in the beta phase.* Journal of Non-Crystalline Solids, 2006. **352**(21-22): p. 2226-2229.

12.   Mendes, S., et al., *Effect of filler size and concentration on the structure and properties of poly(vinylidene fluoride)/BaTiO<sub>3</sub> nanocomposites.* Journal of Materials Science: p. 1-11.

13.   Shah, D., et al., *Dramatic enhancements in toughness of polyvinylidene fluoride nanocomposites via nanoclay-directed crystal structure and morphology.* Advanced Materials, 2004. **16**(14): p. 1173-+.

14.   Priya, L. and J.P. Jog, *Poly(vinylidene fluoride)/clay nanocomposites prepared by melt intercalation: Crystallization and dynamic mechanical behavior studies.* Journal of Polymer Science Part B-Polymer Physics, 2002. **40**(15): p. 1682-1689.

15.   Patro, T.U., et al., *Studies on poly(vinylidene fluoride)-clay nanocomposites: Effect of different clay modifiers.* Polymer, 2008. **49**(16): p. 3486-3499.

16.   Benz, M., W.B. Euler, and O.J. Gregory, *The role of solution phase water on the deposition of thin films of poly(vinylidene fluoride).* Macromolecules, 2002. **35**(7): p. 2682-2688.

17. Ma, W.Z., et al., *beta-Phase of poly(vinylidene fluoride) formation in poly(vinylidene fluoride)/poly(methyl methacrylate) blend from solutions.* Applied Surface Science, 2008. **254**(17): p. 5635-5642.

18. Martins, P., C.M. Costa, and S. Lanceros-Mendez, *Nucleation of electroactive beta-phase poly(vinilidene fluoride) with CoFe2O4 and NiFe2O4 nanofillers: a new method for the preparation of multiferroic nanocomposites.* Applied Physics a-Materials Science & Processing, 2011. **103**(1): p. 233-237.

19. Tuncer, E., et al., *Enhancement of dielectric strength in nanocomposites.* Nanotechnology, 2007. **18**(32).

20. Nelson, J.K. and J.C. Fothergill, *Internal charge behaviour of nanocomposites.* Nanotechnology, 2004. **15**(5): p. 586-595.

21. Zhong, G.J., et al., *Understanding polymorphism formation in electrospun fibers of immiscible Poly(vinylidene fluoride) blends.* Polymer, 2011. **52**(10): p. 2228-2237.

22. Mayes, A.M., *Nanocomposites: Softer at the boundary.* Nature Materials, 2005. **4**(9): p. 651-652.

23. Bansal, A., et al., *Quantitative equivalence between polymer nanocomposites and thin polymer films.* Nature Materials, 2005. **4**: p. 693-698.

24. Tanaka, T., et al., *Proposal of a multi-core model for polymer nanocomposite dielectrics.* Ieee Transactions on Dielectrics and Electrical Insulation, 2005. **12**(4): p. 669-681.

25. Lewis, T.J., *Interfaces: nanometric dielectrics.* Journal of Physics D-Applied Physics, 2005. **38**(2): p. 202-212.

26. Eerenstein, W., N.D. Mathur, and J.F. Scott, *Multiferroic and magnetoelectric materials.* Nature, 2006. **442**(7104): p. 759-765.

27. Sencadas, V., et al., *Influence of Ferrite Nanoparticle Type and Content on the Crystallization Kinetics and Electroactive Phase Nucleation of Poly(vinylidene fluoride).* Langmuir, 2011. **27**(11): p. 7241-7249.

28. Kobayashi, M., K. Tashiro, and H. Tadokoro, *Molecular Vibrations of 3 Crystal Forms of Poly(Vinylidene Fluoride).* Macromolecules, 1975. **8**(2): p. 158-171.

29. Miranda, D., et al., *Influence of Silver Nanoparticles Concentration on the alpha- to beta-Phase Transformation and the Physical Properties of Silver Nanoparticles Doped Poly(vinylidene fluoride) Nanocomposites.* Journal of Nanoscience and Nanotechnology, 2009. **9**(5): p. 2910-2916.

30. Song, R., D. Yang, and L.H. He, *Effect of surface modification of nanosilica on crystallization, thermal and mechanical properties of poly(vinylidene fluoride).* Journal of Materials Science, 2007. **42**(20): p. 8408-8417.

31. Manna, S., S.K. Batabyal, and A.K. Nandi, *Preparation and characterization of silver-poly(vinylidene fluoride) nanocomposites: Formation of piezoelectric polymorph of poly(vinylidene fluoride).* Journal of Physical Chemistry B, 2006. **110**(25): p. 12318-12326.

32. Wang, W., et al., *Gold-Nanoparticle- and Gold-Nanoshell-Induced Polymorphism in Poly(vinylidene fluoride).* Macromolecular Materials and Engineering, 2011. **296**(2): p. 178-184.

33. Yu, L. and P. Cebe, *Crystal polymorphism in electrospun composite nanofibers of poly(vinylidene fluoride) with nanoclay.* Polymer, 2009. **50**(9): p. 2133-2141.

34. Bhatt, A.S., D.K. Bhat, and M.S. Santosh, *Crystallinity, Conductivity, and Magnetic Properties of PVDF-Fe3O4 Composite Films.* Journal of Applied Polymer Science, 2011. **119**(2): p. 968-972.

35. Tang, Z., et al., *Surface treatment of CoFe2O4 nanoparticles to improve their dispersibility in aqueous phase with new fluorine-contain polymers.* Applied Surface Science, 2008. **255**(5, Part 1): p. 2125-2128.

36. Ramasundaram, S., et al., *Preferential Formation of Electroactive Crystalline Phases in Poly(vinylidene fluoride)/Organically Modified Silicate Nanocomposites.* Journal of Polymer Science Part B-Polymer Physics, 2008. **46**(20): p. 2173-2187.

37. Kannappan, V. and S.C. Vinayagam, *Ultrasonic investigation of ion-solvent interactions in aqueous and non-aqueous solutions of transition and inner transition metal ions.* Indian Journal of Pure & Applied Physics, 2007. **45**(2): p. 143-150.

6 The role of nanoparticle surface charge on the nucleation of the electroactive β-PVDF for sensor and actuator applications
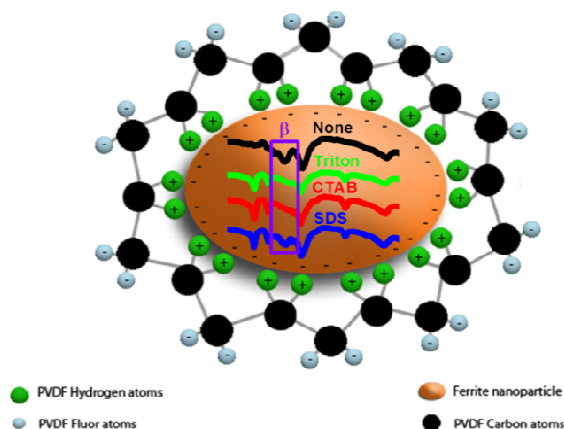
The electroactive β-Poly(vinylidene fluoride (PVDF) can be nucleated by introducing $CoFe_2O_4$ nanoparticles within the polymer matrix, leading to electroactive materials with large potential for sensor and actuator applications. The effects of the $CoFe_2O_4$ nanoparticle electrostatic charge on the phase crystallization of PVDF polymer is reported. For this purpose, the $CoFe_2O_4$ nanoparticles were coated with anionic sodium dodecyl sulfate (SDS), non-anionic (Triton X-100) and cationic cetrimonium bromide (CTAB) surfactants and the obtained coated nanoparticles were used as fillers. It is found that the piezoelectric β-form of the polymer increases when $CoFe_2O_4$ nanoparticles with higher negative electrostatic charge are added. The magnetostriction of the ferrite nanoparticles and the proven piezoelectricity of the polymer allows the use of the material for piezoelectric and ME sensors or/and actuators.

6.1 Introduction

Advanced polymers have found distinct applications in diversified areas such as packing, tissue engineering, drug delivery, energy harvesting, storage, sensors and actuation, among others [1-5]. One of the most interesting and used polymer in the sensor and actuator areas is PVDF, which is a semi-crystalline polymer that shows five crystalline forms namely α, β, γ, δ, and ε [6-9]. The common use of polymer fillers is to improve their stiffness and toughness, to enhance their barrier properties or to develop fire and ignition resistance, among others [10-11]. Addition of fillers sometimes induces drawbacks to the resulting composites such as brittleness or opacity [10]. In the case of PVDF, the addition of nanofillers is often performed aiming the nucleation of the electroactive β-phase of the polymer [12]. The electroactive phase of the polymer is usually achieved either by mechanical stretching from the α-phase [13], a method non compatible with micro fabrication, or by low temperature solvent evaporation, which results in PVDF samples with higher degree of porosity, opaque and fragile [14]. The interest of obtaining the electroactive phase of the polymer stems from the fact that β-phase is piezoelectric allowing possible applications in the areas of sensors, actuators, batteries, filters, chemical warfare protection, ME and, more recently, in the biomedical field [15-21].

The direct nucleation of the electroactive phase of the polymer will allow to save processing steps when the material is obtained by extrusion technologies and to allow micro technology compatible processes by direct deposition of the polymer in the electroactive phase in the desired size and shape.

A variety of methods have been reported to obtain the electroactive β-phase, including the use of $BaTiO_3$ [22], clay [23-25], hydrated ionic salt [26], PMMA [27], TiO_2 [28] or ferrite nanoparticles [29]. The presence of such type of nanofillers in the polymer matrix leads to significant modifications of the breakdown field, charge transport, and charge distribution of the dielectric materials due to the interfacial effects [30-31].

It has been shown that the presence of $BaTiO_3$ ceramic nucleates the β-PVDF phase, being this effect strongly dependent on filler size and almost independent on filler content. In this way, the nucleation of the ferroelectric phase should be strongly influenced by the geometry of the fillers through the interface interactions between the local electric field of the filler and PVDF dipoles [32]. These local field-dipole

interactions can have different nature such as ion-dipole and dipole-dipole , among others [33].

In this way, understanding interfaces in nanocomposites is an important issue for the design of nanocomposite materials with tailored properties [34-35].

Although the literature already suggested that the key factor to the PVDF β-phase nucleation is the electric interaction between the bonds of the PVDF chains and the electric charged surface of nanofillers [33, 36], only recently the effect of the nanoparticle surface charge on the β-phase nucleation mechanism has been studied [32]. In a previous study, different nanoparticles were used to introduce different surface charges into the polymeric matrix, so the nucleation could be affected by two distinct factors: i) the charge and ii) the type of nanoparticle. To definitively set light on the relevance of the key factor influencing the nucleation of the electroactive phase of this important polymer, the aim of the present work was to change the surface charge of the same type of nanoparticles by a surfactation process and evaluate the effect on the β-phase nucleation, allowing in this way a direct correlation between type and content of surface charge and nucleation ability of the nanoparticles.

6.2   Experimental

6.2.1   *Preparation of the nanocomposites*

$CoFe_2O_4$ nanoparticles were purchased from Nanoamor. The ferrite dimensions indicated by the supplier are between 35-55 nm. DMF (pure grade) was supplied by Fluka and PVDF (Solef 1010) was supplied by Solvay. All the chemicals and nanoparticles were used as received from the suppliers.

Three types of surfactants were used to change the surface charge of the nanoparticles: SDS, CTAB and Triton X-100 that induce negative, positive and almost zero surface charge respectively. In a typical procedure, 100 mg of nanoparticles were mixed with 100 ml of a surfactant aqueous solution of 0.1 mM. The solution was rigorously stirred and maintained at 60ºC for 60 min. The prepared suspension was washed and magnetically separated to remove the excess of surfactant: first with distilled water, then with ethanol and, finally, resuspended in distilled water. At last, the surfactated nanoparticles were dried in order to proceed to the following step.

Pedro Martins

For composite preparation, the initial concentration of solution was 0.2 g of PVDF for 1 ml of DMF. The desired amounts of nanoparticles were then mixed in DMF by ultrasound for 6 h in order to obtain nanocomposites with 5 wt.% of $CoFe_2O_4$ nanoparticles. Then, PVDF powder was added to the mixture and placed in a Teflon mechanical stirrer with ultrasound during 1h for complete dissolution of the polymer. After the nanoparticles dispersion in the polymer solution, flexible films were obtained by spreading the solution on a clean glass substrate.

Solvent evaporation was performed inside the oven for 10 min at 210 ºC to ensure the complete melting of the nanocomposite and solvent evaporation. Crystallization was then achieved by cooling down to room temperature.

6.2.2 Characterization

Zeta potential measurements were carried out in order to determine the surface charge of the nanoparticles in a Zetasizer NANO ZS-ZEN3600 (Malvern Instruments Limited, UK) provided with a He/Ne laser of 633 nm wavelength and a detection angle of 173° (backscatter detection). Measurements were performed at 25 ºC using the appropriated sample dilution in ultra-pure water to prevent multiscattering events. The average value for each sample was obtained from 10 measurements.

The average hydrodynamic size of ferrite nanoparticles was assessed by DLS in a Zetasizer NANO ZS-ZEN3600. Measurements were performed at 25ºC using the appropriated sample dilution in ultra-pure water to prevent multiscattering events. The average value for each sample was obtained from 10 measurements.

FTIR spectra of the films were recorded on a PERKIN-ELMER SPECTRUM 100 in ATR mode from 700 to 1100 cm^{-1} with a resolution of 4 cm^{-1}. 32 scans were performed to each sample in order to identify and quantify phase content in PVDF.

After 30 min of corona poling at 80ºC in a home-made chamber, the piezoelectric response (d_{33}) of the poled samples was analyzed with a wide range d_{33}-meter (model 8000, *APC Int Ltd*) to prove the piezoelectric response of the nanocomposites.

6.3   Results and discussion

Zeta potential analysis was used to evaluate the electrostatic charge on the surface of the ferrite nanoparticles [37-38] and the experimental size of nanoparticles was determined

by DLS. Since the surface charge depends strongly on the pH of the suspension, the zeta potential of the nanoparticles was determined at the same pH of the PVDF/ferrite mixture (pH≈6).

The obtained results for the different surfactated nanoparticles are represented in Figure 6.1 and Table 6.1.
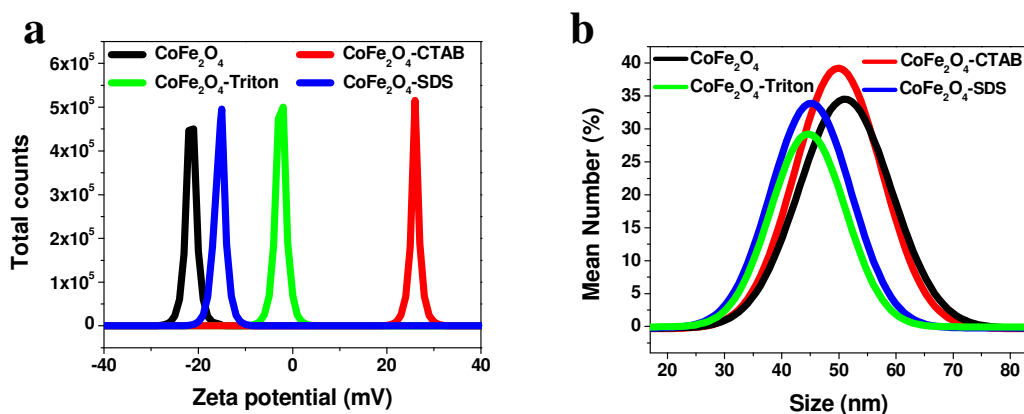
Figure 6.1 − (a) Zeta potential of the nanoparticles with and without surfactation. (b) Size distribution of the nanoparticles with and without surfactation.

In Figure 6.1a it is possible to observe the effect of the different surfactants in the electric charge of the nanoparticle surface. Without any surfactant, $CoFe_2O_4$ nanoparticles exhibit negative surface charge (-22 mV), which is in agreement with previous studies [32]. SDS, CTAB and Triton X-100 induce -15, 26 and -2 mV surface charge, respectively.

Table 6.1 − Zeta potential, β-phase content and size values of the different nanoparticles.

Ferrite	Zeta potential (mV)	F(β) (%)	Size* (nm)	Experimental size (nm)
$CoFe_2O_4$	-22±5	90		
$CoFe_2O_4$-Triton	-2±3	0		
$CoFe_2O_4$-CTAB	26±3	0	35-55	30-70
$CoFe_2O_4$-SDS	-15±4	30		

* provided by Nanoamor

Based on Figure 6.1b and in Table 6.1, there is an expected discrepancy between the physical size of the nanoparticles provided by Nanoamor and the hydrodynamic size determined by DLS, due to the different factors affecting the hydrodynamic measurements [39].

To study the effect of the nanoparticle surface charge on the PVDF β-phase nucleation mechanism FTIR has been used, as this method has been proven to be as suitable as XRD for the determination of the different phases of PVDF [12-13]. Specific bands such as 766 and 840 cm^{-1} have been identified to correspond to the α- and β-phase respectively [40-41] and have been used for identification and quantification of the phases [29].

Assuming that the infrared absorption follows the Lambert-Beer law for a system containing α and β-phases, the relative β-phase fraction, F(β), can be determined using equation 6.1:

$$F(\beta) = \frac{X_\beta}{X_\alpha + X_\beta} = \frac{A_\beta}{\left(\frac{K_\beta}{K_\alpha}\right) A_\alpha + A_\beta} \qquad \textbf{(6.1)}$$

Where K_β =7.7×10^4 cm^2/mol) and K_α=6.1×10^4 cm^2/mol) [6, 18, 29, 42].

FTIR measurements performed in order to identify the F(β) in the different nanocomposites are presented in Figure 6.2.
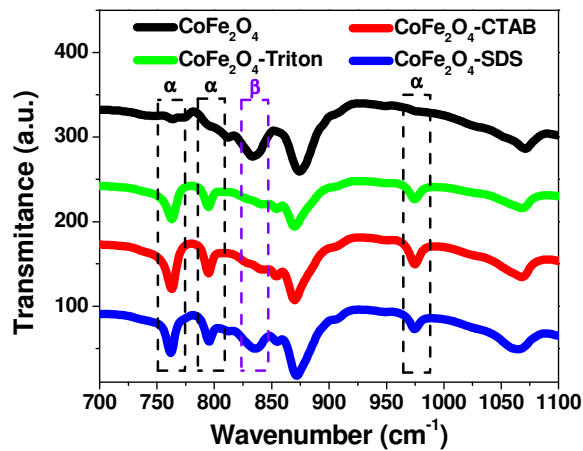
Figure 6.2 − Infrared transmittance vs. wavenumber for PVDF/CoFe$_2$O$_4$ (95/5 wt.%) samples with non surfactated ferrite nanoparticles and surfactated with Triton X-100, CTAB and SDS.

Based on Figure 6.2 it is possible to conclude that only the nanoparticle surfaces significantly negatively charged can nucleate the polymer β-phase.

Since the surface of the $CoFe_2O_4$ nanoparticles is more negatively charged than the $CoFe_2O_4$-SDS ones, the electrostatic interactions will be stronger in the PVDF/$CoFe_2O_4$ nanocomposites [43]. This will lead to a larger interaction and a larger nucleation effect all along the sample has proved by the higher F(β) obtained to the PVDF/$CoFe_2O_4$ nanocomposites (90%) comparatively to the $CoFe_2O_4$-SDS ones (30%). The almost zero surface charge of the $CoFe_2O_4$-Triton and the positive surface charge of the $CoFe_2O_4$-CTAB nanoparticles don´t allow the β-phase formation [32].

Since the size and type of the nanoparticles are all the same for the different nanocomposites, it is undoubtedly determined that β-phase nucleation process can only be explained by the electric interactions between the negative charged $CoFe_2O_4$ nanoparticles and the partially positive CH_2 bonds of the PVDF. The schematic showing of the proposed interaction is represented on Figure 6.3.

● PVDF Hydrogen atoms	● Ferrite nanoparticle
● PVDF Fluor atoms	● PVDF Carbon atoms
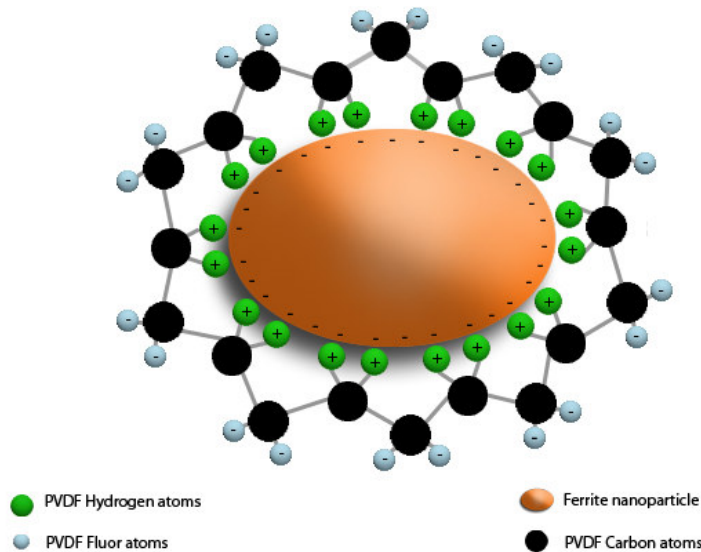
Figure 6.3 – Schematic representation of the proposed mechanism of the beta phase formation.

To prove the piezoelectricity of the β-phase nucleated samples, the piezoelectric response (d_{33}) of the poled samples was analyzed after corona poling and a slight stretching in order to eliminate the center of symmetry of the spherulitic structure [44-46].

The obtained piezoelectric coefficients placed in Table 6.2 are in agreement with the ones reported from Gomes *et al* [47] for the same electroactive phase content.

Table 6.2 – β-phase content and piezoelectric coefficient values.

Sample	F(β) (%)	d_{33} (pC/N)
PVDF/CoFe$_2$O$_4$	90	33
PVDF /CoFe$_2$O$_4$-SDS	30	23

With the addition of low quantity of ferrite nanoparticles, the stretching of the film in order to obtain the β-phase is unnecessary since the material crystallizes in its ferroelectric phase immediately upon cooling from the melt, allowing miniaturization and the preparation of the material into complex shapes [48]. This novel way of preparing β-PVDF matches the request of films with good piezoelectric coefficients, directly from melt and without porosity to be used in technological applications such as sensors and actuators. Additionally, the piezoelectricity of the polymer phase and the magnetostriction of the ferrite nanoparticles results in composites with ME response, depending the magnitude of the ME response on the ferrite content [19-20].

6.4   Conclusions

It is demonstrated that high electroactive β-phase content PVDF films can be obtained from the melt by adding a small quantity of CoFe$_2$O$_4$ nanoparticles. The nucleation is explained by the electrical interactions due to the presence of negative nanoparticle surfaces that will interact with the polymeric CH$_2$ groups that have positive charge density. This interaction induces the polymer chains to align on the surface of the nanoparticles in an extended TTTT conformation resulting in formation of the β-PVDF phase with piezoelectric and ferroelectricity properties.

The use of appropriate surfactants causes variations in the surface charge of the nanoparticles opening the possibility of the β-phase nucleation in different nanofillers, leading to hybrid composites that can take advantage of the properties of the fillers and the electroactive phase of the polymer. For example, in the present case, the magnetostriction of the filler and the piezoelectricity of the polymer allow the magnetoelectric response of the composite and its applications as sensors or/and actuators.

6.5 References

1. Croce, F., et al., *Nanocomposite polymer electrolytes for lithium batteries.* Nature, 1998. **394**(6692): p. 456-458.
2. Burroughes, J.H., et al., *Light-emitting diodes based on conjugated polymers.* Nature, 1990. **347**(6293): p. 539-541.
3. Discher, D.E. and A. Eisenberg, *Polymer vesicles.* Science, 2002. **297**(5583): p. 967-973.
4. Zelikin, A.N., et al., *A general approach for DNA encapsulation in degradable polymer miocrocapsules.* Acs Nano, 2007. **1**(1): p. 63-69.
5. Norrman, K., S.A. Gevorgyan, and F.C. Krebs, *Water-Induced Degradation of Polymer Solar Cells Studied by H(2)(18)O Labeling.* Acs Applied Materials & Interfaces, 2009. **1**(1): p. 102-112.
6. Salimi, A. and A.A. Yousefi, *Conformational changes and phase transformation mechanisms in PVDF solution-cast films.* Journal of Polymer Science Part B-Polymer Physics, 2004. **42**(18): p. 3487-3495.
7. Lovinger, A.J., *Ferroelectric polymers.* Science, 1983. **220**(4602): p. 1115-1121.
8. Rankin, C., et al., *Polarization and local reactivity on organic ferroelectric surfaces: Ferroelectric nanolithography using poly(vinylidene fluoride).* Acs Nano, 2007. **1**(3): p. 234-238.
9. Magasinski, A., et al., *Toward Efficient Binders for Li-Ion Battery Si-Based Anodes: Polyacrylic Acid.* Acs Applied Materials & Interfaces, 2010. **2**(11): p. 3004-3010.
10. Alexandre, M. and P. Dubois, *Polymer-layered silicate nanocomposites: preparation, properties and uses of a new class of materials.* Materials Science and Engineering: R: Reports, 2000. **28**(1-2): p. 1-63.
11. Zhou, T., et al., *Improving Dielectric Properties of BaTiO(3)/Ferroelectric Polymer Composites by Employing Surface Hydroxylated BaTiO(3) Nanoparticles.* Acs Applied Materials & Interfaces, 2011. **3**(7): p. 2184-2188.
12. Martins, P., C.M. Costa, and S. Lanceros-Mendez, *Nucleation of electroactive beta-phase poly(vinilidene fluoride) with CoFe(2)O(4) and NiFe(2)O(4) nanofillers: a new method for the preparation of multiferroic nanocomposites.* Applied Physics a-Materials Science & Processing, 2011. **103**(1): p. 233-237.
13. Salimi, A. and A.A. Yousefi, *FTIR studies of beta-phase crystal formation in stretched PVDF films.* Polymer Testing, 2003. **22**(6): p. 699-704.
14. Sencadas, V., R. Gregorio Filho, and S. Lanceros-Mendez, *Processing and characterization of a novel nonporous poly(vinilidene fluoride) films in the β phase.* Journal of Non-Crystalline Solids, 2006. **352**(21-22): p. 2226-2229.
15. Martins, P., et al., *Local variation of the dielectric properties of poly(vinylidene fluoride) during the alpha- to beta-phase transformation.* Physics Letters A, 2009. **373**(2): p. 177-180.
16. Ribeiro, C., et al., *Influence of Processing Conditions on Polymorphism and Nanofiber Morphology of Electroactive Poly(vinylidene fluoride) Electrospun Membranes.* Soft Materials, 2010. **8**(3): p. 274-287.
17. Lanceros-Mendez, S., et al., *FTIR and DSC studies of mechanically deformed beta-PVDF films.* Journal of Macromolecular Science-Physics, 2001. **B40**(3-4): p. 517-527.
18. Foster, F.S., E.A. Harasiewicz, and M.D. Sherar, *A history of medical and biological imaging with polyvinylidene fluoride (PVDF) transducers.* Ieee

Pedro Martins

Transactions on Ultrasonics Ferroelectrics and Frequency Control, 2000. **47**(6): p. 1363-1371.

19. Martins, P., et al., *Optimizing piezoelectric and magnetoelectric responses on CoFe2O4/P(VDF-TrFE) nanocomposites* Journal of Physics D: Applied Physics, 2011. **44**(49): p. 1-7.

20. Martins, P., et al., *Linear anhysteretic direct magnetoelectric effect in Ni0.5Zn0.5Fe2O4/poly(vinylidene fluoride-trifluoroethylene) 0-3 nanocomposites* Journal of Physics D: Applied Physics, 2011. **44**(48).

21. Hansen, B.J., et al., *Hybrid Nanogenerator for Concurrently Harvesting Biomechanical and Biochemical Energy.* Acs Nano, 2010. **4**(7): p. 3647-3652.

22. Mendes, S., et al., *Effect of filler size and concentration on the structure and properties of poly(vinylidene fluoride)/BaTiO<sub>3</sub> nanocomposites.* Journal of Materials Science, 2012. **47**(3): p. 1378-1388.

23. Shah, D., et al., *Dramatic enhancements in toughness of polyvinylidene fluoride nanocomposites via nanoclay-directed crystal structure and morphology.* Advanced Materials, 2004. **16**(14): p. 1173-+.

24. Priya, L. and J.P. Jog, *Poly(vinylidene fluoride)/clay nanocomposites prepared by melt intercalation: Crystallization and dynamic mechanical behavior studies.* Journal of Polymer Science Part B-Polymer Physics, 2002. **40**(15): p. 1682-1689.

25. Patro, T.U., et al., *Studies on poly(vinylidene fluoride)-clay nanocomposites: Effect of different clay modifiers.* Polymer, 2008. **49**(16): p. 3486-3499.

26. Benz, M., W.B. Euler, and O.J. Gregory, *The role of solution phase water on the deposition of thin films of poly(vinylidene fluoride).* Macromolecules, 2002. **35**(7): p. 2682-2688.

27. Ma, W.Z., et al., *beta-Phase of poly(vinylidene fluoride) formation in poly(vinylidene fluoride)/poly(methyl methacrylate) blend from solutions.* Applied Surface Science, 2008. **254**(17): p. 5635-5642.

28. An, N.L., et al., *Preparation and electroactive properties of a PVDF/nano-TiO2 composite film.* Applied Surface Science, 2011. **257**(9): p. 3831-3835.

29. Martins, P., C.M. Costa, and S. Lanceros-Mendez, *Nucleation of electroactive beta-phase poly(vinilidene fluoride) with CoFe2O4 and NiFe2O4 nanofillers: a new method for the preparation of multiferroic nanocomposites.* Applied Physics a-Materials Science & Processing, 2011. **103**(1): p. 233-237.

30. Tuncer, E., et al., *Enhancement of dielectric strength in nanocomposites.* Nanotechnology, 2007. **18**(32).

31. Nelson, J.K. and J.C. Fothergill, *Internal charge behaviour of nanocomposites.* Nanotechnology, 2004. **15**(5): p. 586-595.

32. Martins, P., et al., *On the origin of the electroactive poly(vinylidene fluoride) [small beta]-phase nucleation by ferrite nanoparticles via surface electrostatic interactions.* CrystEngComm, 2012.

33. Zhong, G.J., et al., *Understanding polymorphism formation in electrospun fibers of immiscible Poly(vinylidene fluoride) blends.* Polymer, 2011. **52**(10): p. 2228-2237.

34. Mayes, A.M., *Nanocomposites: Softer at the boundary.* Nature Materials, 2005. **4**(9): p. 651-652.

35. Bansal, A., et al., *Quantitative equivalence between polymer nanocomposites and thin polymer films.* Nature Materials, 2005. **4**: p. 693-698.

36. Yu, L. and P. Cebe, *Crystal polymorphism in electrospun composite nanofibers of poly(vinylidene fluoride) with nanoclay.* Polymer, 2009. **50**(9): p. 2133-2141.

37. Tang, Z., et al., *Surface treatment of CoFe2O4 nanoparticles to improve their dispersibility in aqueous phase with new fluorine-contain polymers.* Applied Surface Science, 2008. **255**(5, Part 1): p. 2125-2128.

38. Zhou, L., C. Gao, and W. Xu, *Magnetic Dendritic Materials for Highly Efficient Adsorption of Dyes and Drugs.* Acs Applied Materials & Interfaces, 2010. **2**(5): p. 1483-1491.

39. Watanabe, Y. and Y. Inoko, *Further application of size-exclusion chromatography combined with small-angle X-ray scattering optics for characterization of biological macromolecules.* Analytical and Bioanalytical Chemistry, 2011. **399**(4): p. 1449-1453.

40. Kobayashi, M., K. Tashiro, and H. Tadokoro, *Molecular Vibrations of 3 Crystal Forms of Poly(Vinylidene Fluoride).* Macromolecules, 1975. **8**(2): p. 158-171.

41. Miranda, D., et al., *Influence of Silver Nanoparticles Concentration on the alpha- to beta-Phase Transformation and the Physical Properties of Silver Nanoparticles Doped Poly(vinylidene fluoride) Nanocomposites.* Journal of Nanoscience and Nanotechnology, 2009. **9**(5): p. 2910-2916.

42. Sencadas, V., R. Gregorio, and S. Lanceros-Mendez, *Processing and characterization of a novel nonporous poly(vinilidene fluoride) films in the beta phase.* Journal of Non-Crystalline Solids, 2006. **352**(21-22): p. 2226-2229.

43. Kannappan, V. and S.C. Vinayagam, *Ultrasonic investigation of ion-solvent interactions in aqueous and non-aqueous solutions of transition and inner transition metal ions.* Indian Journal of Pure & Applied Physics, 2007. **45**(2): p. 143-150.

44. Zerfoss, S. and L.R. Johnson, *Crystal chemical relations in inorganic piezoelectric materials.* American Mineralogist, 1949. **34**(1-2): p. 61-67.

45. Kawai, H., *Piezoelectricity of Poly (vinylidene Fluoride).* Japanese Journal of Applied Physics, 1969. **8**(7): p. 975-&.

46. Martins, P., et al., *Correlation between Crystallization Kinetics and Electroactive Polymer Phase Nucleation in Ferrite/Poly(vinylidene fluoride) Magnetoelectric Nanocomposites.* Journal of Physical Chemistry B, 2012. **116**(2): p. 794-801.

47. Gomes, J., et al., *Influence of the beta-phase content and degree of crystallinity on the piezo- and ferroelectric properties of poly(vinylidene fluoride).* Smart Materials & Structures, 2010. **19**(6): p. 65010-65010.

48. Akdogan, E.K., M. Allahverdi, and A. Safari, *Piezoelectric composites for sensor and actuator applications.* Ieee Transactions on Ultrasonics Ferroelectrics and Frequency Control, 2005. **52**(5): p. 746-775.

Pedro Martins

7 Dielectric and magnetic properties of PVDF/ferrite nanocomposites
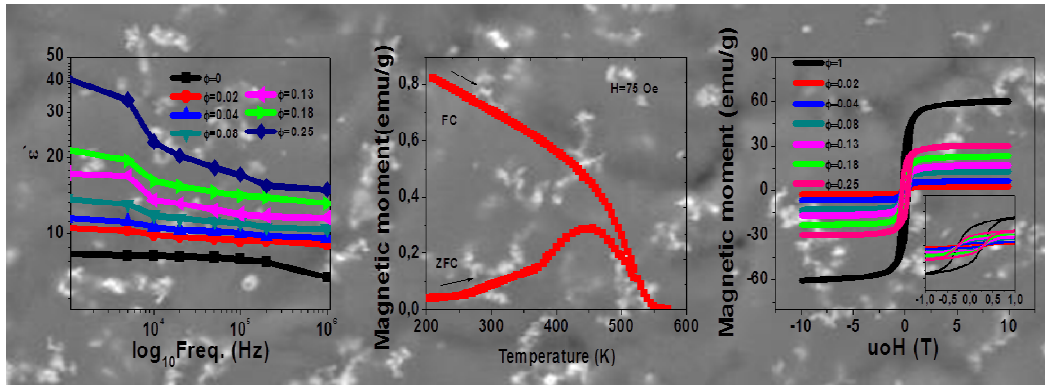
Particulate composite films of Poly(vinylidene fluoride) (PVDF) and ferrires ($CoFe_2O_4$ and $NiFe_2O_4$) were prepared from solvent casting and melt processing. The well dispersed ferrite nanoparticles nucleate the piezoelectric β-phase of the polymer, but the different ferrites nucleate the whole polymer crystalline phase at different filler concentrations. The macroscopic magnetic and dielectric response of the composites demonstrates a strong dependence on the volume fraction of ferrite nanoparticles, with both magnetization and dielectric constant increasing for increasing filler content. The β-relaxation in the composite samples is similar to the one observed for β-PVDF obtained by stretching. A superparamagnetic behaviour was observed for PVDF/$NiFe_2O_4$ composites, whereas PVDF/$CoFe_2O_4$ samples develop a hysteresis cycle with coercivity of 0.3 T.

7.1 Introduction

PVDF is a semicrystalline polymer with one of the largest pyro- and piezoelectric properties among polymers [1]. These properties combined with its high elasticity, transparency and easy processing make this material suitable for numerous technological applications [2].

PVDF is also well known for its polymorphism, showing at least four crystalline phases called α, β, δ and γ [3]. The α and β polymorphs are most common: melt processing of the material typically results in the nonpolar α-phase [4], whereas the polar β-phase is technologically the most interesting one for sensor and actuator applications at it shows the largest piezoelectric, pyroelectric and ferroelectric coefficients, as well as a high dielectric constant [1]. The β-phase of PVDF is commonly obtained by mechanical stretching of films originally in the non-polar α-phase, resulting in films mostly in the β-phase, but with some percentage of α-phase [5]. Further, this method is not appropriate for the preparation of polymer composites, as the stretching process is either hindered for high filler loadings and/or leads to non-controlled reconfigurations of the fillers, as well as their agglomeration [1].

β-PVDF films can be also obtained directly by solution casting but the material shows high porosity leading to an opaque appearance and a decrease of the electrical and mechanical properties. Further, due to their increased fragility the films cannot be oriented by stretching [4, 6]. The development of polymer nanocomposites is a subject of intensive research [7]. In the simplest case, adding nanoparticles to a polymer matrix such as PVDF can enhance its performance or provide new responses, by simply capitalizing on the nature and properties of the nanoscale filler [8]. This is the case of composite materials consisting of magnetic nanoparticles dispersed in a polymer matrix. On the one hand, the processability and mechanical quality of the matrix is an advantage compared to ferrites. On the other hand, despite a restricted particle concentration, a sufficiently high magnetic permeability can be achieved within the polymer composite [9], finally the ME effect can be also observed in such composites [10-12].

Van Suchtelen introduced the idea of the two-phase particulate composites [13], which was supported by the van den Boomgaard's synthesis conditions [14]. The composites with a ferrite and a ferroelectric phases have the ability to show product and sum properties [15]. In such composites, electromechanical coupling occurs:

magnetostriction in the ferrite phase give rise to a mechanical stress within the ferroelectric phase, resulting in variations of the electrical polarization and therefore in a ME effect [16]. MF materials are in this way excellent candidates as memory elements, smart sensors, etc [17].

Due to the magnetic and dielectric properties of ferrites, much interest has been focused on polymer-based composites filled with ferrite nanoparticles, such as Cobalt-ferrite [18], and Nickel-ferrite [19] for their applications in various areas such as information storage, electromagnetic wave absorption, bio-separation, and diagnostics. Their magnetostrictive properties also make them good candidates for ME composites [20].

Three kinds of bulk ME composites have been reported: magnetic metals/alloys, laminated Terfenol-D and piezoelectric ceramics or polymers and most recently particulate composites of ferrite and piezoelectric ceramics e.g., PZT [21]. The ME coefficients obtained in ceramic particulate or laminated composites are typically three orders of magnitude higher than in single phase materials [22-23]. On the other hand, the composites become fragile and are limited by deleterious reactions at the interface regions making such ceramic composites not suitable for device applications [24]. To overcome some of the problems polymer based ME materials are developed such as particulate composite of Terfenol-D, PZT and a polymer matrix has been developed [25]. In this three-phase ME composite, the magnetostrictive Terfenol-D grains are randomly oriented in a matrix of piezoelectric PZT with the polymer as a binder between the phases. In these materials, the incorporation of PZT into the polymeric matrix makes the composite more brittle [25-26] and although Terfenol-D has the highest magnetostriction amongst all known magnetostrictive materials, this rare-earth iron alloy is quite costly and also very brittle.

One approach to obtain highly flexible and non brittle ME composites is to use two phase polymer based composites without any ceramic filler, in which the polymer itself is piezoelectric, such as PVDF in its β-phase.

In this paper, PVDF-based nanocomposites with either Co or Ni ferrites fillers are investigated. The effect of the filler concentration on the dielectric and magnetic properties are discussed, as they are at the base of the different potential applications of these materials. It is particularly important to notice that the electroactive phase of the polymer is nucleated by the ferrites, leading in this way to a simplified processing method for the preparation of ME composites.

Pedro Martins

7.2 Experimental

7.2.1 Preparation of the nanocomposites

$CoFe_2O_4$ and $NiFe_2O_4$ nanoparticles were purchased from Nanoamor. The ferrite dimensions are between 35-55 and 20-30 nm and the densities 5.30 and 5.37 g/cm^3 for $CoFe_2O_4$ and $NiFe_2O_4$, respectively. DMF (pure grade) was supplied by Fluka and PVDF (Solef 1010) with a density of 1.78 g/cm^3 was supplied by Solvay. All the chemicals and nanoparticles were used as received from the suppliers.

For the preparation of the nanocomposite films with thickness around 40-50 μm the initial concentration of solution was 0.2 g of PVDF for 1 ml of DMF. In order to obtain a good dispersion of the ferrite nanoparticles within the polymeric matrix, the following procedure was applied: the desired amount of nanoparticles was added to 12 ml of DMF and then placed in an ultrasound bath during 6 h, in order to ensure that the nanoparticles are well dispersed in the solution; then 3 g of PVDF were subsequently added. Further, the obtained mixture was placed in a Teflon mechanical stirrer during 1h for complete dissolution of the polymer. Flexible films were obtained by spreading the solution on a clean glass substrate. Solvent evaporation and polymer crystallization was performed inside an oven at controlled temperature: the samples were maintained inside the oven for 10 min at 210 ºC to ensure the complete melting of the nanocomposite and solvent evaporation. Crystallization was achieved by cooling down to room temperature. The wt.% of ferrite nanoparticles varied from 0.001 to 50 in the case of Co-ferrite and 5 to 50 in the case of Ni-ferrite, corresponding to $3x10^{-6}$ to 0.25 and 2 to 0.25 in ɸ, respectively.

7.2.2 Characterization of the nanocomposites

SEM was performed in a Leica Cambridge S360 apparatus in order to evaluate composite microstructure and nanoparticle dispersion. XRD measurements were performed using a Philips PW1710 diffractometer equipped with Ni-filtered Cu Kα radiation (λ=0.1542nm) in order to identify and quantify the crystalline phase of the polymer.

Measurements of ε', real part of the dielectric function, and tan δ, dielectric loss were performed with an automatic Quadtech 1929 Precision LCR meter in a Linkam THMSE 600 oven. The applied signal for frequencies in the range 1 Hz to 1 MHz was 0.5 V. The

samples were coated by thermal evaporation with circular Au electrodes of 5mm diameter onto both sides of the sample. Sample thickness was ~50 μm for all samples. Temperature scans were performed at a temperature rate of 1 °C/min from −120 to 150 °C.

For the magnetic characterization, Zero Field Cooled (ZFC) and Field cooled (FC) low field magnetization vs. temperature curves and room temperature hysteresis loops were performed by conventional magnetometry using both a Superconducting quantum interference device (SQUID) and a vibrating sample magnetomer. For the ZFC and FC the characterization was performed at low field (75 Oe) in a range of temperature from 200 K to 575 K in the case of CoFe2O4 nanocomposites and from 4 K to 300 K in the case of nickel ferrite samples.

To the room temperature hysteresis loops H_{DC} was varied from -10 to 10 T and from -1.8 to 1.8 for $CoFe_2O_4$ and $NiFe_2O_4$ films respectively.

7.3 Results and discussion

Figure 7.1 shows typical SEM images of nanocomposite films of PVDF/$CoFe_2O_4$ with ϕ=0.02 (a and b) and ϕ=0.25 (c and d). For low Co or Ni ferrite filler concentrations, the microstructure of PVDF is spherulitic, just like pure PVDF in the α-phase [5, 27] as it can be observed in Figures 7.1a and 7.1b. For higher concentrations (ϕ=0.08 or higher) of ferrite particles, the spherulitic structure is destroyed and the polymer material just agglomerates on the ferrite particles, as it may be observed in Figures 7.1c and 8.1d. Further, ferrite aggregates are formed for these concentrations. The crystallization kinetics of α-PVDF is characterized by a spherulitic growth with heterogeneous nucleation [28]. Typical spherulite sizes range from 10 to 100 μm, depending on the crystallization temperature [29]. The presence of the ferrite particles will interfere both in the nucleation process and in the growth kinetic of the spherulites [30]. For low concentration of ceramic particles, mostly the nucleation process will be affected. Further, the change in the crystallization kinetics will have an influence on the polymer phase and degree of crystallinity of the polymer as well [30]. For higher concentrations, on the other hand, the filler particles will hinder the spherulites to grow and therefore will prevent the formation of the characteristic spherulitic microstructure of the polymer (Figure 7.1c and 7.1d). In fact the polymer phase in these composites is dispersed in very small domains which constrain crystal growth. A fraction of the

polymer chains is confined between the nanoparticle aggregates and probably inside of the aggregates shown in Figures 7.1c and 7.1d. Finally, the SEM micrograph of the nanocomposites also shows that a good dispersion of the ferrite nanoparticles within the polymer is achieved.
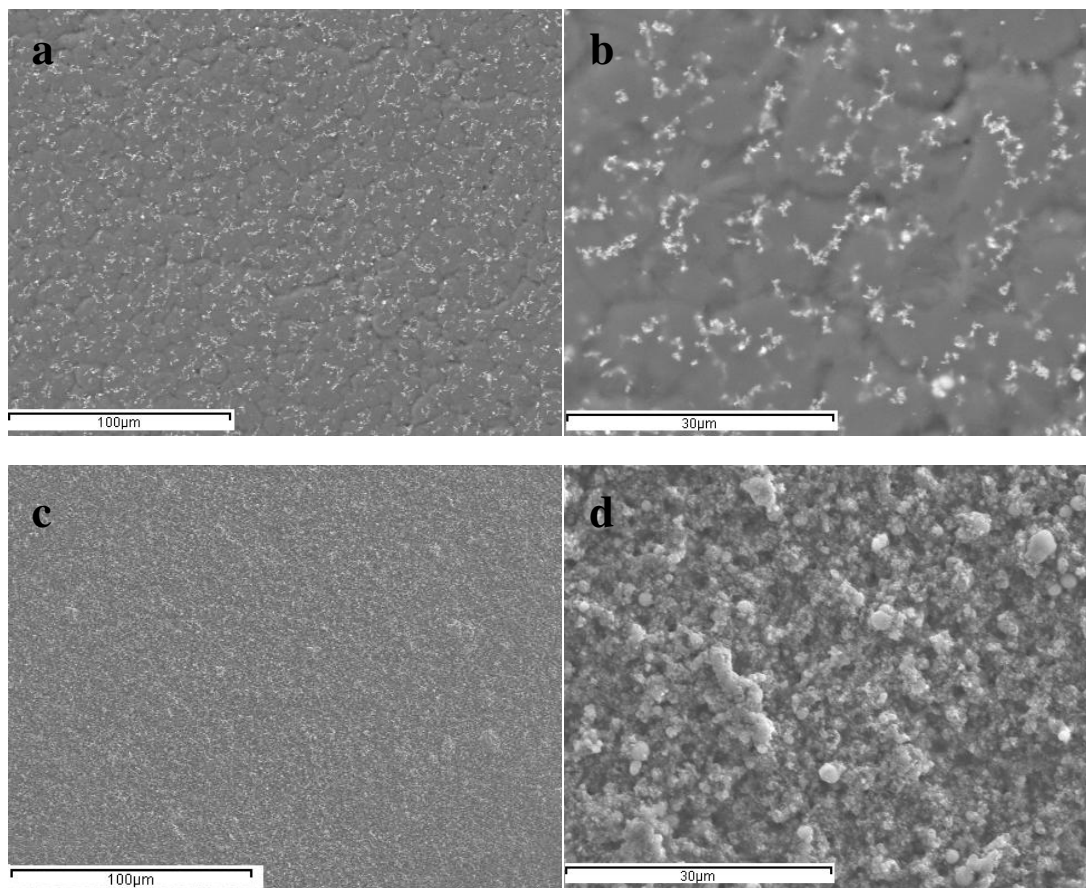
Figure 7.1 − SEM images of PVDF/CoFe$_2$O$_4$ nanocomposites with ferrite φ=0.02 (a and b) and φ=0.25 (c and d).

The evolution of the crystalline phases of the polymer present in the PVDF/CoFe$_2$O$_4$ and PVDF/NiFe$_2$O$_4$ composites as a function of ferrite concentration was obtained by XRD (Figure 7.2).
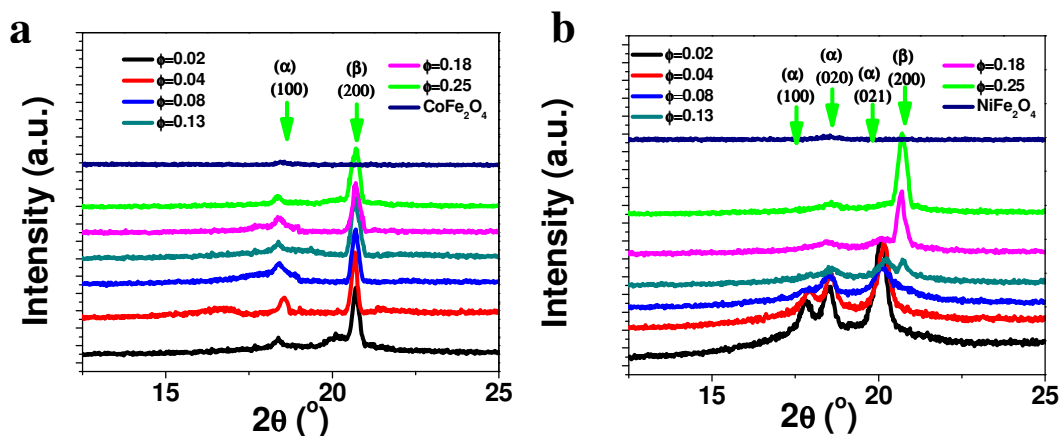
Figure 7.2 − XRD patterns for PVDF/CoFe$_2$O$_4$ (a) and PVDF/NiFe$_2$O$_4$ (b) nanocomposites as for composites with different ferrite contents.

At room temperature, α-PVDF is characterized by three strong reflections at 2θ=17.7º, 18.4º, and 19.9º, corresponding to the (100), (020) and (021) crystalline planes. On the other hand, the β-phase of PVDF is characterized by the peak at 2θ=20.7 and 20.8 matching the (200) and (110) planes [27, 31].

As already shown elsewhere, adding ferrite nanoparticles results in the α to β phase transformation (Figure 7.2 and 7.3) [6]. This fact is confirmed by the peak evolution of the XRD spectra of Figure 7.2. The evolution of the phase content, calculated by the baseline method [32-33] is represented in Figure 7.3.
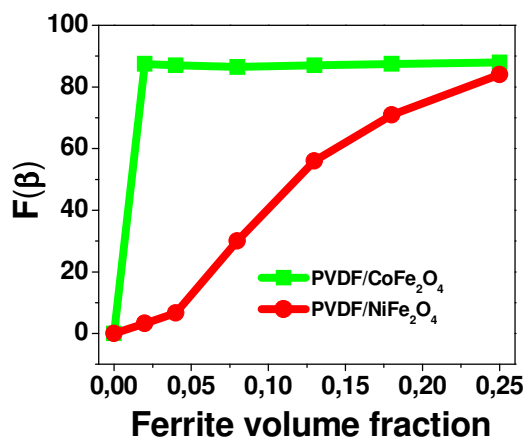
Figure 7.3 − β-phase content of the PVDF nanocomposites as a function of CoFe$_2$O$_4$ and NiFe$_2$O$_4$ ferrite content.

The nucleation effect of the β-phase of the polymer is stronger for the Co-ferrite nanoparticles than for the Ni-ferrite ones. In the first case, for nanoparticle contents lower than ϕ=0.05 the 90% of the polymer crystalline phase nucleates in the piezoelectric β-phase. This fact is only achieved for the Ni-ferrite composite for nanoparticle contents around ϕ=0.25. This variation is to be attributed to the different polymer/filler surface interactions as the geometrical factors are similar with both fillers [30].

Figure 7.4 shows the variation of the dielectric constant at room temperature of PVDF/CoFe$_2$O$_4$ (a) and PVDF/NiFe$_2$O$_4$ (b) composites. In both cases there is an increase of ε' for the composites with respect to the pure polymer.
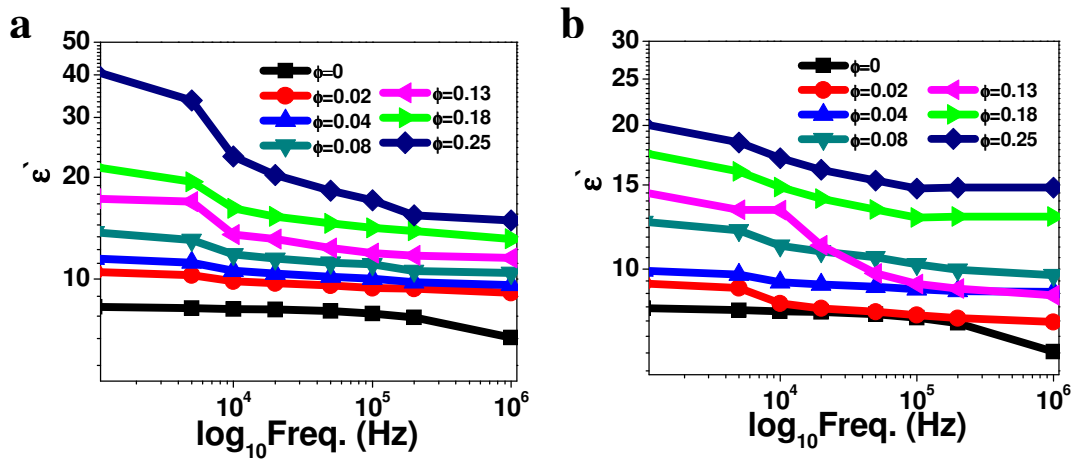
Figure 7.4 – Frequency-dependent dielectric constant for PVDF/ CoFe$_2$O$_4$ (a) and PVDF/ NiFe$_2$O$_4$ (b) nanocomposites.

The higher values obtained for the dielectric constant of the composites are for the PVDF/CoFe$_2$O$_4$ nanocomposites.

The dielectric losses increase almost linearly with increasing nanoparticle loading, maintaining nevertheless values lower that 0.3 even for the largest nanoparticle loadings.

Figure 7.5 shows the variation of the dielectric constant of the nanocomposites with ferrite wt.% for a frequency of 10 kHz.
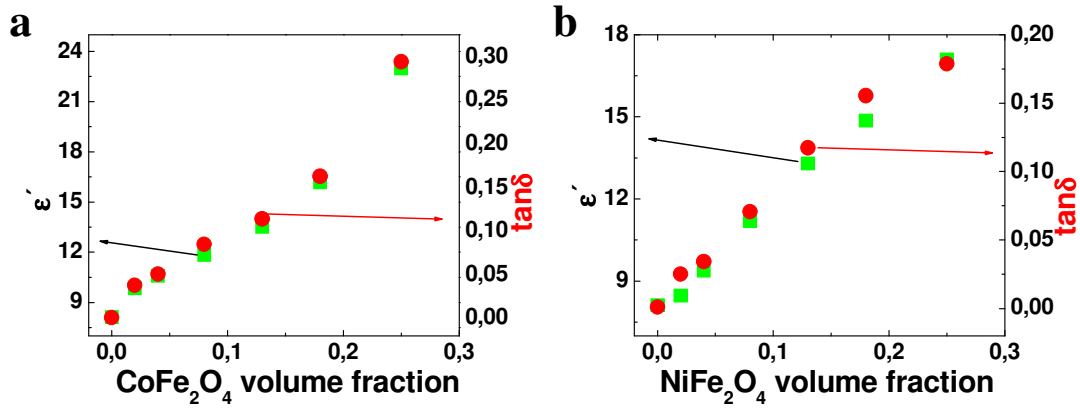
Figure 7.5 − Variation of the dielectric constant of the nanocomposites as a function of CoFe$_2$O$_4$ (a) and Ni Fe$_2$O$_4$ (b) content at room temperature for a frequency of 10 kHz.

Figure 7.5 shows that the inclusion of ferrite nanoparticles in the PVDF matrix leads to a gradual increase of the ε' as the amount of nanoparticles is increased. The increase of ε' is practically linear with increasing ferrite concentration for both ferrites. The dielectric constant is larger for the Co-ferrite composites due to the early nucleation of the β−phase of the polymer which shows a polar nature and larger dielectric constant than the α-phase of PVDF [1]. The dielectric losses shows a similar trend that the dielectric constant and also reflect the differences between the α and β-phases of PVDF, being the losses larger for the Co-ferrites that nucleate the polar β-phase of the polymer. The dielectric response as a function of temperature and frequency was also measured for the composites. Figure7.6 shows the variation of ε´ (a) and tan δ(b) for the PVDF/CoFe$_2$O$_4$ sample with 0.08 volume fraction of magnetic nanoparticles as a function of the temperature for several frequencies.
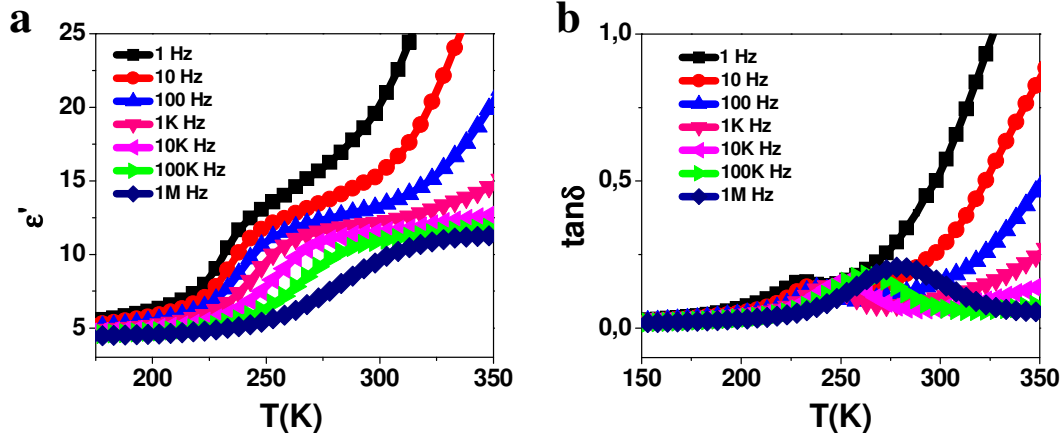
Figure 7.6 − ε' and tan δ vs temperature for the sample with 0.08 volume fraction of $CoFe_2O_4$ at several frequencies between 1 Hz and 1 MHz.

Figure 7.6 reveals that both the real part of the dielectric function and the dielectric losses show a similar behaviour as the pure polymer. The main difference is just the general increase of the dielectric response showing, on the other hand, the same characteristic features [4]. The low-temperature β-relaxation assigned to the glass transition dynamics of the pure polymer matrix is still present probing that the cooperative segmental motions within the amorphous phase [34] are also present in the composites.

The dynamics of the β-relaxation was analyzed by the Vogel–Fulcher–Tammann (VFT) relaxation formalism [34-36]:

$$\tau(T) = \tau_0 e^{\frac{B}{k_B(T-T_0)}} \tag{7.1}$$

Where τ is the relaxation time, τ_0 is the preexponential factor, B is the VTF energy, k_B is the Boltzmann constant, T_0 is the Vogel temperature at which molecular motions in the material becomes infinitely slow and T the temperature.

Figure 7.7 shows fittings obtained from the *VFT* formalism (equation 7.1) to PVDF/$CoFe_2O_4$ and PVDF/$NiFe_2O_4$ composites with ϕ=0.08 of ferrite nanoparticles content.
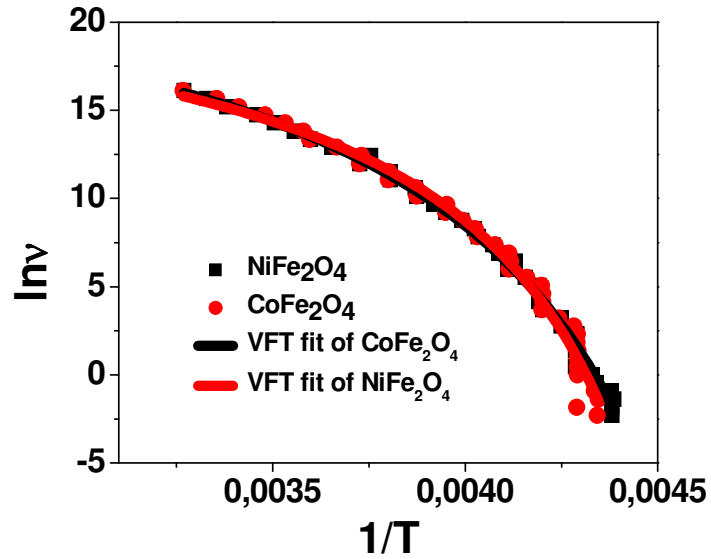
Figure 7.7 − *VTF* fittings of the **β**-relaxation of PVDF/CoFe$_2$O$_4$ and PVDF/NiFe$_2$O$_4$ with 0.08 of ferrite volume fraction.

The fitting parameters for the ϕ=0.08 nanocomposites are summarized in Table 7.1, in comparison with the results obtained for pure *α* and *β*-PVDF. Further, a consequence of the values of the fitting parameters of the VTF relaxation plot is the calculation of the fragility parameter [37]:

$$m = \frac{B / kT_g}{(\ln 10)(1 - T_c / T_g)^2} \qquad (7.2)$$

The *m(Tg)* value calculated with the VTF parameters is determined at the *Tg* where the relaxation time is equal to 100 s. The parameter *m* is an indication of the steepness of the variation of the material properties (viscosity, relaxation time) as T$_g$ is reached. A high *m* value defines a fragile material whereas a strong one will be characterized by small *m* values.

Pedro Martins

Table 7.1 − Vogel–Tammann–Fulcher and fragility parameters for the β-relaxation for α and β-PVDF and for the PVDF/$CoFe_2O_4$ and PVDF/$NiFe_2O_4$ nanocomposites with ferrite ϕ=0.08.

Sample	τ_0 s⁻¹	B eV	T_0 K	T_g K	m
α-PVDF [34]	$5.96E^{-13}$	0.13	168.00	213.00	67.00
β-PVDF [36]	$3.00E^{-12}$	0.06	201.50	228.67	99.00
PVDF/$CoFe_2O_4$	$4.93E^{-10}$	0.05	205.28	227.10	117.68
PVDF/$NiFe_2O_4$	$9.29E^{-11}$	0.07	197.18	225.08	97.08

Table 7.1 confirms that the inclusion of ferrite nanoparticles in PVDF actually nucleates the β-phase of the material as the characteristic parameters of the β-relaxation of the polymer are maintained with respect to the values obtained for β-phase obtained by stretching from the α-phase material (Table 7.1).) B, T_0 and T_g are independent of the processing method (stretching or nucleation) and are not affected by the type of ferrite [34]. This fact is also supported by the fragility parameters of PVDF/ferrites composites: these are higher than the ones calculated for the α-PVDF, demonstrating that the inclusions of ferrite nanoparticles has an effect on the relaxation process and affects in a significant way the amorphous part of the polymer. In fact, it is possible to observe from the *m* value that the ferrite particles immersed in the polymeric matrix make the composites more fragile (the *m* factor of the composite is higher than the pure polymer *α*-phase sample). The values are similar to the ones obtained for β-PVDF.

The magnetic characterization was performed by analyzing the low field (75 Oe) magnetization dependence with temperature (under zero field and field cooling conditions, ZFC-FC curves) of the pure ferrite powders and the room temperature hysteresis loops of the composites with different ferrite contents. In Figure 7.8 the obtained ZFC-FC curves for $CoFe_2O_4$ and $NiFe_2O_4$ are shown. There is a remarkable similarity between the low field magnetization behaviour for both ferrites, indicating that the magnetization process is basically the same. The degree of irreversibility of such processes is high, as indicated by the splitting between ZFC and FC curves. This irreversibility in nanoparticles arises from the competition between the energy needed for a particle moment reorientation against the energy concerning shape, magnetoelasticity and crystalline anisotropy. The bifurcation of both curves occurs at a temperature T_b (525 K and 300 K for the Co- and Ni- ferrites, respectively)

corresponding to the blocking temperature of the largest magnetic entities in the assembly. That is, T_b defines also a temperature above which magnetization processes are fully reversible. Below T_b , there is a maximum in the ZFC curve at a temperature T_p that hints for the blocking of all (any size) particles. However, while this maximum is sharp (at 450 K) for the $CoFe_2O_4$ ferrite, it turns out to be much broader and centred at 225 K for the $NiFe_2O_4$ ferrite, hinting for a larger particle size distribution present in this sample.
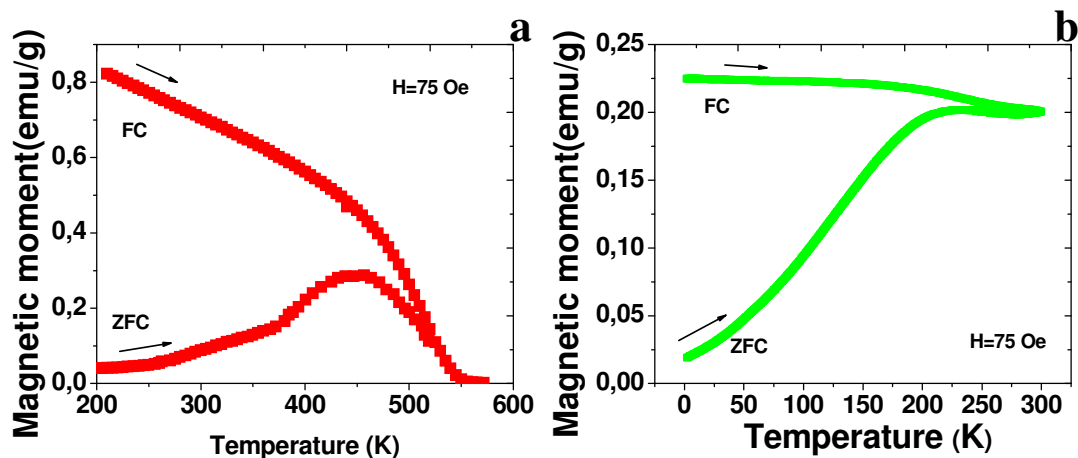
Figure 7.8 – Zero field cooled – field cooled low field (75 Oe) magnetization curves measured for (a) $CoFe_2O_4$ and (b) $NiFe_2O_4$ nanoparticles.

The value of the blocking temperature also marks a lower limit in temperature for superparamagnetic behaviour. Thus, at room temperature ($\approx$300 K) the $CoFe_2O_4$ has to behave as a ferromagnet with blocked magnetic moment within the particle, while the $NiFe_2O_4$ is just on the limit for superparamagnetic behaviour. This is fully confirmed by the room temperature hysteresis loops of the pure ferrite powders (Figure 7.9): while the Co- ferrite develops a hysteresis loop with coercivity of 0.27 T and reaches a saturation magnetic moment of 60 emu/g at a 10 T applied magnetic field, the Ni-ferrite shows almost absence of hysteresis, remanence and coercivity. For this last compound, room temperature is at or above the blocking temperature and the magnetic moment of the particle is free to rotate in response to the applied magnetic field.
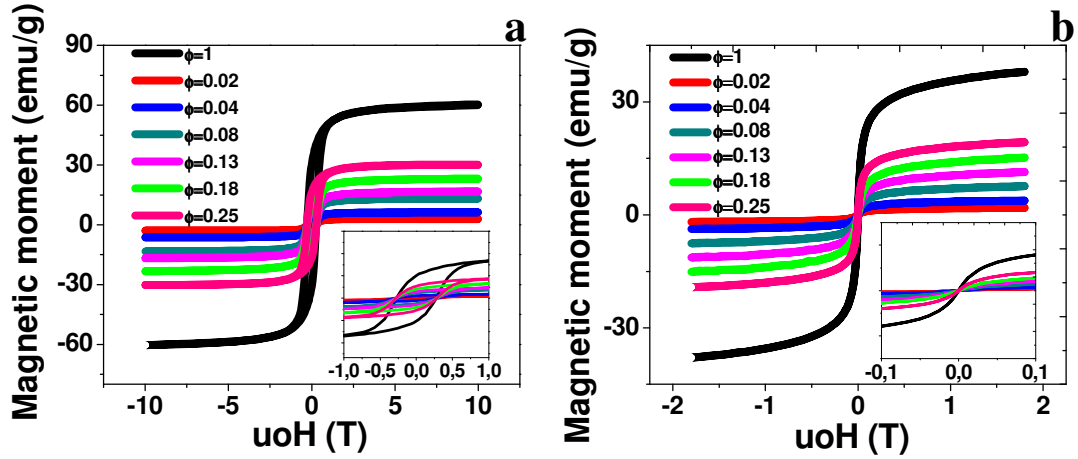
Figure 7.9 – Room temperature hysteresis measured for (a) PVDF/CoFe$_2$O$_4$ and (b) PVDF/NiFe$_2$O$_4$ nanocomposites with different ferrite contents. The hysteresis loops of the pure ferrite powders are also shown.

Since both ferrites have been supplied with almost the same size of the nanoparticles, the origin of such different magnetic behaviour must be elsewhere; in fact, Co^{+2} is highly anisotropic when compared to the Ni^{+2} ion [38], giving rise to a much higher anisotropy value for the CoFe$_2$O$_4$ ferrite than for the NiFe$_2$O$_4$ one. The effective value K_{eff} of that anisotropy inside the PVDF matrix can be evaluated by taking care of the different magnetic behaviours exhibited at room temperature. Thus, for the 50 wt.% PVDF/CoFe$_2$O$_4$ composite the fit of the magnetization data at high fields using the Law of Approach to Saturation [39]

$$\chi = \frac{\partial M}{\partial H} \approx \frac{\alpha` K_{eff}^2}{M_S H^3} \qquad (7.3)$$

where χ is the magnetic susceptibility, M the magnetization, H the magnetic field, K$_{eff}$ is the anisotropy constant, and M$_s$ is the saturation magnetization, gives as result a value of the anisotropy constant $K_{eff} = $ 1.58 x 10^5 ergs/cm^3, where $\alpha´ = 0.533$ was used as for the uniaxial anisotropy case [40]. This value is four times higher than the magnetic anisotropy constant in bulk Co ($\approx$ 0.4 x 10^5 ergs/cm^3 [41]).

This is not the case of the Ni- ferrite, where it is needed to analyze the approach of the magnetization to saturation in a system of particles that are not coupled by an exchange interaction. This approach is given by the Akulov law [42],

$$\frac{M(H)}{M_S} = 1 - \frac{1}{15}\left(\frac{H_a}{H}\right)^2, \qquad\qquad \textbf{(7.4)}$$

where $H_a = 2K_{eff}/M_S$ is the local magnetic anisotropy field of the Ni-ferrite nanoparticle and the rest of the terms are the same as in equation 7.3. From the fit of that curve in the case of the 5 wt.% PVDF/NiFe$_2$O$_4$ composite, a value of $K_{eff} = 0.12 \times 10^5$ ergs/cm^3 is obtained, that is one order of magnitude lower than for the Co-ferrite case. The obtained results for the anisotropy constant values fully support our previous assumptions.

The magnetic grain sizes of the composites can be also estimated by using the measured values of the blocking temperature (T$_b$) and the calculated values of the anisotropy K_{eff}. Both values are related by

$$T_b = \frac{K_{eff}V}{25k_B}, \qquad\qquad \textbf{(7.5)}$$

where V is the magnetic grain volume and k_B is the Boltzmann constant. From this equation they are obtained grain sizes of about 30 and 50 nm for the CoFe$_2$O$_4$ and the NiFe$_2$O$_4$ ferrites respectively, values that roughly agree with the sizes given by supplier and that also indicate, as a relevant result, that these nanoparticles behave as magnetic monodomains.

The shape of the measured *M(H)* loops of the nanocomposites along different directions (in-plane and out of plane of the composites) of the applied magnetic field also demonstrates that magnetic particles are randomly oriented within the polymer matrix (Figure 7.10).
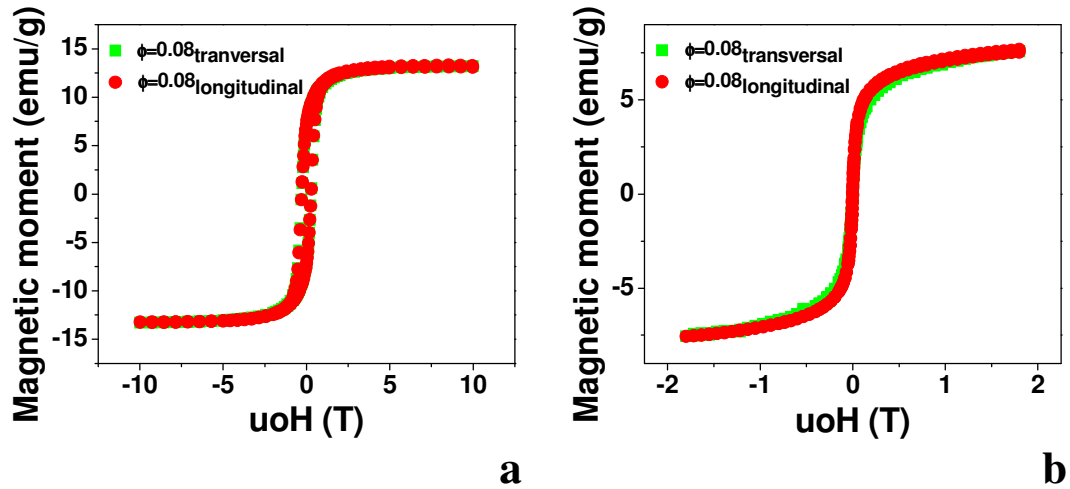
Figure 7.10 – Room temperature hysteresis loops measured along different relative directions of the field and the nanocomposite for (a) φ=0.08 of $CoFe_2O_4$ and (b)) φ=0.08 of $NiFe_2O_4$ nanocomposites.

From these hysteresis loops it is determined the experimental value of the room temperature saturation magnetic moment M_S by using Arrott plots [43]. Figure 7.11 shows how M_S continuously increases with ferrite content in the composite. This fact shows that the net magnetic moment exhibited by the composites turns out to be directly the vector sum of the individual contributions of the ferrite grains inside the PVDF matrix.
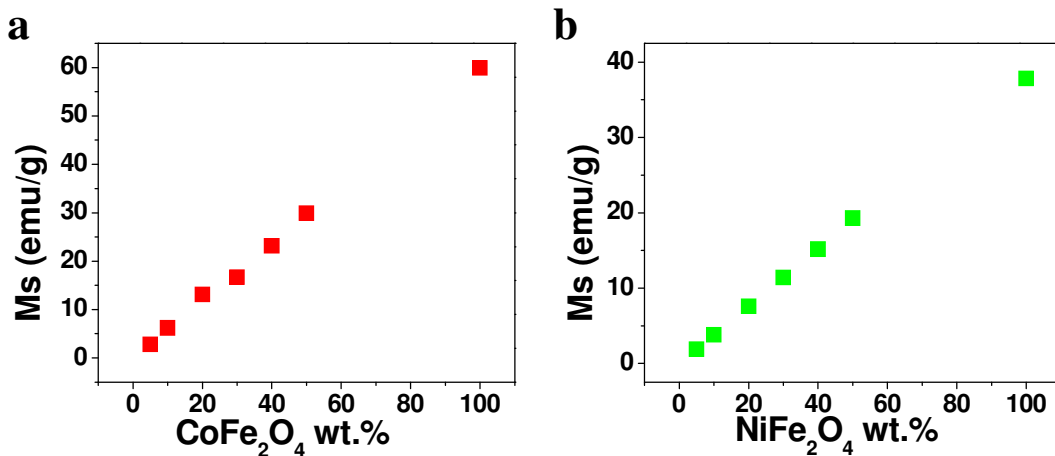
Figure 7.11 – Saturation magnetization dependence with the respective ferrite content for (a) PVDF/$CoFe_2O_4$ and (b) PVDF/$NiFe_2O_4$ nanocomposites.

This measured linearity in M_S value vs. % ferrite is a clear indication of the fact that ferrite particles are very well dispersed in the composite.

7.4   Conclusions

Composites consisting in $CoFe_2O_4$ and $NiFe_2O_4$ nanopowders as ferrite phase and PVDF as ferroelectric phase were prepared by solution method. XRD of the composites reveals the formation of the ferroelectric phase of the polymer with increasing ferrite content. The nucleation of the β-phase of the polymer is more effectively nucleated for the Co-ferrite nanoparticles, as the whole crystalline phase of the polymer is within the ferroelectric phase for ferrite concentrations as low as $\phi=0.02$. On the other hand, for Ni-ferrite nanocomposites as higher ferrite content ($\phi=0.25$) is needed to nucleate the whole polymer crystalline phase into the electroactive phase. This fact is due to nanoparticle surface/polymer interactions and not to size effects as the size of the ferrite nanoparticles are similar. The dielectric constant at room temperature of all nanocomposites increases with increasing ferrite content being the dielectric constant larger for the Co-ferrite composites, due to the polar nature of the polymer phase even for low ferrite concentrations. The β-relaxation related to the amorphous part of the polymer was identified in the composite samples and it is demonstrated that its behaviour is the same as the one observed for the β-PVDF obtained by stretching. While the PVDF/$CoFe_2O_4$ composites exhibit a hysteresis cycle with coercivity of 0.27 T, both missing coercitivity and hysteresis loop represent an evidence for quasi-superparamagnetic behaviour for PVDF/$NiFe_2O_4$ composites. That behaviour is also evidenced from the FC and ZFC dependences of the magnetization vs. temperature. From those ZFC-FC measurements it is also inferred that the nanopowders of both ferrites inside the polymeric matrix behave as magnetic monodomains. Finally, from both hysteresis loops shape and the linearity in M_s value vs. % content of ferrite it is concluded that the ferrite nanoparticles are homogeneously distributed within the composite and that the individual ferrite grains act as individual centers of magnetization.

7.5   References

1.   Sencadas, V., et al., *alpha-to-beta transformation on PVDF films obtained by uniaxial stretch.* Advanced Materials Forum Iii, Pts 1 and 2, 2006. **514-516**: p. 872-876.

2.   R. Gregono, M.C., N. Chaves, *The Polymeric Material Encyclopedia.* 1996, Boca Raton: CRC Press.

3.   Kang, S.J., et al., *Localized pressure-induced ferroelectric pattern arrays of semicrystalline poly(vinylidene fluoride) by microimprinting.* Advanced Materials, 2007. **19**(4): p. 581-+.

4.   Gregorio, R., M. Cestari, and F.E. Bernardino, *Dielectric behaviour of thin films of beta-PVDF/PZT and beta-PVDF/BaTiO3 composites.* Journal of Materials Science, 1996. **31**(11): p. 2925-2930.

5.   Sencadas, V., R. Gregorio, and S. Lanceros-Mendez, *alpha to beta Phase Transformation and Microestructural Changes of PVDF Films Induced by Uniaxial Stretch.* Journal of Macromolecular Science Part B-Physics, 2009. **48**(3): p. 514-525.

6.   Martins, P., C. Costa, and S. Lanceros-Mendez, *Nucleation of electroactive β-phase poly(vinilidene fluoride) with CoFe$_2$O$_4$ and NiFe$_2$O$_4$ nanofillers: a new method for the preparation of multiferroic nanocomposites.* Applied Physics A: Materials Science & Processing, 2010: p. 1-5.

7.   Hussain, F., et al., *Review article: Polymer-matrix nanocomposites, processing, manufacturing, and application: An overview.* Journal of Composite Materials, 2006. **40**(17): p. 1511-1575.

8.   Kanamadi, C.M., et al., *Dielectric and magnetic properties of (x)CoFe2O4 + (1-x)Ba0.8Sr0.2TiO3 magnetoelectric composites.* Materials Chemistry and Physics, 2009. **116**(1): p. 6-10.

9.   Hallouet, B., B. Wetzel, and R. Pelster, *On the dielectric and magnetic properties of nanocomposites.* Journal of Nanomaterials, 2007.

10. Ramprasad, R., et al., *Magnetic properties of metallic ferromagnetic nanoparticle composites.* Journal of Applied Physics, 2004. **96**(1): p. 519-529.

11. Dikeakos, M., et al., *Fabrication and characterization of tunable magnetic nanocomposite materials.* Polymer/Metal Interfaces and Defect Mediated Phenomena in Ordered Polymers, 2003. **734**: p. 315-320.

12. Bregar, V.B., *Advantages of ferromagnetic nanoparticle composites in microwave absorbers.* Ieee Transactions on Magnetics, 2004. **40**(3): p. 1679-1684.

13. Vansucht.J, *Product properties: a new application of composite materials.* Philips Research Reports, 1972. **27**(1): p. 28-&.

14. Vandenboomgaard, J., A. Vanrun, and J. Vansuchtelen, *Magnetoelectricity in piezoelectric-magnetostrictive composites.* Ferroelectrics, 1976. **10**(1-4): p. 295-298.

15. Uchino, K., *Ferroelectric Devices.* second ed. 2009, New York: TAYLOR & FRANCIS INC.

16. Devan, R.S. and B.K. Chougule, *Magnetic properties and dielectric behavior in ferrite/ferroelectric particulate composites.* Physica B-Condensed Matter, 2007. **393**(1-2): p. 161-166.

17. Srinivasan, G., et al., *Magnetoelectric effects in bilayers and multilayers of magnetostrictive and piezoelectric perovskite oxides.* Physical Review B, 2002. **65**(13).

18. Vaishnava, P.P., et al., *Magnetic properties of cobalt-ferrite nanoparticles embedded in polystyrene resin.* Journal of Applied Physics, 2006. **99**(8).

19. Sindhu, S., et al., *Synthesis and characterization of ferrite nanocomposite spheres from hydroxylated polymers.* Journal of Magnetism and Magnetic Materials, 2006. **296**(2): p. 104-113.

20. Zhang, J.X., et al., *The effect of magnetic nanoparticles on the morphology, ferroelectric, and magnetoelectric behaviors of CFO/P(VDF-TrFE) 0-3 nanocomposites.* Journal of Applied Physics, 2009. **105**(5).

21. Nan, C.W., et al., *Multiferroic magnetoelectric composites: Historical perspective, status, and future directions.* Journal of Applied Physics, 2008. **103**(3).

22. Sim, C.H., A.Z.Z. Pan, and J. Wang, *Thickness and coupling effects in bilayered multiferroic CoFe2O4/Pb(Zr0.52Ti0.48)O-3 thin films.* Journal of Applied Physics, 2008. **103**(12).

23. Nie, J.W., et al., *Strong magnetoelectric coupling in CoFe2O4-BaTiO3 composites prepared by molten-salt synthesis method.* Materials Chemistry and Physics, 2009. **115**(1): p. 400-403.

24. Mitoseriu, L., et al., *BaTiO3-(Ni0.5Zn0.5)Fe2O4 ceramic composites with ferroelectric and magnetic properties.* Journal of the European Ceramic Society, 2007. **27**(13-15): p. 4379-4382.

25. Nan, C.W., et al., *A three-phase magnetoelectric composite of piezoelectric ceramics, rare-earth iron alloys, and polymer.* Applied Physics Letters, 2002. **81**(20): p. 3831-3833.

26. Wan, J.G., et al., *Giant magnetoelectric effect of a hybrid of magnetostrictive and piezoelectric composites.* Journal of Applied Physics, 2003. **93**(12): p. 9916-9919.

27. Hasegawa, R., et al., *Crystal-Structures of 3 Crystalline Forms of Poly(Vinylidene Fluoride).* Polymer Journal, 1972. **3**(5): p. 600-&.

28. Mancarella, C. and E. Martuscelli, *CRYSTALLIZATION KINETICS OF POLY(VINYLIDENE FLUORIDE).* Polymer, 1977. **18**(12): p. 1240-1242.

29. Silva, M.P., et al., *alpha- and gamma-PVDF: Crystallization kinetics, microstructural variations and thermal behaviour.* Materials Chemistry and Physics, 2010. **122**(1): p. 87-92.

30. Sencadas, V., et al., *Influence of Ferrite Nanoparticle Type and Content on the Crystallization Kinetics and Electroactive Phase Nucleation of Poly(vinylidene fluoride).* Langmuir, 2011: p. null-null.

31. Scheinbeim, J.I., et al., *Poling-time dependence of the field-induced phase transition and piezoelectric response of poly(vinylidene fluoride) films.* Journal of Polymer Science Part B-Polymer Physics, 1980. **18**(11): p. 2271-2276.

32. Devan, R.S., S.B. Deshpande, and B.K. Chougule, *Ferroelectric and ferromagnetic properties of (x)BaTiO3+(1-x)Ni0.94Co0.01Cu0.05Fe2O4 composite.* Journal of Physics D-Applied Physics, 2007. **40**(7): p. 1864-1868.

33. Branciforti, M.C., et al., *New technique of processing highly oriented poly(vinylidene fluoride) films exclusively in the beta phase.* Journal of Polymer Science Part B-Polymer Physics, 2007. **45**: p. 2793-2801.

34. Mendes, S.F., et al., *Effect of the ceramic grain size and concentration on the dynamical mechanical and dielectric behavior of poly(vinilidene fluoride)/Pb(Zr0.53Ti0.47)O-3 composites.* Applied Physics a-Materials Science & Processing, 2009. **96**(4): p. 899-908.

35. Angell, C.A., *Why C-1=16-17 in the WLF equation is physical - and the fragility of polymers.* Polymer, 1997. **38**(26): p. 6261-6266.

36. Sencadas, V., et al., *Poling of beta-poly(vinylidene fluoride): dielectric and IR spectroscopy studies.* E-Polymers, 2005.

37. Lanceros-Mendez, S., et al., *Dielectric behavior in an oriented beta-PVDF film and chain reorientation upon transverse mechanical deformation.* Ferroelectrics, 2002. **273**: p. 2393-2398.

38. Carling, R.L., *Magnetochemistry.* 1986, Berlin Heidelberg: Springer-Verlag.

39. Chikazumi, S., *Physics of Ferromagnetism.* 1997, Oxford: Clarendon Press.

40. Ibusuki, T., et al., *Magnetic anisotropy and behaviors of Fe nanoparticles.* Ieee Transactions on Magnetics, 2001. **37**(4): p. 2223-2225.

41. Bozorth, R.M., *Ferromagnetism.* 1993, New York: IEEE Press.

42. Akulov, N.S., *Über den Verlauf der Magnetisierungskurve in starken Feldern.* Zeitschrift für Physik A Hadrons and Nuclei, 1931. **69**(11): p. 822-831.

43. Arrott, A., *Criterion for Ferromagnetism from Observations of Magnetic Isotherms.* Physical Review, 1957. **108**(6): p. 1394-1396.

8 Optimizing piezoelectric and magnetoelectric responses of P(VDF-TrFE)/CoFe$_2$O$_4$ and PVDF/CoFe$_2$O$_4$ nanocomposites
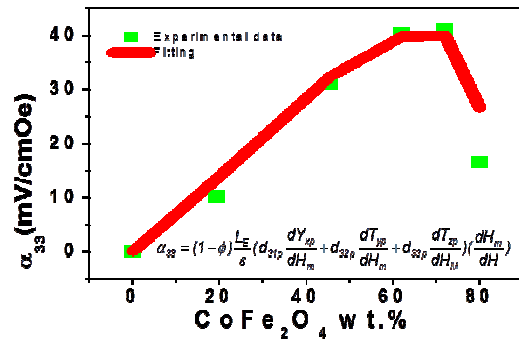
ME nanocomposite films composed of magnetostrictive CoFe$_2$O$_4$ nanoparticles embedded in Poly(vinylidene trifluorethylene) P(VDF-TrFE) and Poly(vinylidene fluoride) PVDF matrices have been successfully prepared by a solvent casting method. Ferroelectric and piezoelectric properties were improved when small amount of ferrite nanoparticles were added to the P(VDF-TrFE) matrix. Magnetic properties vary linearity with ferrite content in nanocomposites with both polymeric matrices. The highest ME response of 41.3 mV/cm.Oe was found in the composite P(VDF-TrFE)/CoFe$_2$O$_4$ (28/72 wt.%) when H$_{DC}$=0.25T was transversely applied to the sample surface. Two main differences were observed in the ME response in function of the H$_{DC}$ between nanocomposites with different polymer matrices:

i) ME response is higher in the unstretched P(VDF-TrFE) sample;

ii) PVDF based sample shows a linear behaviour contrary to the P(VDF-TrFE) samples that shows a non-linear response with a maximum for a given magnetic field.

Both differences were attributed to the existence of voids in the PVDF based ME nanocomposite. The good values of the ME coefficient and the flexibility of the films make these composites suitable for applications in ME smart devices.

8.1   Introduction

ME and MF materials with coexistence of at least two ferroic orders (ferroelectric, ferromagnetic or ferroelastic) have attracted increasing attention due to their potential device applications in areas such as data storage, switching, modulation of amplitudes, polarization and filters, waveguides, sensors, transducers and spin wave generation, among others [1-4]. One of the most promising ideas is that ME bits may be used to store information both in the magnetization M and polarization P. This type of encoding information in such four-state memory has recently been demonstrated [5-6].

In single phase MFs the magnetic and ferroelectric orders frequently occur largely independent of each other and as a result the ME coupling tends to be very small or occurs at temperatures too low for practical applications [3, 7]. On the other hand, and with larger design flexibility, MF ME composites fabricated by combining piezoelectric and magnetostrictive materials have drawn significant recent interest due to their multifunctionality, in which the coupling interaction between the piezoelectric and magnetostrictive phases produce a large ME response [8]. Due to their technologically viable ME response, different ME composites have been investigated in recent years, including multilayer and particulate composites [3].

So far, three main types of bulk ME composites have been investigated both experimentally and theoretically: a) magnetic metals/alloys e.g., laminated Terfenol-D and Metglas and piezoelectric ceramics; b) laminated Terfenol-D and Metglas and piezoelectric polymers; c) particulate composites of ferrite and piezoelectric ceramics e.g., PZT [3].

The ME coefficients obtained in ceramic particulate or laminated composites are typically three orders of magnitude higher than in single phase materials [9-10]. Ceramic composites, on the other hand, may become fragile and are limited by deleterious reactions at the interface regions leading to low electrical resistivities and high dielectric losses >0.1, hindering in this way the incorporation into devices of these materials [11].

Another promising and less explored approach to obtain a good ME coupling is the development of particulate composites of Terfenol-D and PZT within a polymer matrix [12]. Such composites can be easily fabricated by conventional low-temperature processing methods into a variety of forms such as thin sheets and moulded shapes. The simplest three-phase ME composite is a quasi 0-3 type particulate composite where

Terfenol-D grains are randomly oriented in a matrix of PZT and polymer. The incorporation of PZT into the polymeric matrix makes the composite more brittle [12-13] and although Terfenol-D has the highest magnetostriction amongst all known materials, this rare-earth iron alloy is quite costly and very brittle.

One way to avoid some of the aforementioned problems related to the use of ceramics and to obtain ME composites with high ME coupling is the use polymer based composites, where the polymer matrix is the piezoelectric phase.

PVDF and its copolymers have the best electroactive performance in the small class of polymers displaying piezo, pyro and ferroelectricity. These properties are originated from the strong molecular dipoles within the polymer chains [14]. From the four crystal modifications known for PVDF, denoted as α, β, γ and δ, the highest piezo-, pyro- and ferroelectric properties are associated to the β-phase.

P(VDF-TrFE) copolymers, containing VDF between 55 and 82 mol%, have been widely studied for their interesting ferroelectric properties. Besides the pyro- and piezoelectric activities of PVDF, those copolymers exhibit a ferro- to paraelectric phase transition at a temperature Tc which is below the melting temperature of the material and whose value increases with increasing VDF mol% content. Contrary to the PVDF homopolymer, when crystallized from the melt these copolymers present the ferroelectric phase, which is an essential factor for the preparation of ME composites [15-16].

Piezoelectric properties of PVDF polymers and co-polymers, that strongly influence the ME response are dependent of the experimental processing conditions [17-18].

Preliminary studies on MF nanocomposite films composed of P(VDF-TrFE) and $CoFe_2O_4$ nanoparticles have been conducted in films prepared by a complex processing method involving vacuum treatment [19]. This study shows the potential of these composites for ME applications but effect of low ferrite concentrations in the ferroelectric, piezoelectric and magnetic responses was not been reported. Further, the effect of magnetic field direction and the composite thickness in the magnetic and ME response also needs to be addressed in order to obtain suitable materials for useful applications. Since copolymer crystallizes from the melt directly in the electroactive phase which is an essential requirement for the preparation of ME composites, P(VDF-TrFE) is being used in ME composites instead of PVDF, but to their distinct morphological and physical properties, it would be useful to implement also PVDF based ME composite materials.

In this work P(VDF-TrFE)/$CoFe_2O_4$ and PVDF/$CoFe_2O_4$ ME composites were prepared by a simplified solvent casting method without vacuum treatment have been investigated addressing the aforementioned issues.

Further, the size of the nanoparticles is half of the ones used in [19], looking for a larger interaction area between the piezoelectric and magnetostrictive phases.

8.2   Experimental

$CoFe_2O_4$ nanoparticles were purchased from Nanoamor with dimensions between 35-55 nm. The synthesis of this kind of nanoparticles is well discussed in the literature [20-22]. DMF (pure grade) was supplied by Fluka. P(VDF-TrFE) and PVDF (Solef 1010) were supplied by Solvay Solexis. All the chemicals and nanoparticles were used as received from the suppliers.

For composite preparation, the desired amount of nanoparticles was added to DMF and then placed in ultrasound bath during 8h to ensure that nanoparticles were well dispersed in the solution and also to avoid loose aggregates [23]. Then polymer powder was subsequently added. Further, the obtained mixture was placed in a Teflon mechanical stirrer with ultrasound bath for complete dissolution of the polymer during 2 h. Flexible films were obtained by spreading the solution on a clean glass substrate. Solvent evaporation and polymer crystallization were performed inside an oven at controlled temperature. The samples were maintained inside the oven for 10 min at 210 ºC. Crystallization was achieved by cooling down the samples to room temperature. In the P(VDF-TrFE) based nanocomposites, the content of ferrite nanoparticles was varied from 3 to 80 wt.% (0.01 to 0.59 in volume fraction) and the thickness of samples was controlled to be approximately 25, 50 and 75 μm. In order to study the effect of the polymer matrix in the ME response of the nanocomposite, two samples with 7 wt.% of $CoFe_2O_4$ were prepared, one with P(VDF-TrFE) as piezoelectric phase and the other with PVDF. To allow the piezoelectric response in the PVDF based sample, its isotropy was eliminated by submitting the film to a stretching of 100% using a MINIMAT universal testing machine (Polymer Laboratories) in tensile mode, with a 2 mm min^{-1} deformation rate.

The ferroelectric hysteresis loops of the composites were measured at room temperature using Radiant Ferroelectric Premier II LC equipment. After 30 min of corona poling at

120 ºC in a home-made chamber, the piezoelectric response (d_{33}) of the poled samples was analyzed with a wide range d_{33}-meter (model 8000, *APC Int Ltd*).

Magnetic hysteresis loops at room temperature were measured using a vibrating sample magnetometer (Oxford Instruments) up to a maximum field of 1.8 T.

In order to obtain the out of plane and in plane ME coefficient α_{33} and α_{31} respectively, Direct Current Magnetic Field (H_{DC}) and Alternating Current Magnetic Field (H_{AC}) magnetic fields were applied simultaneously in two directions: along the same direction that the electric polarization of the P(VDF-TrFE), that is, perpendicular to the composite´s surface and also parallel to the composite´s surface. The H_{AC} was provided by a pair of Helmholtz coils, being its amplitude of 8.1 mOe at 5 kHz. The external bias field was provided by an electromagnet with a maximum value of 1.2 T. The induced ME voltage in the samples was measured by using a Standford Research Lock-in amplifier.

8.3 Results and discussion

The ferroelectric hysteresis loops of the P(VDF-TrFE) based composites with different ferrite wt.% as well for different thicknesses are presented in Figure 8.1a and Figure 8.1b, respectively.
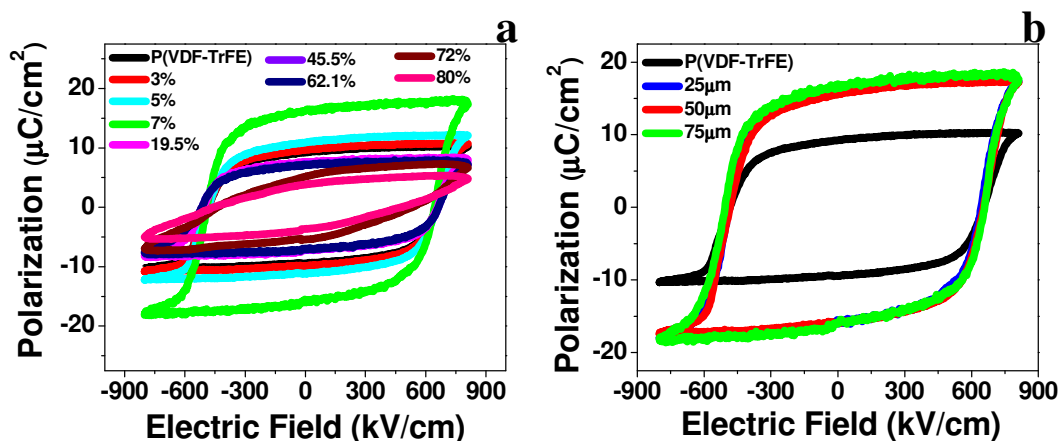

Figure 8.1 – (a) Weight fraction-dependent ferroelectric hysteresis loops for P(VDF-TrFE)/CoFe$_2$O$_4$ nanocomposites. (b) Ferroelectric hysteresis loops for nanocomposites with 7 wt.% for different polymer thicknesses (25μm, 50μm and 75μm) and for pure P(VDF-TrFE).

The ferroelectric properties were tested under an electric field with a maximum strength of 900 kV/cm. In Figure 8.1b it is possible to observe that nanocomposite thickness has no influence in the ferroelectric response of the samples, neither in the spontaneous polarization nor in the coercive field. This important fact is contrary to what is observed in other ferroelectric systems, in particular in composites in which the domain reversal within the films is changed due to the variations in the distribution of the filler in composites of different thickness [24].

All samples exhibit saturated hysteresis loops and the maximum polarization reaches a value of 18.1 $\mu C/cm^2$ with a filler content of 7 wt.%. Increasing ferrite concentration to higher values will cause a drop in the maximum polarization value. This enhancement in the maximum polarization value of polymer/ferrite nanocomposites for low loading contents has been reported previously [25]. Two main effects can be on the basis of this phenomenon: on the one hand ferrite nanoparticles may introduce additional free charges required to compensate and stabilize the polarization domain, on the other hand nanoparticles can act as heterogeneous nucleation centers for ferroelectric domains during the polarization [26]. Moreover, large interfacial areas in the composites containing nanometre scale fillers promote the exchange coupling effect through a dipolar interface layer and results in higher polarization levels and dielectric responses [27]. From ferrite contents higher than 19.5 wt.%, the maximum polarization decreases in comparison with the pure polymer, indicative of the existence of a critical point for the maximum ferrite content optimizing the ferro- and piezoelectric polymer response. At this concentration, the long-range ordered dipole ordering of the polymer chains is destroyed and the polarization decreases significantly due to the fact that nano-sized ferrite particles hinder domain wall movement [25].

It was also observed an increase of the coercive field with increasing ferrite content until a value of 62.1 wt.%. Increasing concentration from this value results in a sharp decrease in the coercive field of the nanocomposites.

The dependence of the maximum polarization and coercive field values with ferrite content in the $P(VDF-TrFE)/CoFe_2O_4$ nanocomposites is represented in Figure 8.2a.
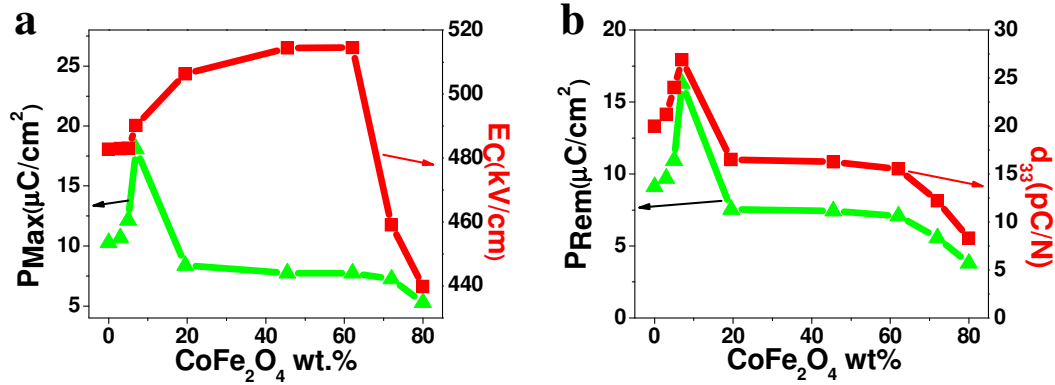
Figure 8.2 − (a) Weight fraction-dependent Maximum Polarization ($P_{Máx}$) and Coercive Electric Field (E_C) of P(VDF-TrFE)/$CoFe_2O_4$ nanocomposites. (b) Weight fraction-dependent Remnant Polarization and Piezoelectric Constant (d_{33}).

Figure 8.2b illustrates the correlation between the remnant polarization and piezoelectric response of the P(VDF-TrFE) based composites. As ferrite concentration increases, both quantities increase until a maximum value of 16.3 $\mu C/cm^2$ and 27 pC/N respectively at a concentration of ~ 7 wt.% content. For higher concentrations, the values of both remnant polarization and piezoelectric response decrease, being this decrease stronger for concentrations above 60 wt.% ferrite. In this way, the presence of small quantities of the magnetostrictive phase in the composite significantly improves the piezoelectric and polarization responses of the copolymer matrix, demonstrating that those nanocomposites are promising candidates for room temperature piezoelectric and ferroelectric applications. On the other hand, as demonstrated later, larger magnetostrictive phase than 7 wt.% is needed in order to obtain suitable ME coupling.

The sample with PVDF (result not shown) as piezoelectric phase and with 7 wt.% of $CoFe_2O_4$ exhibit a piezoelectric coefficient of 31 pC/N, slightly higher than the one obtained for the P(VDF-TrFE) based sample (27 pC/N).

The good ferroelectric and piezoelectric properties of P(VDF-TrFE)/$CoFe_2O_4$ nanocomposites are intimately related to the uniform dispersion of the ferrite nanoparticles [19]. The experimental results confirm that the presence of the nanoparticles significantly influence the polarization and piezoelectric responses of the copolymer matrix, in particular for low ferrite concentrations [28]. It has been reported that cobalt ferrites interact with the PVDF homopolymer matrix in order to favour the crystallization of the electroactive β-phase, which has a polar-all-*trans* conformation, with respect to α phase, which shows *trans*-gauche molecular conformation [23], i.e. Co

nanofillers favour the polar phase of the polymer. Analogously, low nanofiller concentration in the co-polymer matrix may favour arrangement of the polar conformations and therefore the increase of the ferroelectric and piezoelectric responses.

The saturation magnetization of a powder sample of $CoFe_2O_4$ nanoparticles is over 60 emu/g. Saturation magnetization values of the ferrite particles within the polymer matrix fit well to that value when the loops are normalized with the concentration of magnetic particles in the composites. The shape of the measured loops demonstrates that magnetic particles are randomly oriented within the polymer matrix (Figure 8.3).
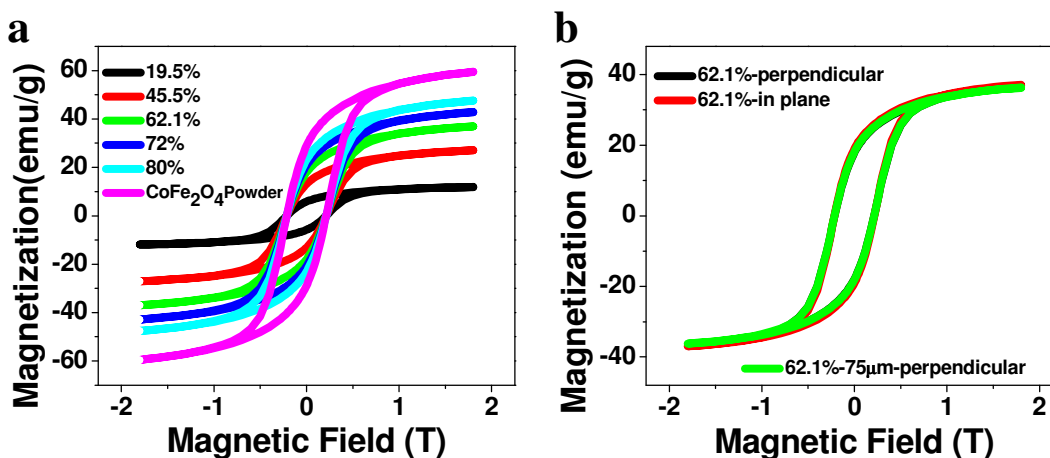
Figure 8.3 – (a) Room temperature hysteresis loops for the pure ferrite nanoparticle powder and for P(VDF-TrFE)/$CoFe_2O_4$ nanocomposites. (b) Room temperature hysteresis loops measured for the composite with 62.1wt.% of ferrite for different field directions.

For all composites a coercive field of 0.21 T was measured, higher than the measured one in similar nanocomposites prepared by other methods [19]. It was found that the thickness of the nanocomposite films, the direction of the magnetic field (in plane and out of plane), and the polymer matrix has no influence in the magnetic response of the nanocomposites.

Figure 8.4a shows the variation of the ME voltage coefficient with the H_{DC} for the different ferrite concentrations, measured under H_{AC} field of 1 Oe with a 5 kHz amplitude in the P(VDF-TrFE)/$CoFe_2O_4$ nanocomposites.
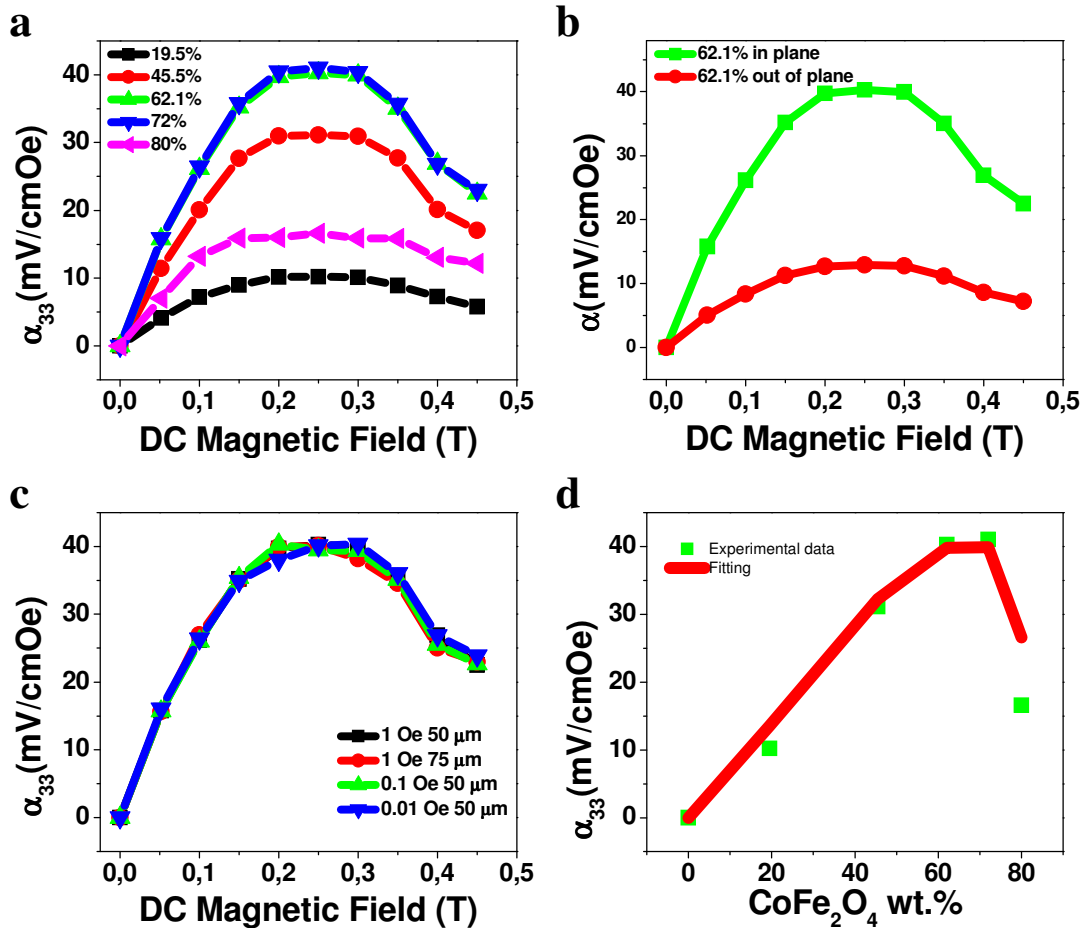
Figure 8.4 – (a) ME coefficients as a function of the bias field and filling fractions of $CoFe_2O_4$ nanoparticle. (b) In plane and out of plane ME response of 62.1 wt.% ferrite content samples. (c) Influence of thickness and H_{AC} in the ME response of 62.1 wt.% ferrite content samples. (d) ME coefficients of nanocomposite with different $CoFe_2O_4$ contents at a H_{DC}= 0.25T.

It can be observed that the induced voltage increases with increasing H_{DC} until a maximum of 41.3 mV/cm.Oe at a magnetic field of 0.25T. With further increase of the H_{DC} a decrease in the induced voltage is observed.

The differences of the in plane (magnetization parallel to the polarization) and out of plane (magnetization perpendicular to the polarization) can be observed in Figure 8.4b. The ME coefficient is three times higher in the out of plane measurement, which is fully to be attributed to the difference in the d_{33} and d_{31} piezoelectric constants of the polymer, since no difference is detected in the in plane and out of plane magnetic response of the nanocomposite [29] (see Figure 8.3b).

As can be seen in Figure 8.4c and as expected for well dispersed composites [30-31] no difference is noted in the ME response when composite thickness and H_{AC} are changed. In this way, it can be concluded that the residual stress status of the composites, that strongly depends on film thickness and deeply affects the ME coupling, together with preferential nanoparticle orientation and interface defects [32], does not play a significant role in the processed composites.

Figure 8.4d shows the ME response of the nanocomposites at a bias field of 0.25T for increasing $CoFe_2O_4$ loading. The initial increase in the ME voltage is explained by the increase of the magnetostriction due to the substantial increase the magnetostrictive phase. This response is optimized at 72 wt.% $CoFe_2O_4$ content. For higher concentrations, nanoparticles lead to the disruption of the ferroelectric copolymer phase [19], having as a result an abrupt decrease in the ME response of the nanocomposite. The theoretical fitting of this behaviour was performed by using the model presented in [30-31]. In this model, the ME response α_{33} can be expressed as:

$$\alpha_{33} = (1-\phi)\frac{L_E}{\varepsilon}(d_{31p}\frac{dY_{xp}}{dH_m} + d_{32p}\frac{dT_{yp}}{dH_m} + d_{33p}\frac{dT_{zp}}{dH_M})(\frac{dH_m}{dH}) \quad \textbf{(8.1)}$$

where L_E and $\frac{dH_p}{dH}$ are given by:

$$L_E = \frac{[\varepsilon_m + 2\varepsilon_p]]}{[(1-\phi)\varepsilon_m + (2+\phi)\varepsilon_p]} \quad \textbf{(8.2)}$$

$$\frac{dH_p}{dH} = \frac{3\xi_p}{(1-\phi)\left(\xi_m + \frac{dM_m}{dH_m}\right) + (2+\phi)\xi_p} \quad \textbf{(8.3)}$$

Here, p and m indicate the polymer and magnetic phase respectively. $\frac{dM_m}{dH_m}$ is obtained from the magnetization curve (Figure 8.3).

As expected and predicted by the theory, the good value of piezoelectric coefficient reached at 7 wt.% is not enough to obtain a good ME coefficient in samples with low magnetostrictive nanoparticle concentrations since it is necessary a substantial presence

of both ferroelectric and magnetostrictive phases [8, 33]. The optimal compromise is obtained for filler concentrations of 72 wt.%.

The significant discrepancy between the theoretical and experimental values in the highest concentrated sample is due to the fact that for these high nanoparticle loadings, filler dispersion cannot be properly achieved. Therefore, this large amount of magnetostrictive phase leads to the disruption of the polymer microstructure and of the ferroelectric properties in the MF nanocomposite [19].

Comparing the ME response of (93/7 wt.%) P(VDF-TrFE)/CoFe$_2$O$_4$ sample with the stretched (93/7 wt.% PVDF/CoFe$_2$O$_4$) sample, different behaviours are observed (Figure 8.5a).
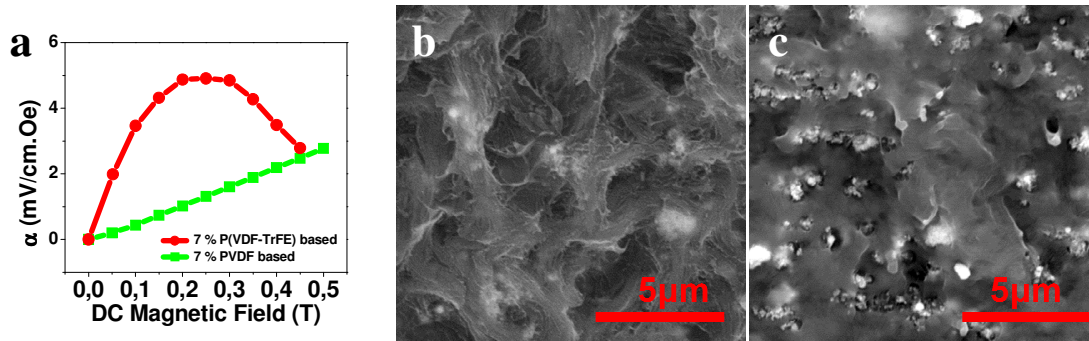
Figure 8.5 – (a) Comparison between the room temperature ME response of 7 wt.% of CoFe$_2$O$_4$ samples with PVDF and P(VDF-TrFE) as piezoelectric matrix as a function of H$_{DC}$ measured under H$_{AC}$ =1 Oe. (b) SEM image of the cross section of the (93/7 wt.%) P(VDF-TrFE)/CoFe$_2$O$_4$ sample. (c) SEM image of the cross section of the (93/7 wt.%) PVDF/CoFe$_2$O$_4$ sample.

The two main differences are that the ME response is higher in the unstretched sample and shows a non-linear response with a maximum for a given magnetic field. On the other hand the stretched samples shows a lower linear ME response as a function of the magnetic field, despite the higher piezoelectric coefficient.

SEM images of Figures 8.5b and 8.5c allow the better understanding of those differences. A detailed view of the microstructure reveals a heterogeneous morphology with the presence of voids resulting from the dragging of the particles in the polymer matrix due to the stretching of the PVDF based nanocomposite (Figure 8.5c). Nanoparticle-polymer interface represents defective structures that can be torn apart under mechanical solicitation.

The lower ME response is explained by the lower mechanical connectivity and the consequent weakening of mechanic-electrical transduction induced by the magnetic field due the existence of voids leading to damping of the elastic vibrations and increasing the loss of energy, contributing therefore to the decrease of the ME voltage coefficient.

Even when the existence of voids and porosity effects in polymer based ME composites has not been considered much in detail so far in the literature, it has been reported that porosity affects the H_{DC} at which the ME voltage coefficient is maximum [34-35] in a similar way as the one observed in the present work.

8.4   Conclusions

ME nanocomposites were successfully produced using P(VDF-TrFE) and its homopolymer PVDF as piezoelectric phase and $CoFe_2O_4$ nanoparticles as magnetostrictive phase. The resultant P(VDF-TrFE) based MF films exhibit saturated hard magnetic properties and a ME coefficient dependent on the loading of the magnetostrictive phase. The presence of low content of nanoparticles in the composite significantly improves the polarization and piezoelectric responses of the copolymer matrix, demonstrating that low filler content P(VDF-TrFE)/$CoFe_2O_4$ nanocomposites are promising candidates for room temperature piezoelectric and ferroelectric applications. The ME response of the P(VDF-TrFE) based nanocomposites is maximized for 72 wt.% filler contents, with a α_{33} value of 41.3 mV/cm.Oe. Since the value is among the highest reported in particulated polymer nanocomposites, this work provides a promising way to produce flexible ME materials to be applied in smart devices.

The ME response in the PVDF based sample was possible due to the destruction of the nanocomposite symmetry by a slight stretching process that allows the piezoelectric response after corona poling. Such process led to the formation of voids that strongly influenced the ME behaviour of the nanocomposites. The ME response is higher in the unstretched P(VDF-TrFE) samples and the PVDF based sample shows a linear ME response as a function of the H_{DC}, contrary to the P(VDF-TrFE) samples that exhibit a non-linear response with a maximum for a given H_{DC}. This distinct behaviour was attributed to the existence of voids in the PVDF based sample.

8.5   References

1.   Nan, C.W., et al., *Coupled magnetic-electric properties and critical behavior in multiferroic particulate composites.* Journal of Applied Physics, 2003. **94**(9): p. 5930-5936.

2.   Zhao, K., et al., *Effect of martensitic transformation on magnetoelectric properties of Ni2MnGa/PbZr0.52Ti0.48O3 composite.* Applied Physics Letters, 2005. **87**(16).

3.   Nan, C.W., et al., *Multiferroic magnetoelectric composites: Historical perspective, status, and future directions.* Journal of Applied Physics, 2008. **103**(3).

4.   Fawzi, A.S., A.D. Sheikh, and V.L. Mathe, *Composition dependent electrical, dielectric, magnetic and magnetoelectric properties of (x)Co0.5Zn0.5Fe2O4 + (1-x)PLZT composites.* Journal of Alloys and Compounds, 2010. **493**(1-2): p. 601-608.

5.   Gajek, M., et al., *Tunnel junctions with multiferroic barriers.* Nature Materials, 2007. **6**(4): p. 296-302.

6.   Shi, Z., et al., *A four-state memory cell based on magnetoelectric composite.* Chinese Science Bulletin, 2008. **53**(14): p. 2135-2138.

7.   Fiebig, M., *Revival of the magnetoelectric effect.* Journal of Physics D-Applied Physics, 2005. **38**(8): p. R123-R152.

8.   Nan, C.W., *Magnetoelectric effect in composites of piezoelectric and piezomagnetic phases.* Physical Review B, 1994. **50**(9): p. 6082-6088.

9.   Sim, C.H., A.Z.Z. Pan, and J. Wang, *Thickness and coupling effects in bilayered multiferroic CoFe2O4/Pb(Zr0.52Ti0.48)O-3 thin films.* Journal of Applied Physics, 2008. **103**(12).

10. Nie, J.W., et al., *Strong magnetoelectric coupling in CoFe2O4-BaTiO3 composites prepared by molten-salt synthesis method.* Materials Chemistry and Physics, 2009. **115**(1): p. 400-403.

11. Mitoseriu, L., et al., *BaTiO3-(Ni0.5Zn0.5)Fe2O4 ceramic composites with ferroelectric and magnetic properties.* Journal of the European Ceramic Society, 2007. **27**(13-15): p. 4379-4382.

12. Nan, C.W., et al., *A three-phase magnetoelectric composite of piezoelectric ceramics, rare-earth iron alloys, and polymer.* Applied Physics Letters, 2002. **81**(20): p. 3831-3833.

13. Wan, J.G., et al., *Giant magnetoelectric effect of a hybrid of magnetostrictive and piezoelectric composites.* Journal of Applied Physics, 2003. **93**(12): p. 9916-9919.

14. Bauer, S., et al., *Piezoelectric polymers.* Electroresponsive Polymers and Their Applications, 2006. **889**: p. 23-30.

15. Legrand, J.F., S*tructure and ferroelectric properties of P(VDF–TrFE) copolymers.* Ferroelectrics, 1989. **91**: p. 303-317.

16. Sencadas, V., S. Lanceros-Mendez, and J.F. Mano, *Behaviour of the ferroelectric phase transition of P(VDF/TrFE) (75/25) with increasing deformation.* Ferroelectrics, 2004. **304**: p. 853-856.

17. Branciforti, M.C., et al., *New technique of processing highly oriented poly(vinylidene fluoride) films exclusively in the beta phase.* Journal of Polymer Science Part B-Polymer Physics, 2007. **45**: p. 2793-2801.

18. Gomes, J., et al., *Influence of the beta-phase content and degree of crystallinity on the piezo- and ferroelectric properties of poly(vinylidene fluoride).* Smart Materials & Structures, 2010. **19**(6): p. 65010-65010.

19. Zhang, J.X., et al., *The effect of magnetic nanoparticles on the morphology, ferroelectric, and magnetoelectric behaviors of CFO/P(VDF-TrFE) 0-3 nanocomposites.* Journal of Applied Physics, 2009. **105**(5).

20. Liu, C., A.J. Rondinone, and Z.J. Zhang, *Synthesis of magnetic spinel ferrite CoFe2O4 nanoparticles from ferric salt and characterization of the size-dependent superparamagnetic properties.* Pure and Applied Chemistry, 2000. **72**(1-2): p. 37-45.

21. Kim, Y.I., D. Kim, and C.S. Lee, *Synthesis and characterization of CoFe2O4 magnetic nanoparticles prepared by temperature-controlled coprecipitation method.* Physica B-Condensed Matter, 2003. **337**(1-4): p. 42-51.

22. Maaz, K., et al., *Synthesis and magnetic properties of cobalt ferrite (CoFe2O4) nanoparticles prepared by wet chemical route.* Journal of Magnetism and Magnetic Materials, 2007. **308**(2): p. 289-295.

23. Martins, P., C. Costa, and S. Lanceros-Mendez, *Nucleation of electroactive β-phase poly(vinilidene fluoride) with CoFe$_2$O$_4$ and NiFe$_2$O$_4$ nanofillers: a new method for the preparation of multiferroic nanocomposites.* Applied Physics A: Materials Science & Processing, 2010: p. 1-5.

24. de la Cruz, J.P., et al., *Thickness effect on the dielectric, ferroelectric, and piezoelectric properties of ferroelectric lead zirconate titanate thin films.* Journal of Applied Physics, 2010. **108**(11).

25. Guo, Y.P., et al., *Giant Magnetodielectric Effect in 0-3 Ni0.5Zn0.5Fe2O4-Poly(vinylidene-fluoride) Nanocomposite Films.* Journal of Physical Chemistry C, 2010. **114**(32): p. 13861-13866.

26. Kusuma, D.Y., C.A. Nguyen, and P.S. Lee, *Enhanced Ferroelectric Switching Characteristics of P(VDF-TrFE) for Organic Memory Devices.* Journal of Physical Chemistry B, 2010. **114**(42): p. 13289-13293.

27. Li Junjun; Seok Sang Il; Chu Boojin; et al., *Nanocomposites of Ferroelectric Polymers with TiO(2) Nanoparticles Exhibiting Significantly Enhanced Electrical Energy Density.* Advanced Materials, 2009. **21**(2): p. 217-221.

28. Chu, B.J., et al., *Large enhancement in polarization response and energy density of poly(vinylidene fluoride-trifluoroethylene-chlorofluoroethylene) by interface effect in nanocomposites.* Applied Physics Letters, 2007. **91**.

29. Bar-Cohen, Y., *Electroactive Polymer (EAP) Actuators as Artificial Muscles: Reality, Potential, and Challenges*, S. Press, Editor. 2004: Bellingham, Washington.

30. Wong, C.K. and F.G. Shin, *Effect of inclusion deformation on the magnetoelectric effect of particulate magnetostrictive/piezoelectric composites.* Journal of Applied Physics, 2007. **102**(6).

31. Zhou, Y. and F.G. Shin, *Magnetoelectric effect of mildly conducting magnetostrictive/piezoelectric particulate composites.* Journal of Applied Physics, 2006. **100**(4).

32. Jing Ma, J.H., Zheng Li, Ce-Wen Nan, *Recent Progress in Multiferroic Magnetoelectric Composites: from Bulk to Thin Films.* Advanced Materials, 20011. **23**(9).

33. Ryu, J., et al., *Magnetoelectric effect in composites of magnetostrictive and piezoelectric materials.* Journal of Electroceramics, 2002. **8**(2): p. 107-119.

34.   Sheikh, A.D. and V.L. Mathe, *Effect of the piezomagnetic NiFe2O4 phase on the piezoelectric Pb(Mg1/3Nb2/3)(0.67)Ti0.33O3 phase in magnetoelectric composites.* Smart Materials & Structures, 2009. **18**(6).

35.   Petrov, V.M., et al., *Magnetoelectric effects in porous ferromagnetic-piezoelectric bulk composites: Experiment and theory.* Physical Review B, 2007. **75**(17).

Pedro Martins

9 Linear anhysteretic direct magnetoelectric effect in P(VDF-TrFE)/Ni$_{0.5}$Zn$_{0.5}$Fe$_2$O$_4$ 0-3 nanocomposites
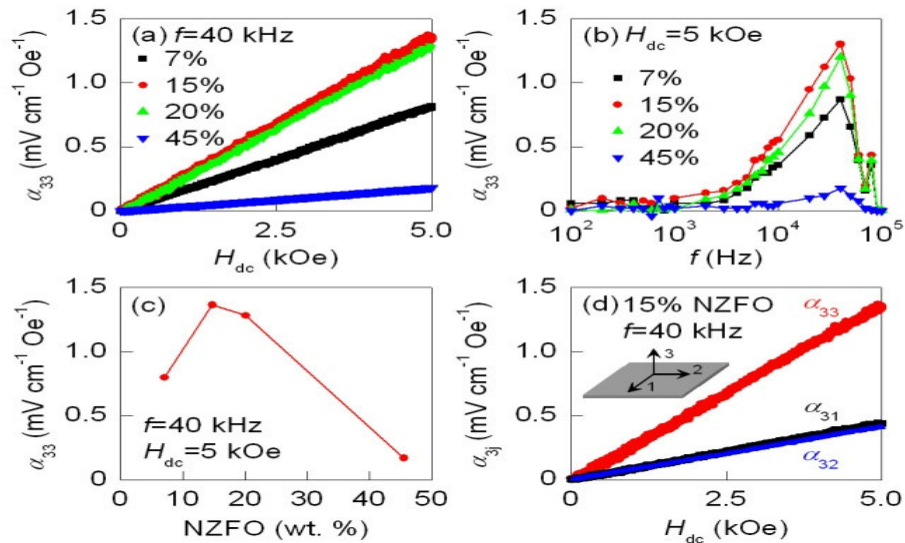
Free-standing flexible ME 0-3 composite films, comprising Ni$_{0.5}$Zn$_{0.5}$Fe$_2$O$_4$ ferrite nanoparticles in a Poly(vinylidene trifluorethylene) (P(VDF-TrFE)) copolymer matrix, have been prepared at low temperatures by solvent casting and melt crystallization. Ferroelectric, piezoelectric, magnetic and direct ME properties of the nanocomposites depend strongly on ferrite concentration. ME voltage coefficients increase linearly with applied H$_{DC}$ up to 0.5T and show no hysteresis. At this field, a maximum ME voltage coefficient of 1.35 mV cm^{-1} Oe^{-1} was obtained for samples with 15 wt. % ferrite using a 40 kHz resonant signal.

9.1 Introduction

ME effects arise in materials, or combinations of materials, that are electrically and magnetically polarisable due to coupling between electrical polarization and magnetization mediated sometimes by strain[1]. The direct ME effect is the modification of electrical polarization P by magnetic field H, and the converse effect is the change of magnetization M by electric field E. Intrinsic ME effects in single-phase materials typically occur at low temperatures and are weak [1,2]. Two-phase composites consisting of strain-coupled piezoelectric (or electrostrictive) and magnetostrictive (or piezomagnetic) materials yield large ME effects at room temperature[3] and are therefore interesting for applications, e.g. magnetic-field sensors, transducers, resonators and energy harvesting [3,4].

The performance of ME composites depends both on the piezoelectric (or electrostrictive) and magnetostrictive (or piezomagnetic) properties of the individual components and their coupling. Strain coupling requires intimate contact between the constituent phases and depends strongly on the geometry of the composite, which is usually described by the connectivity of the phases. Giant direct ME voltage coefficients, $\alpha \sim 7$ V cm^{-1} Oe^{-1} at low frequencies and ~ 300 V cm^{-1} Oe^{-1} at the 50 kHz resonance, have been reported in 2-2 laminate composites of high-magnetic-permeability Fe-Si-Co Metglas and piezoelectric PVDF polymer layers bonded using epoxy resin [5]. Similar values have been observed in 2-1 laminate composites consisting of piezoelectric Pb(Zr,Ti)O$_3$ fibres bonded between Fe-B-Si-C Metglas layers using epoxy resin [6], ~ 20 V cm^{-1} Oe^{-1} at low frequencies and ~ 750 V cm^{-1} Oe^{-1} at the 21 kHz resonance.

The strong ME effects discussed above are non-linear and occur only at low magnetic bias fields (< 20 Oe) such that they are not suitable for use as high-field DC magnetic sensors. Moreover, performance is compromised by the relative brittleness of the epoxy bonding the component phases. However, 0-3 composites of magnetic nanoparticles embedded in a ferroelectric polymer matrix overcome this problem because the magnetic material is in direct contact with, and completely surrounded by, the ferroelectric material. Also, for sufficiently small nanoparticle weight fractions, the mechanical properties of the ferroelectric polymer are preserved and therefore the nanocomposites can be easily processed at low temperatures into a variety of shapes for applications [3,7].

Pedro Martins

Recently, small ME effects up to 40 mV cm^{-1} Oe^{-1} were obtained in P(VDF-TrFE)/CoFe$_2$O$_4$ nanocomposites [7] at high H$_{DC}$ (0.2T). However, the ME response was found to be non-linear at these high fields, and hysteretic at lower fields (CoFe$_2$O$_4$ nanoparticles have coercive field H_c = 0.14T), precluding applications. Here we exploit Ni$_{0.5}$Zn$_{0.5}$Fe$_2$O$_4$ nanoparticles, which are superparamagnetic [8] below 30 nm, in order to achieve linear and anhysteretic direct ME effects in P(VDF-TrFE)/Ni$_{0.5}$Zn$_{0.5}$Fe$_2$O$_4$ nanocomposites.

9.2 Experimental

P(VDF-TrFE) 75/25 mol% powder was purchased from Solvay Solexis, NZFO nanoparticles (10-30 nm) were purchased from Nanoamor and pure grade DMF solvent was purchased from Fluka. P(VDF-TrFE)/NZFO 0-3 nanocomposites were prepared using the procedure described in [9]. NZFO nanoparticles were added to the DMF and the solution was placed in an ultrasonic bath for 8 h. P(VDF-TrFE) powder was subsequently added and the resultant solution was mixed using a Teflon mechanical stirrer and an ultrasonic bath until the polymer was completely dissolved (2 h). Films were obtained by using a coating bar to spread the solution on a clean glass substrate. The solvent was evaporated by heating the films in an oven at 210 ℃ for 10 min. Subsequent cooling to room temperature caused the polymer to crystallize. Finally, free-standing flexible polycrystalline films were obtained by detaching the glass substrate. Films of thicknesses ~ 25, 50 and 75 μm were prepared with nanoparticle content varying from 3 to 45 wt.% (0.01 to 0.23 in ϕ).

9.3 Results and discussion

Ferroelectric $P(E)$ loops were measured using a Radiant Ferroelectric Premier II LC. Out-of-plane piezoelectric coefficients d_{33} were measured using a model 8000 wide range d_{33}-meter (APC Int Ltd). Prior to d_{33} measurements, the films were corona poled for 30 min at 120 ℃ and during the subsequent cooling to room temperature. In-plane E_Y were obtained from the initial slope of strain-stress curves measured for 3.5 mm × 13 mm specimens using a MINIMAT universal testing machine (Polymer Laboratories) in tensile mode, with a 2 mm min^{-1} loading rate. Magnetization $M(H)$ curves were measured up to 1.8T using a vibrating sample magnetometer (Oxford Instruments). For

direct ME measurements, poled nanocomposite films were cut into square specimens (side $l \sim 6 - 10$ mm), and circular 1.4 mm-diameter gold electrodes were sputtered on opposite sides. An electromagnet was used to provide H_{DC} bias, and a Helmholtz coil connected to an HP3245A source was used to generate the H_{AC}. Dynamic ME voltages were measured using a 5302 EG&G lock-in amplifier. All measurements were carried out at room temperature.

Figure 9.1a shows room-temperature ferroelectric $P(E)$ loops of 50 μm-thick P(VDF-TrFE)/NZFO nanocomposites for selected compositions.
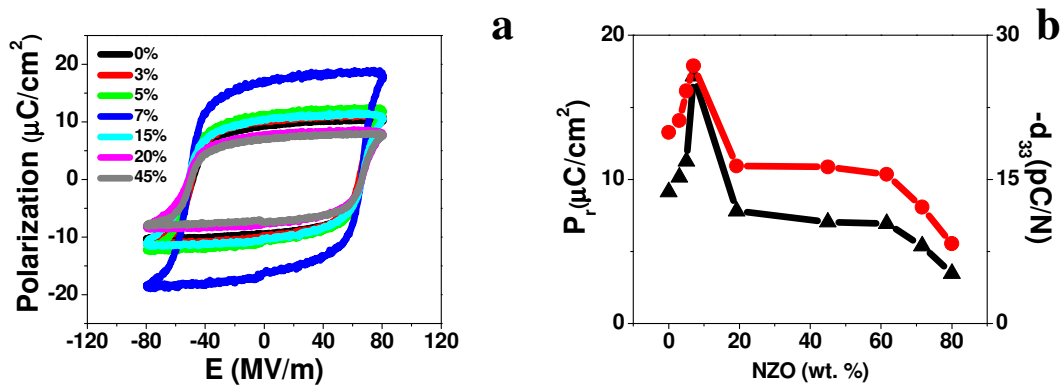

Figure 9.1 − Room-temperature ferroelectric and piezoelectric properties of 50 μm-thick P(VDF-TrFE)/NZFO 0-3 nanocomposites. (a) Polarization P as a function of electric field E for composites with different ferrite concentrations. (b) Remnant polarization P_r and negative piezoelectric coefficient $-d_{33}$ as functions of NZFO content.

The addition of small quantities of NZFO nanoparticles increases P_r and piezoelectric coefficient $-d_{33}$ (Figure 9.1b) because nanoparticles improve the crystallinity of the polymer matrix near the interface [10,11]. For NZFO concentrations higher than 7 wt.%, the ferroelectric polarization decreases with increasing nanoparticles content and at 20 wt.% becomes smaller than the polarization of pure P(VDF-TrFE) due to the disruption of the polymer matrix [7]. 25 μm and 75 μm-thick nanocomposite films possess similar ferroelectric properties (not shown), unlike pure P(VDF-TrFE) thin films whose ferroelectric properties are strongly thickness dependent, e.g. due to changes in crystallinity and domain structure [12,13].

Figure 9.2 shows room-temperature out-of-plane magnetization $M(H)$ loops of 50 μm-thick P(VDF-TrFE)/NZFO nanocomposites for selected compositions.
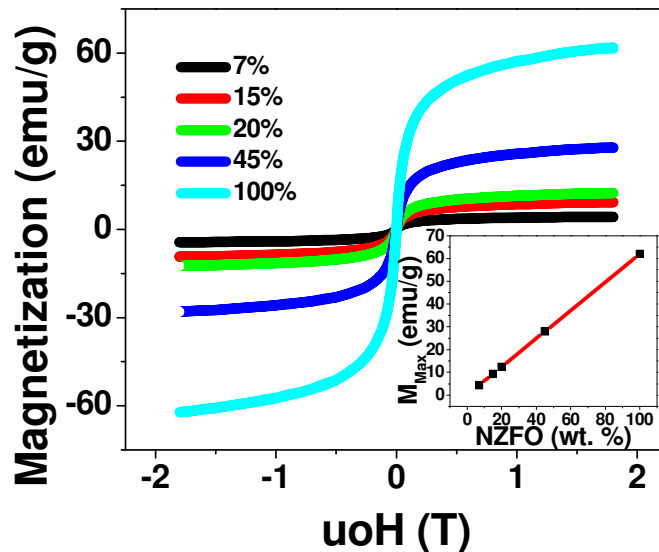
Figure 9.2 – Room-temperature out-of-plane magnetization $M(H)$ of 50 μm-thick P(VDF-TrFE)/NZFO 0-3 nanocomposites with different ferrite concentrations. Inset shows the magnetization M_{max} measured at 1.8T as a function of NZFO content.

As expected, nanocomposite magnetization increases with increasing NZFO content. The nanocomposites show negligible magnetic coercivity and remanence, and the magnetization does not quite saturate at our maximum applied magnetic field of 1.8T, consistent with the superparamagnetic behaviour [8] of nanoparticles whose diameter is less than 30 nm. Additional in-plane $M(H)$ measurements (not shown) evidenced the isotropic magnetic character of the composite films, confirming good nanoparticle dispersion. $M(H)$ measurements of 75 μm-thick films (not shown) revealed no dependence of magnetic properties on nanocomposite thickness.

Figure 9.3a shows that the ME voltage coefficient α_{33} measured at resonance varies as a linear and anhysteretic function of out-of-plane bias field H_{DC}, for several different ferrite concentrations (the first index in α_{ij} indicates the collinear ferroelectric poling and electrical measurement directions, and the second indicates the applied magnetic field direction).
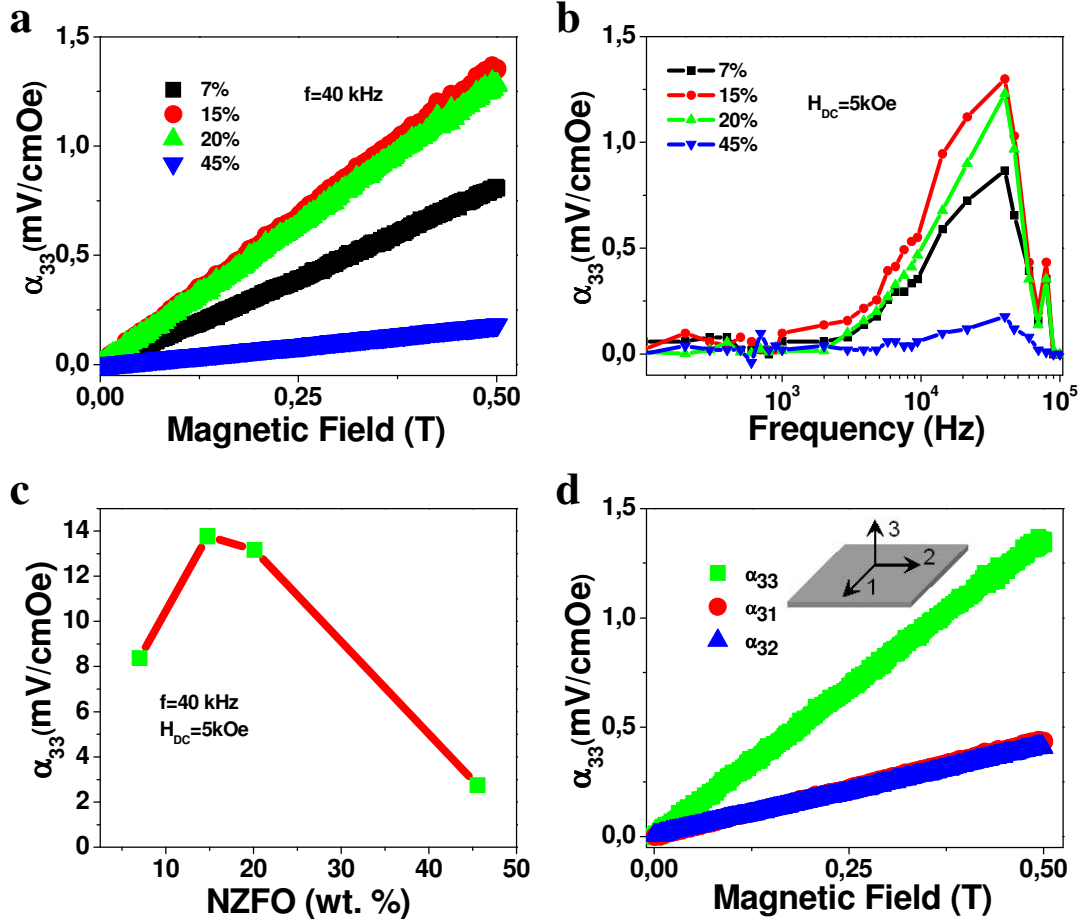
Pedro Martins

Figure 9.3 – Room-temperature dynamic ME response of 50 μm-thick P(VDF-TrFE)/NZFO 0-3 nanocomposites to out-of-plane H_{AC} fields of magnitude 1.27 Oe. (a) ME voltage coefficient α_{33} as a function of H_{DC} at resonance and (b) as a function of frequency at $H_{DC} = 0.5$T. (c) Maximum value of α_{33} as a function of NZFO content. (d) α_{3j} as a function of H_{DC} magnitude and direction (inset) at resonance for the sample with 15 wt.% NZFO. In (a) and (d), ME voltage is plotted for both increasing and decreasing H_{DC}.

The resonant frequency for each concentration was determined from 100 - 100 kHz scans at constant $H_{DC} = 0.5$T (Figure 9.3b). A peak in $\alpha_{33}(f)$ is seen at ~ 40 kHz for all the composites, and corresponds to the expected longitudinal electromagnetic resonance governed by the formula [14]

$$f_n \approx (n/2l)\sqrt{E_Y/\rho} \qquad \textbf{(9.1)}$$

where l is the length along the resonant direction, n is the order of the harmonic mode, and ρ and E_Y are density and Young's modulus, respectively (Table 9.1).

Table 9.1 – Longitudinal resonant frequencies for 50 μm thick P(VDF-TrFE)/NZFO 0-3 nanocomposites with different ferrite concentration, computed from equation 9.1. Volume fraction and density of the nanocomposites were calculated from the density of the components [1900 kg m^{-3} and 5200 kg m^{-3} for P(VDF-TrFE) and NZFO, respectively]. In-plane Young's modulus values E_Y of the composite films were obtained from the initial slope of strain-stress curves (not shown).

NZFO (wt.%)	NZFO (φ)	ρ	E_Y	l	f
7	2.7	(kg m^{-3})	(GPa)	(mm)	(kHz)
15	6.1	1990	0.52	6	42.5
20	8.4	2100	1.06	9	39.5
45	23	2180	1.14	9	40.2

The observed linear behaviour of the ME voltage coefficient may be attributed to linear magnetostriction in our nanocomposites, which has been previously reported at fields < 2-3T in 0-3 composites comprising ferromagnetic particles in a silicone matrix with low concentration of magnetic particles [15], and also in some paramagnetic materials [16]. Note that varying the amplitude of H_{AC} from 0.4 – 1.5 Oe yielded a linear variation in ME voltage (not shown) and therefore did not change α_{33}.

ME performance is maximized for 15 wt.% of NZFO (Figures 9.3a-c). As expected and predicted by the theoretical calculations, higher NZFO concentrated samples do not result in higher ME coupling due to relative decrease of the piezoelectric phase within the composite [7]. In a similar way, note that maximum ME performance is not obtained for the nanocomposite with the largest piezoelectric coefficient (7 wt.% of NZFO) because ME effect is a product property and magnetization, and therefore magnetostriction, of the nanocomposite increases with increasing NZFO content. The maximum value of $\alpha_{33} = 1.35$ mV cm^{-1} Oe^{-1} is smaller than the maximum $\alpha_{33} = 40$ mV cm^{-1} Oe^{-1} observed [7] in P(VDF-TrFE)/CoFe$_2$O$_4$ and the maximum 16 mV cm^{-1} Oe^{-1} predicted [17] for P(VDF-TrFE)/NiFe$_2$O$_4$ 0-3 nanocomposites, but larger than the 0.4 - 0.7 mV cm^{-1} Oe^{-1} response of all-ceramic 3-3 composites (Ni,Zn)Fe$_2$O$_4$/(Ba,Pb)(Zr,Ti)O$_3$ [18,19].

Figure 9.3d shows α_{33} together with α_{32} and α_{31}, as functions of H_{DC}, for the optimal sample with 15 wt.% of NZFO at resonance. The ME response is reduced by a factor of

around 3 when the H_{DC} is applied in-plane, i.e. $\alpha_{33} \sim 3\alpha_{32} \sim 3\alpha_{31}$. Given that the magnetic properties are isotropic (Figure 9.2), this anisotropy is attributed to the piezoelectric response of the polymer, which for highly crystalline pure films of P(VDF-TrFE) obeys [20] $-d_{33} \sim 3d_{31} \sim 3d_{32}$.

9.4 Conclusions

To conclude, we studied the ferroelectric, piezoelectric, magnetic and direct ME properties of free-standing, flexible 0-3 nanocomposite films of NZFO and P(VDF-TrFE) that were processed at low-temperature. Direct ME effects up to 1.35 mV cm^{-1} Oe^{-1} were obtained in a H_{DC}=0.5T, for samples with 15 wt.% of NZFO at the 40 kHz resonance. P(VDF-TrFE)/NZFO nanocomposites improve upon P(VDF-TrFE)/$CoFe_2O_4$ nanocomposites [7] as they show linear and non-hysteretic direct ME responses up to 0.5T. Our findings may be useful for DC magnetic-field sensors.

9.5 References

1.   Eerenstein, W., N.D. Mathur, and J.F. Scott, *Multiferroic and magnetoelectric materials.* Nature, 2006. **442**(7104): p. 759-765.
2.   Fiebig, M., *Revival of the magnetoelectric effect.* Journal of Physics D-Applied Physics, 2005. **38**(8): p. R123-R152.
3.   Nan, C.-W., et al., *Multiferroic magnetoelectric composites: Historical perspective, status, and future directions.* Journal of Applied Physics, 2008. **103**(3).
4.   Ma, J., et al., *Recent Progress in Multiferroic Magnetoelectric Composites: from Bulk to Thin Films.* Advanced Materials, 2011. **23**(9): p. 1062-1087.
5.   Zhai, J., et al., *Giant magnetoelectric effect in Metglas/polyvinilidene-fluoride laminates.* Applied Physics Letters, 2006. **89**(8).
6.   Dong, S., et al., *Near-ideal magnetoelectricity in high-permeability magnetostrictive/piezofiber laminates with a (2-1) connectivity.* Applied Physics Letters, 2006. **89**(25).
7.   Zhang, J.X., et al., *The effect of magnetic nanoparticles on the morphology, ferroelectric, and magnetoelectric behaviors of CFO/P(VDF-TrFE) 0-3 nanocomposites.* Journal of Applied Physics, 2009. **105**(5).
8.   Albuquerque, A.S., et al., *Nanosized powders of NiZn ferrite: Synthesis, structure, and magnetism.* Journal of Applied Physics, 2000. **87**(9): p. 4352-4357.
9.   Martins, P., C.M. Costa, and S. Lanceros-Mendez, *Nucleation of electroactive beta-phase poly(vinilidene fluoride) with CoFe(2)O(4) and NiFe(2)O(4) nanofillers: a new method for the preparation of multiferroic nanocomposites.* Applied Physics a-Materials Science & Processing, 2011. **103**(1): p. 233-237.
10.   Chu, B., et al., *Large enhancement in polarization response and energy density of poly(vinylidene fluoride-trifluoroethylene-chlorofluoroethylene) by interface effect in nanocomposites.* Applied Physics Letters, 2007. **91**(12).
11.   Li, J.J., et al., *Nanocomposites of Ferroelectric Polymers with TiO(2) Nanoparticles Exhibiting Significantly Enhanced Electrical Energy Density.* Advanced Materials, 2009. **21**(2): p. 217-+.
12.   Xia, F., et al., *Thickness dependence of ferroelectric polarization switching in poly(vinylidene fluoride-trifluoroethylene) spin cast films.* Applied Physics Letters, 2001. **78**(8): p. 1122-1124.
13.   Xu, H.S., *Dielectric properties and ferroelectric behavior of poly(vinylidene fluoride-trifluoroethylene) 50/50 copolymer ultrathin films.* Journal of Applied Polymer Science, 2001. **80**(12): p. 2259-2266.
14.   Israel, C., et al., *Magnetically tuned mechanical resonances in magnetoelectric multilayer capacitors.* Applied Physics Letters, 2009. **95**(7).
15.   Bednarek, S., *The giant linear magnetostriction in elastic ferromagnetic composites within a porous matrix.* Journal of Magnetism and Magnetic Materials, 2006. **301**(1): p. 200-207.
16.   Fawcett, E. and G.K. White, *Magnetostriction of Paramagnetic Transition Metals and Alloys.* Journal of Applied Physics, 1968. **39**(2P1): p. 576-&.
17.   Wong, C.K. and F.G. Shin, *Effect of inclusion deformation on the magnetoelectric effect of particulate magnetostrictive/piezoelectric composites.* Journal of Applied Physics, 2007. **102**(6).

Pedro Martins

18. Bammannavar, B.K. and L.R. Naik, *Magnetic properties and magneto electric effect in ferroelectric rich Ni0.5Zn0.5Fe2O4+ BPZT ME composites.* Journal of Magnetism and Magnetic Materials, 2009. **321**(5): p. 382-387.
19. Devan, R.S., et al., *Electrical properties and magnetoelectric effect measurement in (x)Ni0.8Cu0.2Fe2O4+(1-x) Ba0.9Pb0.1Ti0.9Zr0.1O3 composites.* Smart Materials & Structures, 2006. **15**(6): p. 1877-1881.
20. Wang, H., et al., *Piezoelectric, dielectric, and elastic properties of poly(vinylidene fluoride/trifluoroethylene.* Journal of Applied Physics, 1993. **74**(5): p. 3394-3398.

10 Conclusions and future work

10.1
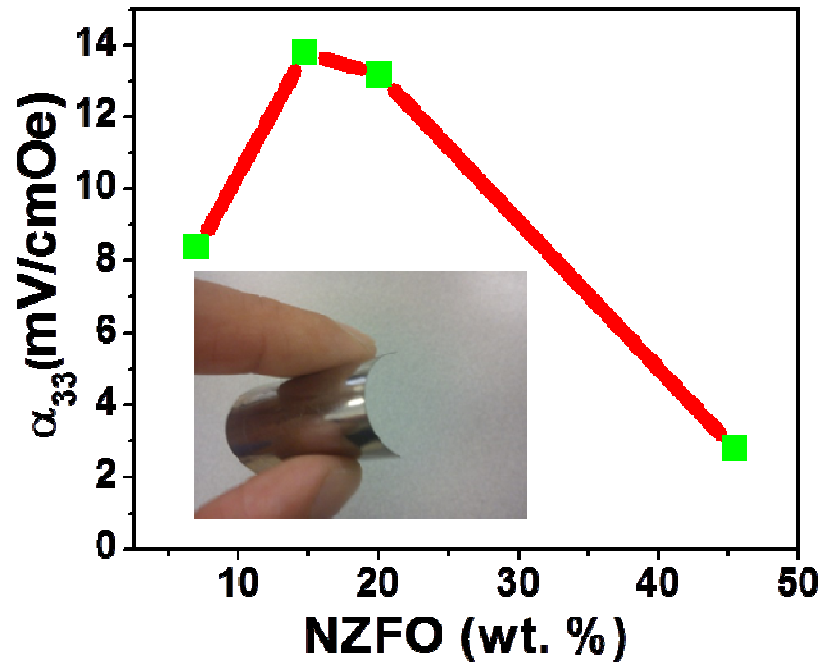
It was shown the need of more and more extensive studies regarding polymer based ME materials. This need derives from the low ME effect in single-phase materials, the fragility of ceramic composites and from an increasing demand of such composites from the industry.

In this way multiferroic and magnetoelectric composites consisting in the mixture of PVDF piezoelectric polymer with $CoFe_2O_4$, $NiFe_2O_4$ and $Ni_{0.5}Zn_{0.5}Fe_2O_4$ nanoparticles have been produced.

10.2 Conclusions

It was verified that composites with more that 90% of the crystalline phase in the ferroelectric β-phase were obtained for 5 wt.% of $CoFe_2O_4$ and 50 wt.% of $NiFe_2O_4$ respectively. In this way, ME polymer nanocomposites can be processed avoiding the usual α to β phase transformation by stretching of the polymer matrix.

It was shown that the nucleation kinetics was enhanced by the presence of the ferrite nanoparticles, as corroborated by the increasing number of spherulites with increasing nanoparticle content and by the variations of the Avrami's exponent. Further, the decrease of the crystalline fraction of PVDF with increasing nanoparticles content indicates that an important fraction of polymer chains are confined in interphases with the filler particle. Additionally, the crystallization velocity was found to be intimately related to the polymer α or β−phase formation in the nanocomposites and followed the order: $PVDF/NiFe_2O_4$> $PVDF/CoFe_2O_4$>$PVDF/Ni_{0.5}Zn_{0.5}Fe_2O_4$ for a given temperature and nanoparticle loading.

The origin of the β-phase nucleation was explained by the electrostatic interactions due to the presence of negative nanoparticle surfaces that interact with the polymeric CH_2 groups that have positive charge density. This interaction induced the polymer chains to align on the surface of the nanoparticles in an extended TTTT conformation resulting in formation of the β-PVDF phase with piezoelectric and ferroelectric properties. The use of appropriate surfactants caused variations in the surface charge of the nanoparticles opening the possibility of the β-phase nucleation in different nanofillers, leading to hybrid composites that can take advantage of the properties of the fillers and the electroactive phase of the polymer. For example, in the present case, the magnetostriction of the filler and the piezoelectricity of the polymer allow the ME response of the composite and its applications as sensors or/and actuators.

The macroscopic magnetic and dielectric response of the composites has demonstrated a strong dependence on the fraction of ferrite nanoparticles, with both magnetization and dielectric constant values increasing for increasing filler content. The β-relaxation in the composite samples was similar to the one observed for β-PVDF obtained by stretching. A superparamagnetic behaviour was observed for $PVDF/NiFe_2O_4$ composites, whereas $PVDF/CoFe_2O_4$ samples develop a hysteresis cycle with coercivity of 0.3 T.

Ferroelectric and piezoelectric properties of the composites were improved when small amount of $CoFe_2O_4$ nanoparticles were added to the P(VDF-TrFE) matrix. The highest

ME response of 41.3 mV/cm.Oe was found in the composite with 72 wt.% of $CoFe_2O_4$ content when H_{DC}=0.25T was transversely applied to the sample surface. A maximum ME voltage coefficient of ≈5mV/cm.Oe was obtained at a 50 kHz resonance frequency, a constant H_{DC} = 0,5T and a H_{AC} = 1 Oe to the PVDF/ $CoFe_2O_4$ (93/7 wt.%) sample. This ME response was possible due to a slight stretching process that allows the piezoelectric response after corona poling. Such process also led to the formation of voids.

At last, direct ME effects up to 1.35 mV cm^{-1} Oe^{-1} were obtained in a H_{DC}=0.5T, for samples with 15 wt.% of $Ni_{0.5}Zn_{0.5}Fe_2O_4$ at the 40 kHz resonance. P(VDF-TrFE)/$Ni_{0.5}Zn_{0.5}Fe_2O_4$ nanocomposites have showed, as compared to P(VDF-TrFE)/$CoFe_2O_4$ nanocomposites, linear and non-hysteretic direct magnetoelectric responses up to 0.5T.

It is in this way, novel polymer based magnetoelectric composites have been produced and characterized suitability for the development of sensors and actuators.

10.3 Future work

Many scientific groups are getting attracted towards the investigation in polymer based ME nanocomposites due to their cross-coupling effect which lead to promising applications in technological devices. However there are still some aspects that require further attention and an exhaustive study. One of these consist in the investigation regarding the effect of nanoparticle shape anisotropy in the ME response of the nanocomposite. Most of the existing studies report on nanocomposites with almost spherical filler nanoparticles. The use of anisotropic nanoparticles may promote the emergence of new effects and the fabrication of anisotropic sensors and actuators.

Other underexplored field lies in the creation of ME materials that can be used in applications that require simultaneously low and high magnetic fields. This can be achieved with the incorporation of distinct magnetostrictive nanoparticles in the same piezoelectric polymer matrix or the use of a bilayer system consisting in one layer of a magnetostrictive alloy and other layer with a polymeric nanocomposite (polymer + magnetostrictive nanoparticles).

It is also necessary to further explore the ME response of PVDF homopolymer based materials since its distinct morphological, physical properties and price show some advantages when compared to its copolymers. The only study which was reported in

Pedro Martins

the literature is the one presented in this thesis. In a similar way, more studies should be devoted to the understanding of the ME response in porous polymer based composites.

Finally, it is scientifically accepted that polymer based ME composites are ready for practical ME device applications such as magnetic field sensors and current sensors due to their good ME effect at room temperature. Although some prototypes of devices based on the polymeric ME laminates have been proposed, much work still remains for their applications in real systems.